NUREG/CR-
BNL-NUREG-

DETERMINATION OF LOCAL CORROSION CONDITIONS APPROPRIATE FOR HIGH LEVEL WASTE CONTAINERS IN A BASALT REPOSITORY

E. P. Gause, C. Brewster and P. Soo

June 1984

Prepared by the Nuclear Waste Management Division
D. G. Schweitzer, Head
Department of Nuclear Energy, Brookhaven National Laboratory
Associated Universities, Inc.
Upton, New York 11973

Prepared for the U. S. Nuclear Regulatory Commission
Office of Nuclear Materials Safety and Safeguards
Contract No. DE-AC02-76CH00016
FIN No. A-3167

ABSTRACT

The objective of this program is to determine the chemical environment that will be present within high level nuclear waste packages emplaced in a basalt repository. For this purpose, low carbon 1020 steel (a current BWIP reference container material), synthetic basaltic groundwater and a mixture of bentonite and basalt were exposed, in an autoclave, to expected conditions after repository sealing (150°C, ≈10.4 MPa). The experimental program consisted of three phases. The Phase I test involved a two-month gamma irradiation test in an inert argon environment. The Phase II test involved an irradiation test in a methane-containing environment also for a period of two months. (Methane was used because of the high concentrations of methane that have been detected in basaltic groundwater samples from Borehole RRL-2 in the Grande Ronde formation.) These two experiments were followed by a Phase III study which was conducted in the absence of radiation in a methane environment. Parameters measured include changes in gas pressure with time and gas composition, variation in dissolved oxygen (DO), pH and certain ionic concentrations of water in the packing material across an imposed thermal gradient, mineralogic alteration of the basalt/bentonite mixture, and steel corrosion behavior.

CONTENTS

ABSTRACT iii
FIGURES vii
TABLES xi
ACKNOWLEDGMENTS xiii
EXECUTIVE SUMMARY

1. INTRODUCTION 3

2. MATERIALS 4

3. AUTOCLAVE SYSTEM DESIGN 8

4. EXPERIMENTAL PROCEDURES 10

4.1 Slurry Preparation 10
4.2 Autoclave Pressurization 12
4.3 Irradiation Procedure 13
4.4 Post-Test Procedures 13

5. RESULTS AND DISCUSSION 14

5.1 Pressure Measurements 14
5.2 Pressure Changes Due to Radiolysis 15

5.2.1 Radiolysis of Water in a Closed System 15
5.2.2 Radiolysis of Methane in Aqueous Solution and in the Gaseous Phase 17

5.3 Gas Analyses Results 22

5.3.1 Phase I Test Gas Analysis Results 22
5.3.2 Phase II Test Gas Analysis Results 22
5.3.3 Phase III Test Gas Analysis Results 23
5.3.4 Comparison of Gas Analyses Results 23

5.4 Measurement of pH and DO and Calculation of Eh 24

5.4.1 Measurement of pH and Dissolved Oxygen of Unreacted Packing Material Slurry 24
5.4.2 Measurement of pH and Dissolved Oxygen of Reacted Packing Material Slurry 25

5.4.2.1 Measurement of Phase I Test pH and Dissolved Oxygen and Eh Calculation 25
5.4.2.2 Measurement of Phase II Test pH and Dissolved Oxygen and Calculation of Eh 26
5.4.2.3 Measurement of Phase III Test pH and Dissolved Oxygen and Calculation of Eh 27

5.4.3 Comparison of pH and DO Measurements and Eh Calculations for All Tests 27

5.5 Measurement of Ionic Concentrations in Slurry Water 28

5.5.1 Measurement of Ionic Concentrations in Phase I Test . . . 30
5.5.2 Measurement of Ionic Concentrations in Phase II Test . . 30
5.5.3 Measurement of Ionic Concentrations in Phase III Test . . 30
5.5.4 Comparison of Measured Ionic Concentrations For All Tests 31

5.6 SEM-EDX Analysis of Colloidal Material 32

5.6.1 SEM-EDX Analysis of Colloidal Material Removed From Phase I Test Solution 32
5.6.2 SEM-EDX Analysis of Colloidal Material Removed From Phase II Test Solution 33
5.6.3 SEM-EDX Analysis of Colloidal Material Removed From Phase III Test Solution 33
5.6.4 Comparison of SEM-EDX Analyses of Colloidal Materials 33

5.7 Analysis of Unreacted Bentonite and Reacted Bentonite Portion of Slurry 41

5.7.1 Analysis of Bentonite 41
5.7.2 Analysis of Montmorillonite Portion of Bentonite 41

5.7.2.1 Montmorillonite XRD Phase I Test 41
5.7.2.2 Montmorillonite XRD Phase II Test 50
5.7.2.3 Montmorillonite XRD Phase III Test 52
5.7.2.4 Comparison of Montmorillonite XRD Studies For All Tests 53

5.8 Analysis of Reacted Basalt 54

5.8.1 Comparison of XRD Patterns of Pulverized Basalt 54
5.8.2 Comparison of Micrographs of Polished Basalt Thin Sections 57

5.9 Metallography of Carbon Steel Sleeve and Identification of Surface Products 57

5.9.1 Metallography of Phase I Test Sleeve 60
5.9.2 Metallography of Phase II Test Sleeve 64
5.9.3 Metallography of Phase III Test Sleeve 69
5.9.4 Comparison of Pitting Corrosion For All Tests 71

6. SUMMARY 71

7. RECOMMENDATIONS FOR FUTURE WORK 75

8. REFERENCES 75

FIGURES

1. Generalized stratigraphy of the Columbia River Basalt Group, Yakima Basalt Subgroup, and intercalated and suprabasalt sediments within the Pasco Basin 5

2. Autoclave system being leak checked 9

3. Cross section through autoclave 10

4. Lengthwise section through autoclave 11

5. Pressure changes with time and temperature in the autoclave system for the three phases of the experiment: Phase I (absence of methane and presence of radiation), Phase II (presence of methane and radiation), Phase III (presence of methane and absence of radiation.) 16

6. Effect of dose rate on H_2 equilibrium pressures for concrete (neat), concrete containing Fe_2O_3, and concrete containing MnO_2 18

7. Solubility of methane in water at high temperatures and pressures . . 19

8. Solubilities of O_2, N_2, and H_2 in water as a function of temperature 24

9. Micrograph of colloidal material recovered from the Phase I test (800X) 34

10. EDX analysis of colloidal material recovered from the Phase I test. . 34

11. EDX analysis of rod in colloidal material recovered from the Phase I test 35

12. EDX analysis of crystal in colloidal material recovered from the Phase I test 35

13. Micrograph of protuberances appearing in colloidal material recovered from the Phase I test after bombardment with 17-kV electrons (1000X). 36

14. Micrograph of colloidal material recovered from the Phase II test heater region (1000X) 36

15. Micrograph of colloidal material recovered from the Phase II test wall region (1000X) 37

16. Micrograph of colloidal material recovered from the Phase II test heater region (300X) 37

17. Micrograph of the colloidal material recovered from the Phase III test heater region (100X) 38

FIGURES (Continued)

18. Micrograph of the colloidal material recovered from the Phase III test wall region (100X) 38

19. EDX analysis of colloidal material recovered from the Phase III test heater region 39

20. EDX analysis of colloidal material recovered from the Phase III test wall region 39

21. EDX(TEM) analysis of colloidal material recovered from the Phase III test wall region 40

22. Micrograph of unreacted bentonite clay (100X) 40

23. Comparison of X-ray diffraction patterns of reacted and unreacted bentonite present in the Phase I centrifuged packing material slurry samples prepared as oriented clay mounts by evaporation of slurry on glass slides. [Range of scan: 2θ = 3-37° (d = 2.43-29.4 Å).] 42

24. Comparison of X-ray diffraction patterns of reacted and unreacted bentonite present in the Phase II test centrifuged packing material slurry samples prepared as oriented clay mounts by evaporation of slurry on glass slides. [Range of scan: 2θ = 3-37° (d = 2.43-2.94 Å)] 43

25. Comparison of X-ray diffraction patterns of reacted and unreacted bentonite present in the Phase III test centrifuged packing material slurry samples prepared as oriented clay mounts by evaporation of slurry on glass slides. [Range of scan: 2θ = 3-37° (d = 2.43-29.4 Å)] 44

26. Appearance of Phase I centrifuged packing material slurries before and after reaction 45

27. Comparison of X-ray diffraction patterns of Phase I test reacted and unreacted montmorillonite present in the centrifuged packing material slurry samples prepared as oriented clay mounts by evaporation of slurry on glass slides; treatment by glycolation, followed by heating to 300°C for one hour. [Range of scan: 2θ = 3-9.5° (d = 9.30-29.4 Å)] 48

28. Comparison of X-ray diffraction patterns of Phase II test reacted and unreacted montmorillonite present in the centrifuged packing material slurry samples prepared as oriented clay mounts by evaporation of slurry on glass slides; heat-treated at 300°C for 18 hours, followed by glycolation at 60°C. [Range of scan: 2θ = 3-9.5° (d = 9.30-29.4 Å)] 49

FIGURES (Continued)

29. Comparison of X-ray diffraction patterns of Phase III test reacted and unreacted montmorillonite present in the centrifuged packing material slurry samples prepared as oriented clay mounts by evaporation of slurry on glass slides; heat-treated at 150°C, followed by glycolation at 60°C, followed by heat-treatment at 300°C, followed by glycolation at 60°C. [Range of scan: 2θ = 3-9.5° (d = 9.30-29.4 Å)] 51

30. Comparison of X-ray diffraction patterns for reacted and unreacted basalt, prepared as unoriented mounts of pulverized basalt. [Range of scan: 2θ = 3-65° (d = 1.43-29.4 Å)] 55

31. Minerals in unreacted basalt as determined with a polarizing microscope under crossed polars (100X) 58

32. Minerals in Phase I test reacted basalt sampled from the heater region as determined with a polarizing microscope under crossed polars (100X) 58

33. Minerals in Phase I test reacted basalt sampled from the wall region as determined with a polarizing microscope under crossed polars (100X) 59

34. Minerals in the Phase III test reacted basalt sampled from the wall region as determined with a polarizing microsope under crossed polars (100X) 59

35. Appearance of carbon steel sleeve prior to reaction (left) and subsequent to Phase I test reaction (right) 61

36. Micrograph of outside diameter of carbon steel sleeve subsequent to Phase I test rection showing metal oxide and thin clay deposition layer (marked by arrow) (250X) 62

37. Micrograph of outside diameter of carbon steel sleeve subsequent to Phase I test reaction showing metal oxide and thick clay deposition layer between arrows (250X) 62

38. SEM-EDX micrograph of iron-rich layered material in Phase I test carbon steel surface product (1000X) 63

39. Micrograph of outside diameter of carbon steel sleeve prior to Phase I test reaction (250X) 63

40. Micrograph of weld metal in carbon steel sleeve subsequent to Phase I test reaction (250X) 65

FIGURES (Continued)

41. Micrograph of outside diameter of carbon steel sleeve subsequent to Phase II test reaction showing metal oxide and thin clay deposition layer (marked by arrows) (250X) 65

42. Micrograph (SEM) of orange-brown sleeve surface product from Phase II test (100X) 66

43. Micrograph (SEM) of magnetic green-yellow sleeve surface product from Phase II test (100X) 66

44. Point plot of EELS spectrum of orangish-brown sleeve surface product from the Phase II test showing well-defined crystalline material containing iron and oxygen 67

45. Debye-Scherrer powder pattern for orange-brown sleeve surface product from Phase III test 68

46. Debye-Scherrer powder pattern for green-yellow sleeve surface product from Phase II test 68

47. Micrograph of outside diameter of carbon steel sleeve subsequent to Phase III test showing pitting, and a thin detached oxide layer (250X) 70

48. Micrograph of Phase III test green carbon steel surface product (100X) 72

49. EDX of Phase III test green carbon steel surface product 72

50. Micrograph of Phase III test orange-brown carbon steel surface product (100X) 73

51. EDX of Phase III test orange-brown carbon steel surface product . . . 73

TABLES

1. Compositions of Middle Sentinel Bluffs Flow basalt and reference Wyoming bentonite 6

2. Petrographic characteristics of primary and secondary phases reported as present in Grande Ronde basalt. 7

3. Composition of synthetic Grande Ronde groundwaters 8

4. Comparison of composition of gases sampled after reaction as determined by mass spectrometry 21

5. pH and DO as measured for packing material slurry and Eh as calculated for all tests 28

6. Comparison of ionic concentrations of reacted Grande Ronde GR-3 groundwater 29

7. Comparison of (00ℓ) d-spacings based on X-ray diffractometer studies of reacted and unreacted bentonite portions of centrifuged packing material slurries prepared as oriented clay mounts by evaporation of centrifuged slurry on glass slides. [Intensities not specified. Range of scan: 2θ = 3-37° (d = 2.43-29.4 Å).] 46

8. Comparison of (00ℓ) d-spacings based on X-ray diffractometer studies of Phase I test reacted and unreacted montmorillonite, prepared as oriented clay mounts by evaporation of centrifuged packing material slurry on glass slides; treatment by glycolation at 60°C, followed by heating to 300°C for one hour. [Intensities not specified. Range of scan: 2θ = 3-9.5° (d = 9.30-29.4 Å).] 47

9. Comparison of (00ℓ) d-spacings based on X-ray diffractometer studies of Phase II reacted and unreacted montmorillonite, prepared as oriented clay mounts by evaporation of centrifuged packing material slurry on glass slides; treatment by heating to 300°C for 18 hours, followed by glycolation at 60°C. [Intensities not specified. Range of scan: 2θ = 3-9.5° (d = 9.30-29.4 Å).] 50

10. Comparison of (00ℓ) d-spacings based on X-ray diffractometer studies of Phase III reacted and unreacted montmorillonite, prepared as oriented clay mounts by evaporation of centrifuged packing material slurry on glass slides; heat-treatment at 150°C, followed by glycolation at 60°C, followed by heat-treatment at 300°C, followed by glycolation at 60°C. [Intensities not specified. Range of scan: 2θ = 3-9.5° (d = 9.30-29.4 Å).] 53

TABLES (Continued)

11. Comparison of (hkℓ) d-spacings based on X-ray diffractometer studies of reacted and unreacted basalt, prepared as unoriented mounts of pulverized basalt. [Intensities not specified. Range of scan: 2θ = 3-65° (d = 1.43-29.4 Å).] 56

12. Calculated d-spacings of Phase II test sleeve surface product based on measured Debye-Scherrer electron diffraction powder patterns . . . 69

ACKNOWLEDGMENTS

The authors would especially like to thank Dr. Ramesh Dayal for his help in utilizing instrumentation, interpreting results, and reviewing the manuscript. They are also grateful to Dr. Harpal Arora for his helpful discussions regarding the use of the X-ray diffractometer and mineralogical identification. Appreciation is also extended to Robert Sabatini and Johan Tafto for performing the SEM-EDX analyses and for their efforts in attempting to identify the composition of the carbon steel surface products. They would also like to thank Eugene Ferreri, Mary Kinsley, Andrew Cendrowski, Sue Oakley, Robert Wilson and John Warren for ion chromatography results, atomic absorption results, metallographic results, silica content determinations, gas analyses and SEM-EDX analysis of the colloidal material, respectively. The authors would also like to express their gratitude to Ms. Grace Searles for her patience and skill in the typing and preparation of this report.

EXECUTIVE SUMMARY

The objective of this program is to determine the chemical environment that will be present within high level nuclear waste packages emplaced in a basalt repository. For this purpose, low carbon 1020 steel (a current BWIP reference container material), synthetic basaltic groundwater and a mixture of bentonite and basalt were exposed in an autoclave to expected repository conditions shortly after repository sealing (150°C, 10.4 MPa). The experimental program consisted of three phases. Phase I involved a two-month irradiation test (3.8 ± 0.5) x 10^4 rad/h in an argon environment. The Phase II test was similar but was conducted in a methane environment. These two tests were followed by a Phase III control test which was similar to the Phase II study but it was performed in the absence of radiation.

All of these studies concentrated on changes in gas pressure and composition; on the differences in pH, dissolved oxygen (DO), calculated Eh and the concentration of those ions, which have been implicated in the corrosion of carbon steel, as sampled across a thermal gradient; on alterations of the packing material as determined by X-ray diffraction (XRD); and on the determination of localized and uniform corrosion of the carbon steel sleeve.

Trends in gas pressure were similar in each of the three tests. Over the two-month test periods, the gas pressure in the autoclave ranged from 9.3-9.7 MPa (1357 psi to 1404 psi) in the Phase I test, from 11.1-13.2 MPa (1612 psi to 1919 psi) in the Phase II test and from 9.8-11.7 MPa (1416 psi to 1702 psi) in the Phase III test. There was an early trend to decreasing pressures followed by a trend to pressures approaching or slightly exceeding the initial values. This indicates that pressure in a sealed repository environment may initially decrease and be followed by a slow increase. Overall, in all three tests, hydrogen was produced and oxygen was consumed, as determined by gas analyses and dissolved oxygen measurements. More hydrogen was produced in the Phase II test than in the Phase I and III tests due to the radiolysis of methane. Similar amounts of hydrogen were produced in the irradiated Phase I test and in the non-irradiated Phase III test. These results indicate that, in a repository, hydrogen will be produced and oxygen will be consumed but that some residual oxygen may be present, at least in the short term. Carbon-containing gases were produced in the Phase I test (CO_2 and CH_4) and in the Phase II test (CO_2 and C_2H_6) and possibly in the Phase III test.

There were different thermal gradients established across the packing material in each test. For Phase I, II, and III tests, these were, respectively, 1.0, 0.6, and 2°C/mm. After cooling the autoclave over a period of 25 minutes, the pH of the water in the basalt/bentonite packing material measured at room temperature was nearly neutral. There did not appear to be a significant change in pH across the thermal gradient in the packing material in any of the three tests. There did not appear to be a significant change in DO across the thermal gradient of the packing material in any of the tests. The calculated Eh values indicate that an oxidizing environment existed after quenching the contents of the autoclave. Reducing environments were not achieved under the current test conditions.

The concentrations of Cl^- and SO_4^{2-} measured at room temperature were greater near the cooler end of the thermal gradient in the tests. Changes in ionic concentrations occur across the thermal gradients but bulk changes in ionic concentrations, relative to the groundwater composition, may be more significant in terms of corrosive environments. The bulk of the Fe and Si content of the liquid system is present as colloidal material that is filterable. Colloids are formed in the absence of radiation but their production seems to be enhanced if radiation is present.

Hydrothermal conditions cause some change in the bentonite component of the packing material as determined by X-ray diffraction (XRD). The expandability of the bentonite portion of the wet packing material may be affected by periods of heating and simultaneous dehydration. Radiation may enhance expandability. Optical and XRD studies indicate that some changes occur in the mineralogical content of basalt during hydrothermal testing. The alteration of the pyroxenes in the basalt is one mineralogical change that was observed. Other alteration also occurs in the presence or absence of radiation as evidenced by changes in XRD patterns.

Adherent surface products removed from the carbon steel sleeve in the Phase I test contained mainly montmorillonite clay. Scanning electron microscope (SEM-EDX) analysis indicated the presence of other materials containing more Fe than that found in montmorillonite. Surface products removed from the carbon steel sleeve in the Phase II test were analyzed by SEM-EDX and electron diffraction but were not readily identifiable. (An orange-brown product contained large amounts of Si, Fe, and Al, while the green-yellow product was largely composed of Fe and Si.) Identification was also not possible for the Phase III surface products, which were analyzed by SEM-EDX and XRD. (Both Phase III surface products contained large amounts of Si and Fe, with the green phase also containing a large amount of Ca.)

There was no pitting on the carbon steel sleeve or the steel weldment in the Phase I test. There were hemispherically-shaped pits approximately 12 microns in depth in the Phase II test, and shallower (approximately 8 microns in depth) and more closely-spaced pits were formed in Phase III. Under the conditions of these tests, the maximum predicted pit depth in 300 years is estimated to be <2.2 cm.

1. INTRODUCTION

The objective of this program is to determine the chemical environment that will be present in high level nuclear waste packages emplaced in a basalt repository. For this purpose, low carbon steel (a current Basalt Waste Isolation Project, BWIP, reference container material), a basalt/bentonite packing material, and synthetic Grande Ronde basaltic water were reacted in an autoclave at 150°C and ≈10.4 MPa (1500 psi) pressure. The tests lasted for two-month periods and the gamma irradiation flux, when used, was $(3.8 \pm 0.5) \times 10^4$ rad/h. The Phase I irradiation test used an inert argon environment and Phase II involved a similar set of experimental conditions but used a methane cover gas. This was performed because high methane concentrations have been detected in basaltic water samples taken from Borehole RRL-2 in the Grande Ronde formation. The Phase III control test was also conducted in a methane environment, but in the absence of irradiation.

Measurements on the packing material slurry at the conclusion of the tests included pH and dissolved oxygen (DO) determinations. The Eh could have also been measured but, according to available information (NUREG/CR-3389, 1984), its observed value may not be very meaningful[1]. The concentrations of Cl^-, total Fe (measured as Fe^{2+}), and SO_4^{2-} ions in the filtrate were also measured, since these ions are associated with the corrosion of carbon steel[2]. Gases generated during the irradiation period may include H_2, O_2, N_2 and CO_2. Since several of these gases could have a deleterious effect on the waste container, gas analyses were made at the conclusion of the test period. The carbon steel sleeves were metallurgically evaluated for uniform and pitting corrosion. Hydrothermal alteration of the rock and clay constituents of the packing material was also investigated.

---

[1]There is no reason to believe that the potential of a platinum (or other noble metal) electrode immersed in a solution is a thermodynamic potential or even a reasonably reproducible potential. Most likely, such a measured potential is a mixed potential dependent on the kinetics of the various redox processes occurring in the system. In the absence of significant concentrations of oxygen and other possible redox active species, the potential may depend on the corrosion rate, however small, of the indicator electrode (NUREG/CR-3389, 1984).

[2]Basaltic groundwater contains F^- ion but this has not been associated with the corrosion of carbon steel (Hall, E., 1982). Qualitative tests for H_2S and S^{-2} were to be performed in the current study to determine if quantitative tests were needed.

2. MATERIALS

Basalt from the Cohassett Flow of the Sentinel Bluffs Sequence of the Grande Ronde Formation (see Figure 1) and bentonite clay from Wyoming[3], saturated with simulated Grande Ronde groundwater, were used to prepare the packing material slurry. The major-element oxide compositions for the Middle Sentinel Bluffs Flow (assumed to be representative of other flows in the Sentinel Bluffs Sequence, including the reference Cohassett Flow) and the reference Wyoming bentonite (coded SWy-1 by the Clay Minerals Society) are given in Table 1. Analyses for S and F contents were not reported for the basalt but were reported as 0.05% S and 0.11% F for the bentonite. Some information is also available on the carbonate content of the bentonite. Upon ignition to 1000°C, the bentonite lost 6.43% of its weight [assumed to be due to the loss of adsorbed and structural water (5.1%) and CO_2] (Van Olphen, H., 1979). An infrared spectrum of the bentonite confirmed the trace carbonate content and a moderate content of iron in the lattice in the ferric state (Van Olphen, H., 1979). The availability of information, e.g., the infrared spectrum, and the characterization of the standard clay, SWy-1, was a primary reason for its use in the experiment. As a reference clay, it is reported to have a surface area of 31.82 ± 0.22 m^2/g (Van Olphen, H., 1979), as determined at 77K using the BET gas (N_2) adsorption method designed by S. Brunauer, P. H. Emmett and E. Teller (1938). However, it should be noted that surface areas determined by gas adsorption techniques on SWy-1 clay do not necessarily correspond to the the reactive surface areas in solution (Lerman, A., 1979). The surface that reacts with the solution may be smaller than the total measured. It is not expected that the use of an argon or methane overpressure will block reactive sites of the clay in solution, based on results of Stoessel and Byrne (1982). They showed that methane solubilities in water at 25°C and at pressures of methane up to ≈5 MPa were not significantly affected by the presence of clay and that there was no detectable sorption of methane onto SWy-1 clay, under these conditions. It is assumed that argon will behave similarly to methane because of its inertness. It is also assumed, without evidence to the contrary, that at higher pressures and temperatures, there is no blocking of reactive sites by argon or methane.

---

[3]Reference basalt and clay as specified by BWIP Rockwell-Hanford personnel. The density of the basalt rock that was crushed to pellet size was measured to be 2.8 g/cc. These basalt pieces are not uniform in size but are chips ranging in size from 0.187 to 0.250 inches in diameter.

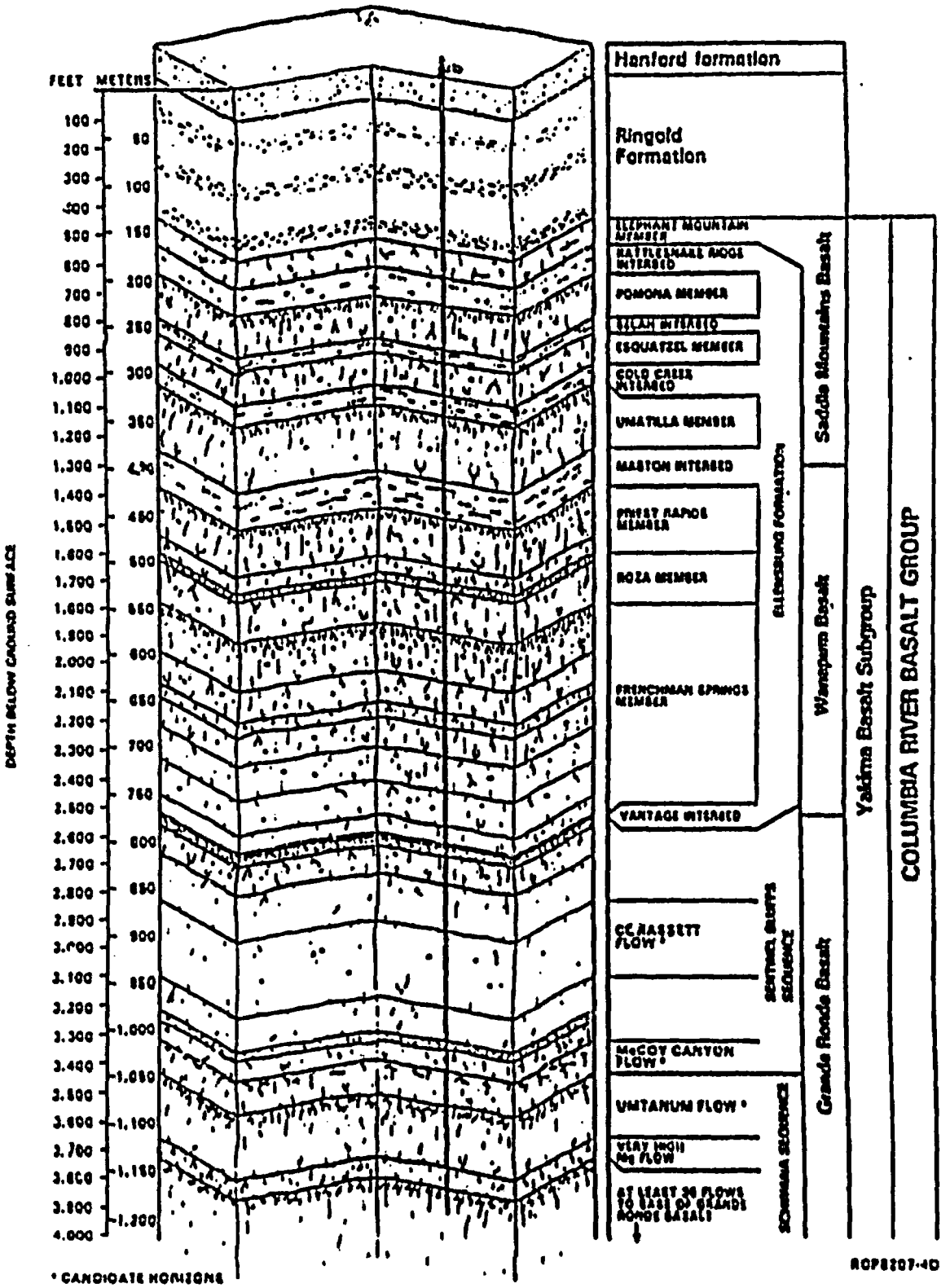

Figure 1. Generalized stratigraphy of the Columbia River Basalt Group, Yakima Basalt Subgroup, and intercalated and suprabasalt sediments within the Pasco Basin (RHO-BW-SA-303P, 1983). (Details of the stratigraphy are not discussed in this report.)

Table 1. Compositions of Middle Sentinel Bluffs Flow basalt and reference Wyoming bentonite.

Oxide Component	Basalt (Weight Percent) (DOE/RL 82-3, Vol. II, 1982)	Bentonite (Weight Percent) (Van Olphen, H, 1979)
SiO_2	53.4	62.9
TiO_2	1.79	0.09
Al_2O_3	15.0	19.6
FeO	11.7	0.32
Fe_2O_3	---	3.35
MnO	0.21	0.006
MgO	4.99	3.05
CaO	8.86	1.68
Na_2O	2.48	1.53
K_2O	1.03	0.53
P_2O_5	0.29	0.049

Mineralogically, bentonite is montmorillonite clay with some quartz present (Van Olphen, H., 1979)[4]. Steindler and others (ANL 83-19, 1983) reported the mineralogical composition of SWy-1 clay to consist of montmorillonite, quartz, calcite, and K-feldspars. No gypsum was detected.

The Grande Ronde basalt flows of the Columbia Plateau are continental flood basalts. Mineralogically, these basalts contain the principal minerals pyroxene, plagioclase, titaniferous magnetite, olivine and interstitial glass

[4]Montmorillonite is a mineral which is essentially a hydrated aluminosilicate with some substitution within the lattice. A "typical" packet of montmorillonite is formed by the bonding of a layer of alumina octahedra with two layers of silica tetrahedra. In general, Wyoming bentonite contains a mineral of the montmorillonite type as the principal component with the structural formula:

$$(Al_{1.53}\ Fe^{3+}_{0.18}\ MgO_{0.33})(Al_{0.13}\ Si_{3.87})\ O_{10}\ (OH)_2$$

(Grimshaw, R. W., 1971). (This notation indicates that Al, Fe, and Mg are present in dioctahedral coordination and that Al and Si are present in tetrahedral coordination. There are also ten divalent oxygen and two hydroxyl anions per packet, as shown by the formula.) The presence of adsorbed cations (i.e. the exchangeable cations such as Ca^{2+}, Na^{+}, Mg^{2+}, K^{+} and H^{+}) and other minerals (e.g. quartz) present in the Wyoming bentonite are not indicated by this formula.

of variable composition (DOE/RL 82-3, Vol. II, 1982). The secondary minerals are predominantly smectite clays and zeolite (clinoptilolite), with lesser amounts of SiO_2. Textures vary considerably, with typical textures dominated by a lath-shaped plagioclase and pyroxene grains locked together by an interstitial glassy matrix. Primary and secondary phases in Grande Ronde basalt are listed in Table 2.

Table 2. Petrographic characteristics of primary and secondary phases reported as present in Grande Ronde basalt (DOE/RL 82-3, Vol. II, 1982).

Characteristic Primary Phase	Abundance Volume %	Chemical Formula
Plagioclase (anorthite)	25-50	$CaAl_2Si_2O_8$
Pyroxene		
Augite	20-45	$(Ca)(Mg,Fe^{2+},Fe^{3+},Al,Ti)(Si,Al)_2O_6$
Pigeonite	0-10	$(Mg,Fe^{2+},Ca,Mn)(Mg,Fe^{2+},Mn)[Si,Al]_2O_6$
Orthopyroxene	0-trace	$(Ca,Mg,Fe^{2+})(SiO_3)$
Glassy Mesostasis	15-70	SiO_2 = 60 to 74% (by weight)
Titaniferous Magnetite	0-7	$FeO\cdot(Fe_2O_3,TiO_2)$
Apatite	0-2	$Ca_5(PO_4)_3F$, occurs as acicular crystals in the mesostasis.
Olivine	0-3	$(Mg,Fe^{2+})_2\ SiO_4$
Alteration Products (secondary phases)	1-9	Includes smectites, zeolites, SiO_2

The nominal composition of the synthetic Grande Ronde water identified as GR-3 is given in Table 3. Its pH at 25°C is 9.74 (RHO-RE-SR-5, 1982). In addition to the components listed, GR water has been found to contain the following gases: 25 ppm N_2, 10 ppm Ar, and up to 700 ppm CH_4 at 25°C (RHO-BW-SA-315P, 1983). The results of an analysis of the synthetic groundwater used in this experiment are also given in Table 3. The recipe for the synthetic groundwater is based on analyses of water samples collected from the DC-6 well in the test horizon just below the Umtanum basalt flow (990-1075 m). (The composition of GR-4 synthetic groundwater is given in Table 3 for comparison and is based on analysis of a Cohassett flow bottom sample from Borehole RRL-2 in the reference repository location. It should be noted that GR-4 water has much less sulfate content than the GR-3 water which was used in the present experiment.)

Table 3. Composition of synthetic Grande Ronde groundwaters.

Chemical Species	GR-3 Nominal Composition (ppm) (RHO-RE-SR-5, 1982)	GR-3 Experimental Composition (ppm)	GR-4 Nominal Composition (ppm) (SD-BWI-TP-022, 1984)
Na^+	358	363	334
Cl^-	312	312	405
SO_4^{2}	173	165	40
Si as SiO_2*	76.2	79.3	96.4
Inorganic C as HCO_3^-	54.6	---	92.0
F^-	33.4	29.9	19.9
K^+	3.43	3.63	13.8
Ca^{2+}	2.78	2.10	2.20
Mg^{2+}	0.032	0.030	---

*Total dissolved silica content is not partitioned in its speciated forms, $H_3SiO_4^-$ and H_4SiO_4.

3. AUTOCLAVE SYSTEM DESIGN

The hydrothermal conditions in the current tests were achieved by use of a stainless steel autoclave, which was pressurized with Ar and/or CH_4 to approximately 6.9 MPa (1000 psi) at room temperature to obtain the expected hydrostatic pressure at temperature. (The contribution to the pressure due to water vapor at 150°C is 0.52 MPa, 75 psi.) Figure 2 shows the exterior of the autoclave. The placement of internal components is shown in Figures 3 and 4. The autoclave weighs approximately 20.4 kg and is approximately 15.2 cm in depth and has an internal diameter of 6.3 cm. A rod-shaped resistance heater was placed vertically near the wall of the autoclave to ensure the development of a thermal gradient across the packing material. A 1/4 carbon 1020 steel sleeve was placed over the heater to simulate actual waste container/packing material conditions. It has a welded-on cap and is 2.5 mm in diameter, 143 mm in length and 2 mm in thickness. The sleeve was heated to 150°C and a temperature differential was established across the 38-mm thickness of the packing material. The temperatures at the heater (T_2) and at the wall (T_1) were monitored by Type 316 stainless steel thermocouples which were 3 mm in diameter and were inserted to a depth of approximately 75 mm and bent to contact the heater and wall. It is assumed that thermocouples maintain contact during test. During the tests, packing material was extruded into the space between the heater and the inner surface of the steel sleeve. This would act as an insulating medium which, together with the excellent thermal conductivity of the sleeve, would greatly minimize local hot spots on the latter. In the Phase I test an

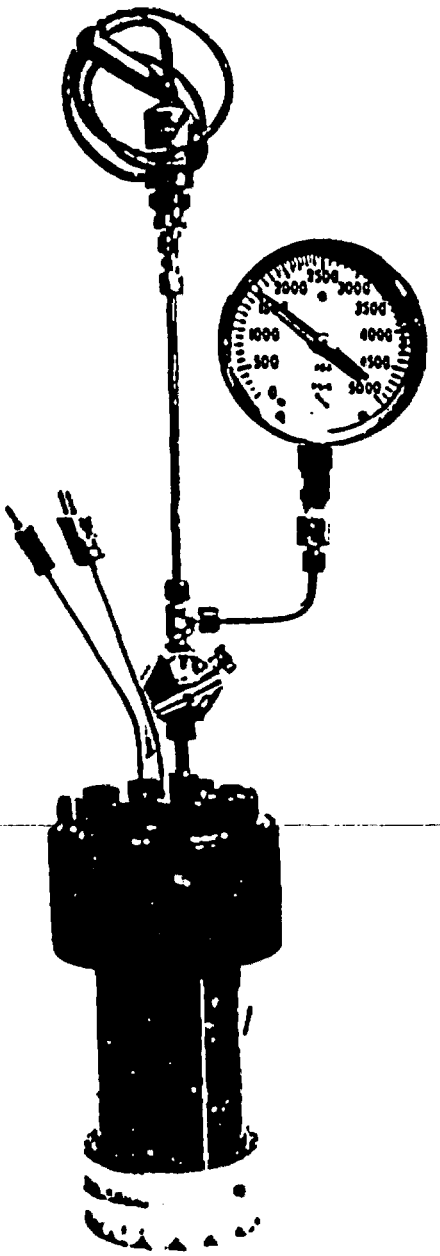

Figure 2. Autoclave system being leak checked. (Pressure gauge was removed prior to placement in gamma pool.) Magnification is 0.2X.

attempt was made to obtain water samples for analysis by incorporating two Type 304 stainless steel sampling tubes in the packing material. These were 7 mm in diameter and 150 mm in length, and each contained 23 small drilled holes to allow water ingress while retarding passage of the slurry. Since the tubes displace a volume of only 20 mL compared to a slurry volume of 440 mL, no significant changes in thermal conductivity or temperatures in the packing were expected. Sampling tubes were not used in the Phase II and III tests since the volumes of water collected by their use were minimal.

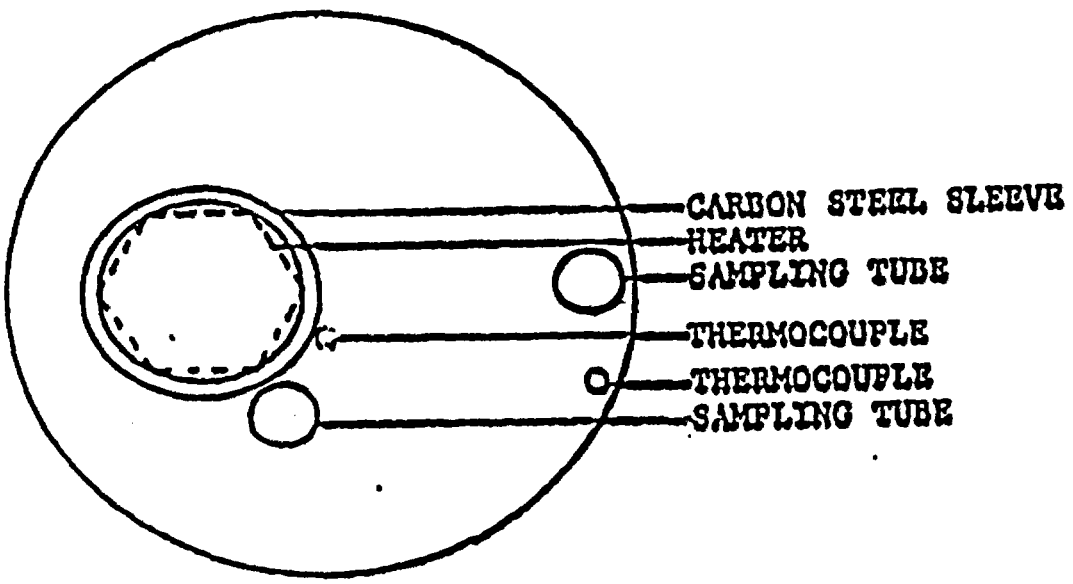

Figure 3. Cross section through autoclave (drawn to scale).

4. EXPERIMENTAL PROCEDURES

4.1 Slurry Preparation

The bentonite was used in the as-received condition (-400 mesh, with a density of 0.78 g/cc). The basalt was crushed to pellets ranging in size from 0.187 to 0.250 inch in diameter. An excess amount of slurry was first prepared by mixing 33.5 g of bentonite with 478 mL of freshly-made synthetic groundwater which was prepared using details given in the literature (RHO-RE-SR-5, 1982). The ratio of 7:100 (by weight) of bentonite to water was selected on the basis of BWIP work which showed this composition to be optimal for restricting water flow in basalt repositories (RHO-BWI-C-66, 1980). To minimize the presence of air and voids, the slurry was prepared so that water replaced the air present in the packing material. This mixture was allowed to gel overnight in the presence of air. Pellets of basalt including fines (209 g occupying a volume of ≈129 mL) were then added to the bentonite slurry. This packing material was also allowed to equilibrate overnight in the presence of air. This procedure yielded a 3:1 (by volume) mixture of basalt:bentonite and a solution:solid

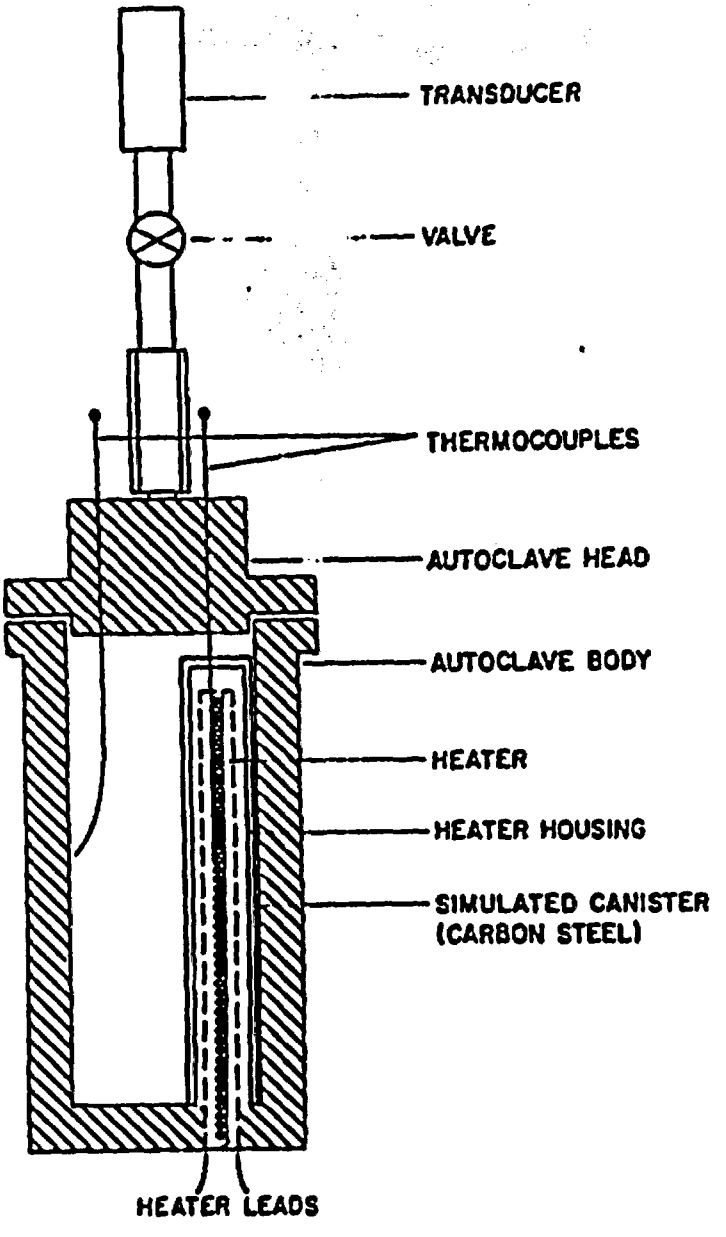

Figure 4. Lengthwise section through autoclave. Magnification is 0.35X.

ratio (by weight) of about 2. Most of the packing material slurry was placed in the autoclave, giving a void space below the autoclave head of approximately 20 mL. (The use of the sampling tubes gave a total void of ≈30 mL.)

4.2 Autoclave Pressurization

In the Phase I test, the slurry was placed in the autoclave leaving a void space of ≈30 mL. The autoclave was flushed with argon and pressurized to 6.9 MPa (1000 psi) with argon at 24°C. After lowering the autoclave and monitoring/control attachments into the gamma pool, the temperature was slowly raised to 150°C ± 2°C over a period of 24 hours. A mean temperature differential of ≈37°C across the packing material test section was achieved and maintained. The temperature at the autoclave wall and pressure transducer readings were recorded hourly by use of an automated data logger. The transducer readings in volts had previously been calibrated to pressure.

In the Phase II test, slurry was placed in the autoclave, with a void space of ≈20 mL remaining. (The sampling tubes were not used in the Phase II and Phase III tests.) Because of the ≈50 mL drop in slurry level discovered at the conclusion of the Phase I test, a different pressurization technique was followed in Phase II. The autoclave was pressurized to 10.4 MPa (1500 psi) at room temperature with argon and maintained overnight. The autoclave was opened and there was again found to be a noticeable drop in the slurry level. Additional slurry was added to keep an estimated void space of ≈20 mL. The autoclave was again pressurized to 10.4 MPa with argon at room temperature to check for leakage. The argon was then bled off and methane (99.93% pure, ethane 0.07%) was added to attain a pressure of 6.2 MPa (900 psi) at 18°C. It was predicted that the system would approach a pressure of ≈9.7 MPa at the test temperature, including a water vapor pressure contribution. However, the pressure attained when the system was at 150°C was in excess of 13.1 MPa (1900 psi). After lowering the autoclave and monitoring/control attachments into the gamma pool[5], the temperature at the heater was slowly raised to 150°C ± 4°C over a period of 52 hours. A temperature differential across the packing of ≈22°C ± 4°C was achieved at the end of that time. After 157 hours of irradiation, a malfunction developed in the heater regulator, causing the temperature to drop to 108°C at the heater (T_2) by morning. After the regulator was replaced, the temperature was increased to normal over a period of 11 hours. The pressure reading at 176 hours (11.9 MPa) was ≈1.0 MPa lower than the pressure reading at 159 hours. It is not known whether this reduction in pressure would have occurred if the regulator had not failed; nor is the cause of the reduction clear. A mean temperature differential of ≈22°C was maintained throughout the Phase II test.

In the Phase III test, a procedure similar to that described for the Phase II test was used to check for leakage. The argon was again bled off and

[5]A methane monitor was emplaced over the tube containing the autoclave in the gamma pool. Continuous purging over the entry of the tube with argon was carried out.

methane added to attain a pressure of 7.4 Mpa (1074 psi) at 18.4°C. It was predicted that the system would approach a pressure of ≈10.4 MPa, with the addition of the water vapor pressure contribution. The actual pressure attained was ≈10.6 MPa. An air blower and/or cooling coils were used in this non-irradiation test in an attempt to obtain a thermal gradient in the packing similar to those obtained for the Phase I and Phase II tests which were placed in the gamma pool. Their use across the body of the autoclave increased the thermal gradient. However, an air stream across the top of the autoclave was used because its use decreased the thermal gradient. Because of the blower tests, there was some fluctuation in autoclave pressure during the first 195 hours of testing.

The initial pressurization value was kept the same for all three phases of the experiment. The fact that the pressure in the Phase II experiment exceeded that predicted may be due to the generation of a radiolytically-produced gas. Differences in pressure developing in the autoclave seem to also be inversely proportional to the size of the thermal differential across the packing material. The effect of this pressure difference between the Phase II and Phase III tests on the results is not known.

4.3 Irradiation Procedure

The ambient air temperature in the gamma pool test hole was 22°C. A dosimetry measurement, which was performed on the empty autoclave, indicated that a dose rate of $(3.8 \pm 0.5) \times 10^4$ rad/h was delivered to the interior of the vessel by the ^{60}Co source. The dose rate was measured by use of radiochromic film which is calibrated to a National Bureau of Standards (NBS) standard by comparing optical densities. No measurement of distribution of the gamma energies from the ^{60}Co source is available. In the Phase I test, the autoclave was irradiated for 1486 h, to a dose of $(5.6 \pm 0.7) \times 10^7$ rad. In the Phase II test, the autoclave was irradiated for 1727 h, to a dose of $(6.6 \pm 0.9) \times 10^7$ rad. The Phase III test did not incorporate any irradiation.

4.4 Post-Test Procedures

Procedures for analyses on the gas, the packing material, water and carbon steel sleeve were initiated after the autoclave had been cooled to room temperature (at a rate of approximately 5°C/min). As many as six gas samples were taken, and analyses carried out by a mass spectrometric technique. Gas remaining in the autoclave was vented to the air and the autoclave was opened in a glove bag filled with argon. Measurements of pH and DO were made at several depths in the slurry both near the heater and near the autoclave wall. The pH electrode had previously been calibrated with buffers having standardized pH values of 2, 7, and 10. Readings are accurate to ±0.05 units. The DO electrode had been calibrated against the DO content of water at 25°C, which is 8.4 ppm. Dissolved oxygen (DO) readings have an estimated accuracy of ±0.5 ppm.

The appearance of the material in the autoclave was changed after reaction in all three tests. There were portions of the slurry which were white and/or orange in comparison to the unreacted slurry color (beige). No caking or odor were detected. Some orange coloration was also evident on the slurry adhering to the steel sleeve.

Two-core samples (each ≈5 mL) were taken from both the heater and autoclave wall regions (these are designated by the letters H and W, respectively, in subsequent discussions). Test tubes containing the slurry were centrifuged for one hour and the liquid portion was removed. Approximately 3 mL of solution were collected from the sample taken from the region near the autoclave wall and approximately 2 mL from the sample taken from the heater region. The liquid was cloudy and was passed through a membrane filter having a pore size of 0.025 μm. The filtrates were analyzed for Fe, Si, Cl^-, and SO_4^{2-} content[6]. After the cores were removed, an additional sample (i.e. samples designated R) was obtained by combining portions of the slurry that were randomly selected. The test tube containing this "combination" sample was also centrifuged, but the supernate was analyzed in the unfiltered form.

Basalt pellets were removed from the corings near the heater and the autoclave wall and prepared as thin-section specimens for microscopic analysis. Unreacted basalt thin sections were also made for comparison. Pulverized basalt and glass slides coated with reacted centrifuged slurry were also prepared for mineralogical studies using a Philips XRG 3100 X-ray diffractometer. Colloidal matter obtained from R samples, by filtration through a 0.025-micron membrane filter, was analyzed by SEM-EDX procedures.

The slurry was removed from the carbon steel sleeve by washing in water. The slurry adhering to the sleeve was isolated for SEM-EDX studies. The carbon steel sleeve was placed in a desiccator and kept for metallographic analysis.

5. RESULTS AND DISCUSSION

5.1 Pressure Measurements

After the test temperature was attained, the pressure within the autoclave was recorded. The following ranges of pressure were found for the three tests over the two-month test periods:

9.3-9.7 MPa (1357-1404 psi) — Phase I
11.1-13.2 MPa (1612-1919 psi) -- Phase II, and
9.8-11.7 MPa (1416-1702 psi) — Phase III.

Note that the initial large pressure fluctuations in the Phase III test caused by attempts to achieve a specific thermal gradient in the packing are not included.

---

[6]The Fe content was determined by atomic absorption (AA). The Si content was determined by an automated standard colorimetric method using ammonium molybdate reagent. The Cl^- and SO_4^{2-} contents were measured by ion chromatography (IC). This analytical technique gives quantification of ionic species in the sub ppb to ppm range and allows for the analysis of small volumes (≈1 mL) of sample. Precision is normally ±5%, but due to the large amount present in our samples, it was approximately ±2%.

A plot of P/T_1 values versus time should be an indicator of change in the number of moles of gas present in the system and/or the volume that the gas occupies, since $P/T_1 = nR/V$, where R is the gas constant. It is assumed that T_1, the temperature at the autoclave wall, is representative of the average temperature experienced by the gases contained in the autoclave. Figure 5 gives P/T_1 values for the three tests conducted. Fluctuations in the P/T_1 values from the mean are less than ±1 percent and may be due to instrumentation characteristics or small fluctuations in volume. There is a basic trend in the pressure changes during each test involving an initial decrease in pressure over the first 500 h followed by an increase for the remainder of each test. For the Phase I test, this trend is more clearly detected by a magnified P/T_1 scale. Although the pressure at the end of each test never exceeded the initial pressure, it is possible that very long term reaction could lead to monotonic pressure increases.

Reasons for the initial decrease in pressure include consumption of gases such as oxygen and an increase in the void space in the autoclave during a test. Pressure decreases in the Phase I, II and III tests are 0.14, 0.83, and 0.48 MPa (20, 120 and 70 psi), respectively. This would represent a decrease in gaseous oxygen (sorbed or dissolved oxygen will not cause a pressure decrease after reaction) of 100-200 mg. This explanation is not likely since this relatively large amount of free oxygen (i.e. not sorbed or dissolved) would not be present in the test system. A more plausible explanation of the initial pressure decrease is a change in the volume above the packing material. Volumetric increases of only 1%, 7%, and 4% would be needed to account for the observed pressure decrease in the Phase I, II and III tests, respectively. This could be caused by shrinkage of the bentonite during hydrothermal interaction. The increases in pressure observed in the later stages of a test are likely to be partly associated with radiolytic gas generation and/or hydrogen generation by basalt/water interaction (see below).

5.2 Pressure Changes Due to Radiolysis

Any radiolytic effects which result in the production or consumption of gas and associated pressure changes are assumed to occur on (1) the slurry water in the Phase I and II tests, (2) methane as dissolved gas in the water in the Phase II test and (3) methane in the void space in the Phase II test. No radiation-induced structural damage to the bentonite silicate lattice is expected (Krumhansl, J. L., 1982).

5.2.1 Radiolysis of Water in a Closed System

Since we are concerned with the radiolytic products of water in a closed system (constant volume) in the Phase I and II tests, pressure buildup studies at Savannah River Laboratory (SRL) on the irradiation of concrete waste forms in sealed containers have yielded specific conclusions (DP-1464, 1978), which may enable an interpretation of our data to be made on the basis of radiolytic effects on the amount of gas present in the system. In the SRL tests, 500-mL glass bottles containing set cement (with voids in different samples ranging from 125 to 223 mL depending on the amount of cement and water that was added to the bottle) were irradiated at 40-50°C. Both high and low dose rate tests established that the initial production rate of H_2 from the radiolysis of water

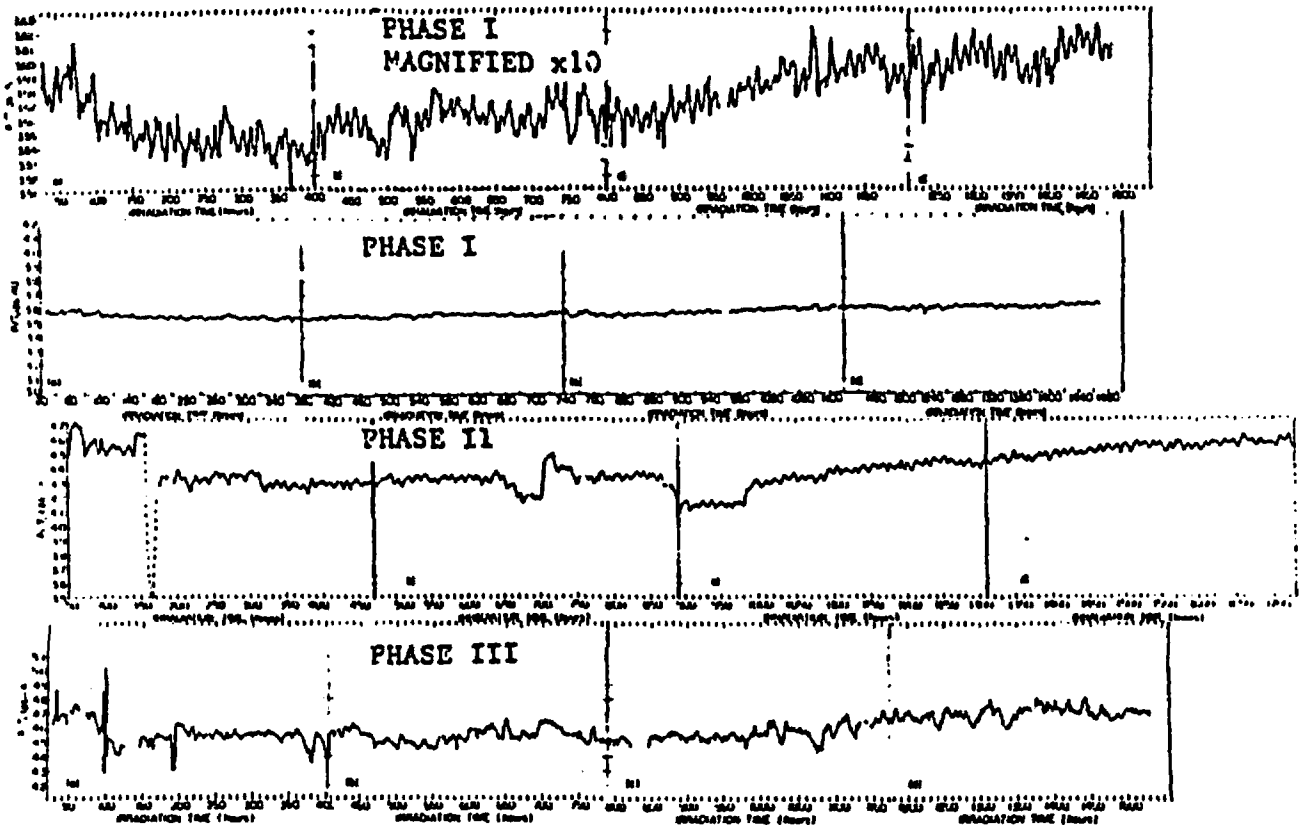

Figure 5. Pressure changes with time and temperature in the autoclave system for the three phases of the experiment: Phase I (absence of methane and presence of radiation), Phase II (presence of methane and radiation), Phase III (presence of methane and absence of radiation.)

was dependent upon the dose rate; but as the H_2 pressure increased, a reaction removing H_2 was initiated and the pressure reached a steady state. This equilibrium pressure was also directly dependent upon the dose rate. The gas volume and the water-to-cement ratio did not affect the pressure attained. Gas composition at the end of the test showed that O_2 content from the air sealed within the concrete was 95% consumed and N_2 content was unchanged. In water containing oxygen, the oxidizing power of the dissolved oxygen is made available by reactions of $e^-(aq)$ and $H^\cdot$ to give O_2^-, which is a powerful oxidizing species. Presumably the consumed oxygen was incorporated in oxidation products. This depletion of oxygen resulted in a 0.014 MPa (≈2 psi) decrease in pressure over a period of 100 days at a constant dose rate (DP-MS-16-51, 1976). See Figure 6 for data on dose rate versus the steady state H_2 pressure.

It is also known that if the radiolysis occurs at a higher temperature, the increase in temperature will lead to an increase in the primary species [i.e. the hydrated electron $e^-(aq)$, the hydrogen atom and the hydroxyl radical OH] and a decrease in the number of molecules (H_2 or H_2O_2) (Draganic, I. G., 1971). It has also been determined that there is no effect of pressure on the yields of primary reducing species, hydrogen atoms, and H_2 (Draganic, I. G., 1971). Thus, we assume that the dose rate is the determinant of the final H_2 pressure from the radiolysis of water. If we chose the largest pressure at the radiation dose of $(3.8 \pm 0.5) \times 10^4$ rad/h, which is what the packing slurry receives in this experiment, this value is less than 0.17 MPa (25 psi) (assuming linear extrapolation) under ambient conditions. For a temperature of 150°C, this would correspond to a pressure of less than 0.24 MPa (35 psi). From the use of the baseline data indicated in Figure 5, it is clear that any increase in pressure due to H_2 production on the order of 0.24 MPa, and any decrease in pressure due to O_2 consumption, will fall within the baseline scatter and will not be observable.

5.2.2 Radiolysis of Methane in Aqueous Solution and in the Gaseous Phase

Gas production and consumption are also affected by the presence of methane in the Phase II test. Methane is the predominant gaseous constituent in the Saddle Mountains and Wanapum basaltic groundwaters, comprising 60 to 98 percent of the total dissolved gas. Methane comprises from <0.01 to 1.6 percent of the total dissolved gas in the groundwater of the Grande Ronde in Boreholes DB-6 and DC-14, but comprises 98 percent of the total dissolved gas in the Grande Ronde groundwater in Borehole RRL-2 (on the order of 10^2 to 10^3 ppm) (NUREG-0960, Vol. 2, 1983).

Methane (99.93%) was used to attain a pressure of 7.4 MPa (1074 psi) at 18.4°C in the Phase II test. The solubility of methane in water at 25°C at 1 atm of methane over-pressure is approximately 21 ppm (Dean, J. A., 1979). The Henry's Law coefficient for methane at this temperature is $\approx 4 \times 10^4$ atm/mole fraction (Himmelblau, D. M., 1960). A calculation using this coefficient gives a concentration of ≈1600 ppm of methane in water at 7.4 MPa pressure. Solubilities at high temperature and high pressure conditions are graphically represented in Figure 7. At 150°C and 10.4 MPa (1500 psi) (see arrows in Figure 7), the solubility is approximately 1500 ppm.

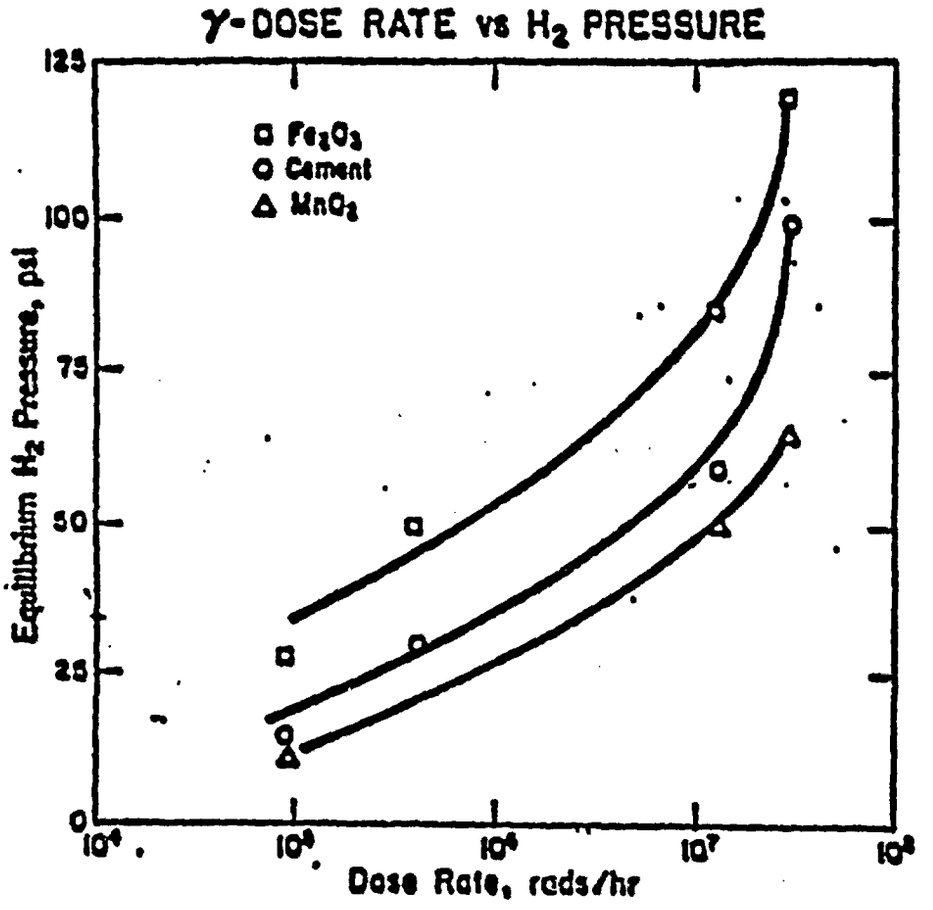

Figure 5. Effect of dose rate on H_2 equilibrium pressures for concrete (neat), concrete containing Fe_2O_3, and concrete containing MnO_2 (DP-MS-76-51, 1976).

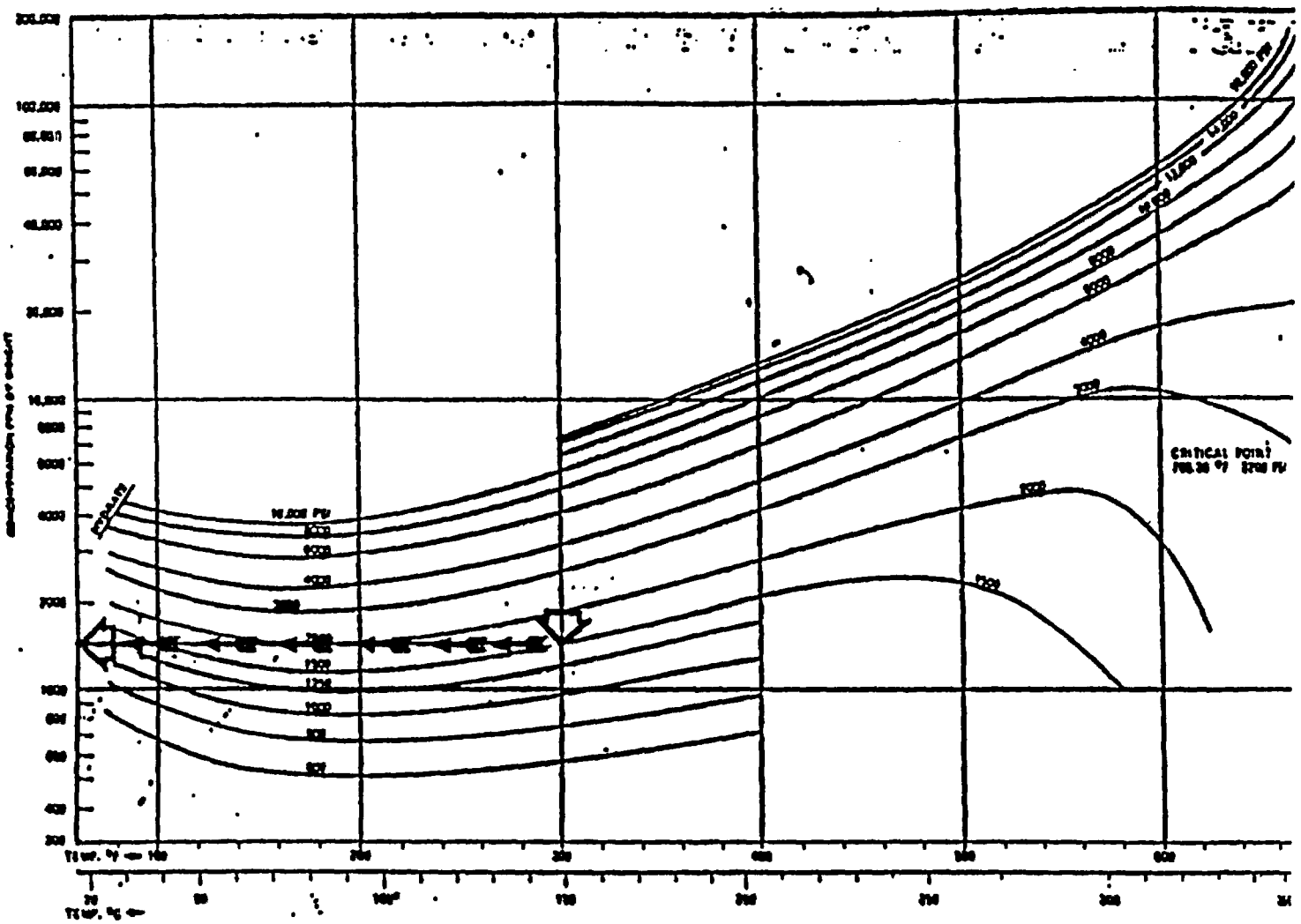

Figure 7. Solubility of methane in water at high temperatures and pressures (Bonham, L. C., 1978).

Results of a study on the gamma radiolysis of aqueous methane solutions (Stevens, G. C., 1972) have indicated that only the OH free radical (from the water radiolysis) reacts with methane to any appreciable extent. Methyl radical is the product of this reaction. Methyl radical then reacts with the radiolysis products of water to yield methane, hydroxyl ion and methanol. It also reacts with another methyl radical to produce ethane. Ethane reacts with the various radicals present in the system to produce ethyl radical, methane and hydrogen. This process could continue as higher alkanes are formed which themselves interact with radicals present in the system to produce hydrogen, ethylene, propane, n-butane, i-butane, n-pentane, i-pentane, neopentane, acetylene, propylene, 1-butene and polymeric type molecules (Arai, H., 1981).

In the BNL tests, gas samples were taken from the autoclave after cooling to room temperature. Detailed data are given in Table 4.

The largest $G(H_2)$ value from the radiolysis of methane in the gas phase and subsequent reactions is 13.26 molecules/100 eV of absorbed radiation (Arai, H., 1981). No $G(H_2)$ value for the aqueous methane solution was reported in the Stevens (1972) study. Although this $G(H_2)$ value is much larger than that obtained for water (0.45), it should be noted that the methane content (≈0.1 mol) in our system is approximately 250 times less than the content of water. Thus, we could estimate that more hydrogen would be produced from the radiolysis of water than the radiolysis of methane. However, as shown in Table 4, more hydrogen was produced in the Phase II test than in the Phase I test.

A valid estimation of the amount of hydrogen produced by the radiolysis of methane is not possible due to the combination of major experimental factors that will affect gas production rates, viz. temperature, pressure, and increased surface area of adsorbent. The presence of other gases initially present in the system and those possibly generated by chemical reactions will also affect the dominant mechanisms in the radiolysis of methane. However, some specific effects from other studies which varied single parameters are summarized as follows:

- The G values for all products are affected by an increase in temperature (Arai, H., 1981). The G values for the formation of n-butane and acetylene decrease with increasing temperature. The G values for the formation of other significant products increase with temperature.

- An increase in pressure causes a decrease in $G(H_2)$ and $G(C_2H_6)$ (Maurin, J., 1962).

- The influence of the basalt/bentonite mixture, due to chemical composition and increased surface area available for reaction, on the production of gases, in combination with the other variables that are present, is not known. Synergistic and/or catalytic effects may be operative. Results from Norfolk (1977) on the gamma radiolysis of methane gas adsorbed on gamma-alumina suggest that methane at the temperature under consideration will react only with radiolytic intermediates derived from surface hydration and that direct energy transfer to the adsorbed methane from the alumina did not occur.

Table 4. Comparison of composition of gases sampled after reaction as determined by mass spectrometry. (Gas composition is given as mole percent.)

Gas	Molecular Weight	Phase I[a]	Phase II[b]	Phase III[c]
H_2	2	3.71	17.6	4.21
CH_4	16	0.019	78.3[d]	91.5[d]
NH_3	17	ND[e]	ND	ND
H_2O	18	0.020	0.028	0.063
CO	28	ND	[f]	ND
C_2H_4	28	ND	ND	0.03
N_2	28	1.00	0.18[f]	0.28
C_2H_6	30	ND	0.43[d]	ND[d]
NO	30	ND	ND	ND
O_2	32	0.027	ND[g]	0.020[h]
H_2S	34	ND	ND	ND
Ar	39.9[i]	95.1	3.04	3.84
CO_2	44	0.12[j]	0.17[j]	0.04[j]
NO_2	46	ND	ND	ND

[a]These values represent compositions averaged from the last two of the three gas samples taken.
[b]These values represent compositions averaged from the fourth and fifth samples of the six gas samples taken.
[c]These values represent compositions averaged from a total of five gas samples taken.
[d]The methane was analyzed and was found to contain 0.07% ethane. On this basis, we would predict that the Phase II test and Phase III test gas analyses would show a maximum ethane content of 0.07%.
[e]ND is an abbreviation for not detected.
[f]Carbon monoxide and nitrogen concentrations are not distinguishable at these low levels.
[g]Minimum detection limit was stated to be 0.017%.
[h]Oxygen was detected in the first two samples out of a total of five samples.
[i]The argon used contains <0.001% oxygen.
[j]Dry air contains by mole percent: 78% N_2, 20.9% O_2, 0.9% Ar, 0.03% CO_2, and 0.2% other gases.

- The presence of other gases initially present in the system and those generated by chemical reactions will also affect the radiolysis of methane. A G value for the depletion of hydrocarbon, G(-hydrocarbon), in a system containing carbon dioxide, carbon monoxide, methane, water and hydrogen has been estimated to be ≈16 (Norfolk, D. J., 1983).

5.3 Gas Analyses Results

5.3.1 Phase I Test Gas Analysis Results

In the Phase I argon-overpressure test, hydrogen, carbon dioxide, and methane were produced and radiolytic and/or adsorbed oxygen was consumed. The source of the nitrogen is assumed to be air remaining after slurry preparation. Some carbon dioxide is also present in the starting slurry, but a source of carbon must be available to account for the presence of methane and additional carbon dioxide. It is known that calcite is present in the bentonite and that the groundwater contains carbonate species. There may also be some organic surface contamination of the basalt that could act as a source of carbon.

5.3.2 Phase II Test Gas Analysis Results

The Phase II test system was pressurized with methane. During the course of irradiation and reaction, hydrogen, ethane, and carbon dioxide are produced and oxygen was consumed overall. A small amount of carbon monoxide may have been produced. There is some residual argon in the system from leak testing and the nitrogen is assumed to be from residual air present in the system.

Work related to the Phase II test has been conducted by PNL (RHO-BW-SA-315P, 1983) on the irradiation of synthetic Grande Ronde (GR-3) basaltic groundwater saturated with methane in the absence of basalt and bentonite at 150°C for 72-hour periods at dose rates ranging from 1.1-5.3 x 10^6 rad/h. The initial methane content of the pressurizing gas used was at least 95%, and the final methane content of the vented gas ranged from 70-85%. This decrease is due to the radiolysis of methane. Hydrogen was produced and its content in the vented gas ranged from 9.9 to 24%. In the Phase II test, the methane content was decreased to ≈78% and ≈18% H_2 was formed. However, different gases and filterable material were produced in the Phase II test than were produced in the PNL work. Carbon dioxide and ethane, and perhaps carbon monoxide, were the only carbon-containing gases found in the Phase II test. In the PNL study, carbon dioxide and higher alkanes, e.g. derivatives of propane and butane, were formed.

The filterable colloidal material in the Phase II test was mainly inorganic and contained 1.8% C, 0.3% H, and <0.03% N. The polymeric solids formed in the PNL work were mainly organic and contained ≈86% C, ≈12% H, and ≈1% O. The extent of polymerization as evidenced by weight-average molecular weights is directly dependent on the dose rate. In the PNL work, the dose rate was three to four orders of magnitude greater and there was no packing material present.

5.3.3 Phase III Test Gas Analysis

During the course of this non-irradiation control test, hydrogen was produced and oxygen was consumed. Small amounts of carbon dioxide may also have been produced. In work performed by Siskind (NUREG/CR-3091, Vol. 3, 1983), gas analyses performed after hydrothermal reaction of packing material at 250°C (in argon and in the absence of irradiation) showed that carbon dioxide, hydrogen, and methane were produced. However, it is not possible to state whether any methane was produced during the Phase III test since this would be masked by the large volume of this gas used for pressurization.

5.3.4 Comparison of Gas Analyses Results

A comparison of the gas compositions from the Phase I, II, and III tests, given in Table 4, results in the following conclusions:

- Hydrogen is produced in all three tests, i.e. in the presence and in the absence of radiation. More hydrogen appears to be produced in the Phase II test, probably as a result of methane radiolysis. Hydrogen in the Phase I and II tests probably forms by basalt/water reactions.

- Since no methane is known to be present in the initial gas composition of the Phase I test, its detection indicates formation during this test. Because methane was used to pressurize the Phase II and Phase III test systems, it is difficult to determine whether any methane was produced. However, there is less methane remaining at the end of the Phase II test when compared to Phase III. This difference may be attributable to the radiolysis of methane which would explain the relatively large volume of hydrogen in Phase II.

- There is more nitrogen present in the gas at the end of the Phase I test than for the other two tests. This difference is indicative of the change in pressurization techniques after the Phase I test (see above).

- Oxygen was detected in the Phase I and III gas samples. The concentrations of 0.027 and 0.020 percent, respectively, correspond to partial pressures (at 6.9 MPa, 1000 psi) of 0.018 atm (0.27 psi) and 0.014 atm (0.20 psi). Using a Henry's Law coefficient of 5×10^4 atm/mole fraction from Figure 8, these oxygen partial pressures give the following DO levels: 0.6 ppm (Phase I) and 0.5 ppm (Phase III). See Section 5.4 for measured values.

- Carbon dioxide in amounts exceeding that in dry air (i.e. 0.03%) was found in all three tests.

5.4 Measurement of pH and DO and Calculation of Eh

5.4.1 Measurement of pH and Dissolved Oxygen of Unreacted Packing Material Slurry

The pH electrode was calibrated with buffer solutions having pH values of 2, 7, and 10. The accuracy of the pH measurement is ±0.05 units. Prior to testing, the pH in the bentonite/basalt packing material was determined to be 8.14 at mid-depth and 7.84 at the bottom of the beaker containing the mixture.

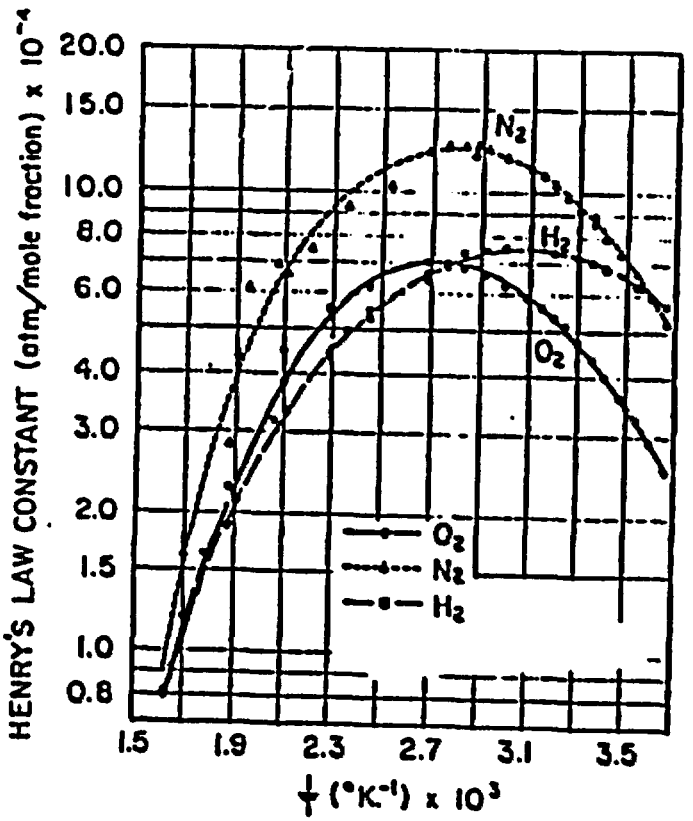

Figure 8. Solubilities of O_2, N_2, and H_2 in water as a function of temperature (Himmelblau, D. M., 1960). Note that the solubility of O_2 goes through a minimum near 100°C.

The DO electrode was calibrated against the DO content of water at 25°C, which is 8.4 ppm. The DO of the starting bentonite slurry without basalt was found to be 8.3 ± 0.5 ppm. It was concluded on the basis of obtaining this 8.3 ppm value that readings are not affected by the presence of a solid phase. After the addition of basalt to the slurry, DO was measured near the surface and at mid-depth, at three locations. Results for the near-surface measurements ranged from 4.1 ppm to 6.5 ppm, with an average value of 5.4 ppm. Results for the mid-depth measurement ranged from 2.8 ppm to 3.7 ppm, with an average value of 3.2. It is clear that the DO content of the bentonite/basalt

slurry is reduced by basalt/water interaction. The wide range of results obtained in the DO values led to uncertainty in the accuracy of the measurements. Accuracy is taken to be ±0.5 ppm based on DO measurements on a solution prepared to contain zero dissolved oxygen (Method 421F, A. Greenberg, 1980).

5.4.2 Measurement of pH and Dissolved Oxygen of Reacted Packing Material Slurry

The following general procedure was used for each of the three tests: The autoclave was opened and kept in a glove bag filled with argon. The pH and DO measurements were made, almost immediately, at several depths in the slurry near the heater and near the autoclave wall. It was felt that these in situ measurements would be most representative of the conditions achieved during a test. It should be noted, however, that autoclave depressurization forces gases such as carbon dioxide and oxygen out of solution and causes the pH reading to be higher and DO to be lower than those under the pressurized condition. The use of these measurements after decompression in the calculation of the Eh would, therefore, result in a more reducing value.

5.4.2.1 Measurement of Phase I Test pH and Dissolved Oxygen and Eh Calculation

In the irradiated Phase I test, pH values near the heater increased from 6.84 to 6.92 as the depth of measurement increased. The three pH values obtained averaged 6.88. Near the autoclave wall, the pH was found to be 7.16 near the surface of the slurry, 6.73 in the middle and 6.88 near the bottom. These pH values averaged 6.92. If the average pH value at the heater is compared to the average pH value at the wall, there does not appear to be a significant difference across the thermal gradient. The average pH of the Phase I test irradiated system was, therefore, taken to be 6.90 in the Eh calculations described below.

Dissolved oxygen measurements taken near the heater gave values of 0.64 ppm near the surface, and 0.56 ppm at a depth of approximately 5 cm. For measurements near the autoclave wall, the DO was found to be 0.70 ppm near the surface and 0.52 ppm at a depth of approximately 5 cm. These values may be compared to the average of 3.2 ppm for a system containing only bentonite, basalt, and synthetic groundwater and open to the air. There is significantly less DO in the reacted system which is probably due to reaction with various system components, i.e. packing and carbon steel, during irradiation to form corrosion products and colloids. However, there does not seem to be a significant difference between the DO content across the thermal gradient. The average DO content of the Phase I irradiated system was taken to be 0.6 ppm for the Eh calculation given below.

It has been speculated by BWIP that the environment in a basalt repository will be sufficiently reducing to inhibit corrosion of the carbon steel. Reducing conditions, however, were not achieved in the Phase I test based on the following calculation of Eh. The Eh was calculated using the experimental DO

and pH results from the following equation (DOE/RL 82-3, Vol. II, 1982)[7] for a temperature of 24°C (297.2°K) to compare with BWIP estimates:

$$Eh\ (V) = 1.23 + 0.0147 \log fO_2 - 0.0590\ pH + 0.000136.$$

If we assume that the pressure exerted by the dissolved oxygen on the system is equivalent to the fugacity of oxygen needed as input to the equation and that the use of this oxygen pressure rather than the oxygen overpressure (1670 Pa)[8] leads to a smaller value for fO_2, then the fugacity is calculated to be 46.3 Pa by use of the Ideal Gas Law, based on a DO content of 0.6 ppm (1.875×10^{-8} mol/mL)[9]. Accordingly, the Eh is +0.85 V, indicating that an oxidizing environment existed in the Phase I test after quenching the autoclave.

5.4.2.2 Measurement of Phase II Test pH and Dissolved Oxygen and Calculation of Eh

Measurements for the Phase II test were similar to those for Phase I. Adjacent to the heater, the pH was 6.62 near the surface of the slurry, 6.52 in the middle, and 6.68 near the bottom, with an average value of 6.61. Adjacent to the wall, the pH was 6.53 near the surface of the slurry, 6.49 in the middle, and 6.70 near the bottom, with an average value of 6.57. Although there

---

[7] The total range of Eh values for the Middle Sentinel Bluffs and Umtanum flows from 51°C to 300°C was estimated to be -0.54 to -0.37 V (DOE/RL 82-3, Vol. II, 1982). The equation used to calculate Eh should be applicable at a temperature of 24°C, because the equations for pH and fO_2 used in the derivation are valid at this temperature (Equations II-6 and II-16, DOE/RL 82-3, Vol. II, 1982).

[8] By use of the Henry's Law coefficient for oxygen at 25°C ($=5 \times 10^4$ atm/mole fraction), it was calculated that an overpressure of 0.0165 atm of oxygen is needed to sustain an oxygen solubility in water of 0.6 ppm (The mole fraction of oxygen was calculated to be 3.3×10^{-7}.) The amount of oxygen overpressure expressed as a volume per cent of the mixture of gases at 1000 psi (68 atm) is 0.024%, which is very close to the measured oxygen content of the gas vented after quenching. It should be noted that an oxygen content of 0.2 ppm in water at 25°C would require an overpressure of 0.0055 atm of oxygen, which would constitute 0.008% of a gas mixture at 68 atm, and which would be below the mass spectrometric detection limit for oxygen of 0.017%.

[9] The compressibility factor of oxygen at 1 atm of oxygen and 300 K is 0.9994, indicating that oxygen behaves as an ideal gas under the conditions for which fugacity is calculated (Braker, W., 1980). It is interesting to also note that the compressibility factors (Z) for 100 atm of methane and 100 atm of argon at 300 K are 0.8493 and 0.9553, respectively. At higher temperatures, the values for Z increase and approach 1.0000, indicating more ideal behavior of methane and argon.

does not seem to be a significant change in pH across the thermal gradient, there does appear to be a significant change in pH with depth. The pH of the Phase II test for the purpose of Eh calculations will be taken as 6.60.

Near the heater, the DO was 0.21 ppm near the surface of the slurry and 0.22 ppm at a depth of approximately 5 cm. The DO near the autoclave wall was 0.16 ppm at similar depths. There does not appear to be a significant change in DO across the thermal gradient. The value of DO for Eh calculations will be taken as 0.2 ppm.

The Eh was calculated to be 0.86 V using the values for pH and fugacity of oxygen of 15.4 Pa (based on a DO of 0.2 ppm).

5.4.2.3 Measurement of Phase III Test pH and Dissolved Oxygen and Calculation of Eh

Adjacent to the heater, the pH was 7.10 near the surface of the slurry, 7.05 in the middle, and 7.28 near the bottom, with an average value of 7.14. Adjacent to the wall, the corresponding pH values were 7.03, 7.02 and 7.06, respectively, with an average value of 7.03. There does not appear to be a significant difference in pH as measured across the thermal gradient. The pH measured at 24°C is taken to be 7.10.

Near the heater, the DO was 0.6 ppm near the surface of the slurry and 0.5 ppm at a depth of approximately 5 cm. The DO near the autoclave wall was 0.4 ppm at similar depths. The DO content does not vary significantly across the thermal gradient. The average DO content in the test is taken to be 0.5 ppm.

Using the equation cited above, the Eh (after quenching) was calculated to be 0.83 V.

5.4.3 Comparison of pH and DO Measurements and Eh Calculations for All Tests

The pH and DO data for the three tests along with the calculated Eh values after quenching are summarized in Table 5.

The unreacted slurry components are basic in contrast to the reacted slurries. The latter are either slightly basic (the non-irradiated Phase III test) or slightly acidic (the irradiated Phase I and Phase II tests). Comparison of the DO data for the reacted (closed system) and unreacted (open system) shows that there is approximately an order of magnitude difference in the DO levels. The addition of basalt in an open system reduced the DO content and it was further reduced in the irradiated and non-irradiated tests. Within the accuracy of the measurements, there is no obvious difference in DO content among the three tests. The calculated Eh values show a more oxidizing environment in the closed reacted systems than in the open unreacted systems, due to lower pH values in the closed reacted system. It would appear that radiation does not significantly affect the Eh of the system under consideration.

Table 5. pH and DO as measured for packing material slurry and Eh as calculated for all tests.

	pH[a]	DO (ppm)[b]	Eh (V)[c]
Phase I test slurry	6.9 ± 0.05	0.6 ± 0.5	0.85 ± 0.01
Phase II test slurry	6.6 ± 0.05	0.2 ± 0.5	0.86 ± 0.01
Phase III test slurry	7.1 ± 0.05	0.5 ± 0.5	0.83 ± 0.01
Unreacted bentonite slurry	8.7 ± 0.05	8.3(mean) ± 0.6(2σ)	0.76
Unreacted bentonite + basalt slurry	8.0(mean)	4.3(mean) ± 3(2σ)	0.79
Unreacted groundwater	9.7 ± 0.05	8.4	0.70

[a]These reported pH values represent the average of six readings made with a pH electrode which was calibrated with buffer solutions having pH values of 2, 7, and 10. The accuracy of the pH measurement is 0.05 units.
[b]The reported DO values represent the average of four or more readings. Accuracy is taken to be 0.5 ppm. The DO electrode was calibrated with the oxygen content of water at 25°C, which is 8.4 ppm.
[c]These Eh values are calculated based on the pH and DO measurements of the slurry at 24°C.

5.5 Measurement of Ionic Concentrations in Slurry Water

It was considered important to measure the concentrations of ions particularly associated with the corrosion of carbon steel and to determine whether significant differences occurred across a thermal gradient. Therefore, the concentrations of Cl^-, Fe(total), and SO_4^{2-} in W samples (filtered) and H samples (filtered) were measured as detailed in the experimental section. These concentrations in R samples (unfiltered) were also measured to determine differences in content between filtered and unfiltered samples. The concentration of Si, reported as SiO_2, was also determined but only for the Phase I test samples. Results of these analyses are summarized in Table 6 and uncertainties are given wherever they are known. However, it must be emphasized that these are the results of one analysis on single samples after quenching has

occurred[10]. Any conclusions derived from these data would have to be supported by valid experiments that have eliminated any effects due to quenching. Therefore, these results should be regarded only as indications of possible differences in ionic concentration across a thermal gradient.

Table 6. Comparison of ionic concentrations of reacted Grande Ronde GR-3 groundwater (in ppm).

Sample	Cl^-	SO_4^{2-}	Fe(Total)	SiO_2
GR-3 (initial composition)	312	165	0	79
Sample H-I (filtered)[a]	305±6	260±5	ND(<2)	29
Sample W-I (filtered)[b]	321±6	300±6	ND(<2)	39
Sample R-I (unfiltered)[c]	357±7	330±7	500±100	116
Sample H-II (filtered)[d]	263±5	220±4	1.4	—
Sample W-II (filtered)[b]	328±7	272±5	0.9	—
Sample R-II (unfiltered)[c]	—[d]	330±7	700±140	—
Sample R-II (filtered)[c]	177±3	145±3	2.4	—
Sample H-III (filtered)[a]	388±8	204±4	0	—
Sample W-III (filtered)[b]	429±9	258±5	1.0	—
Sample R-III (unfiltered)[c]	—[d]	345±7	500±100	—
Sample R-III (filtered)[c]	368±7	200±4	2.5	—

[a]Sample H is the designation for the supernate of the centrifuged slurry removed from the heater region in the autoclave. Experimental phases are designated by Roman numeral I, II or III.
[b]Sample W is the designation for the supernate of the centrifuged slurry, removed from the wall region in the autoclave.
[c]Sample R is the designation for the supernate of the centrifuged slurry removed from random locations in the autoclave.
[d]Insufficient sample remained for this analysis to be performed.

[10]Evidence exists (RHO-BWI-C-105, 1981) that the state of leachates under hydrothermal conditions is not completely preserved in quench rates of ≈25°C/min. Experiments conducted on the interaction of seawater and basalt (Seyfried, W. E., 1979) at 150°C showed that significant retrograde changes occurred in ionic concentrations and pH measurements after a quenching period of 45 minutes. Approximate cooling time for all tests in the current study was 25 minutes.

5.5.1 Measurement of Ionic Concentrations in Phase I Test

The concentrations of Cl^-, SO_4^{2-} and Si were greater near the cooler end (the wall) of the thermal gradient which was at approximately 113°C. The change in concentration of Cl^- across a thermal gradient may be significant. However, the difference in concentration of SO_4^{2-} across the gradient does seem significant, based on these single measurements. It is not known whether the Si concentrations are significant, since the precision is not known and they are an order of magnitude smaller than the Cl^- and SO_4^{2-} concentrations. Comparison of these ionic concentrations with those measured in the synthetic groundwater (see Table 6) reveals a decrease of Si and an increase of SO_4^{2-} in the filtrates. If any Fe was present in the filtrates, it was in amounts <2 ppm, the detection limit of the analysis. Total iron in Sample R-1 was determined quantitatively after acidification of the unfiltered liquid with HF. It was also determined that a significant portion of the total Fe was in the ferrous state (Fe^{2+})[11].

It appears that the bulk of the Fe and Si content of the unfiltered water is present in the colloidal state. This is also reflected by relatively low concentrations of Si and below detection for Fe in filtered samples. The filterable material appears to be acting as a sink for iron, the source of which can be the basalt, bentonite, or carbon steel.

5.5.2 Measurement of Ionic Concentrations in Phase II Test

The only measurements that appeared to change significantly across the temperature differential of ≈22°C were the concentrations of SO_4^{2-} and Cl^-. Concentrations were lower at the hotter end of the gradient, i.e. near the heated carbon steel sleeve.

From the results of these single determinations, it appears that less Cl^- and more SO_4^{2-} than are present in the starting groundwater would be found near the carbon steel sleeve. It is clear that, for the Phase I test results, the bulk of the Fe content of the unfiltered supernate is present in the colloidal form. However, very small amounts of iron remain in the filtered supernates.

5.5.3 Measurement of Ionic Concentrations in Phase III Test

As was the case in the previous tests, concentrations of Cl^- and SO_4^{2-} were significantly lower at the hotter end of the gradient. Again, the bulk of the iron is present in colloidal material.

---

[11] The Fe^{+2} content was estimated using the phenanthroline standard method. Three molecules of 1,10-phenanthroline chelate each atom of ferrous ion to form an orange-red complex. The intensity of the color is dependent on the amount of ferrous ion present. A visual comparison with color standards was made to determine content of ferrous ion. Another portion of Sample R was treated to convert any ferric ion to ferrous and another phenanthroline complexation determination was made. The color of the reduced solution was very similar to that of the first determination, indicating that most of the iron was in the ferrous state in the original sample.

5.5.4 Comparison of Measured Ionic Concentrations For All Tests

The results of the water analyses for Fe(total), Cl^-, and SO_4^{2-} from the three tests were summarized in Table 6. There were different thermal differentials established across the packing materials in each test. For Phases I, II and III, these were, respectively, 1.0, 0.6 and 2°C/mm. Results from the three tests, therefore, cannot be quantitatively compared. However, qualitative differences among ionic concentrations are noted for the three tests. It must be emphasized that these results are from the analyses of single specimens from individual tests. Therefore, in the absence of statistical information, a difference is deemed significant if one measured value differs from another by a quantity that exceeds the experimental error. Experimental precision is indicated in the table where it is known. The results for the chloride and sulfate concentrations are based on IC measurements and are estimated to vary by ±2%. On this basis the following conclusions can be drawn by comparing and contrasting the ionic concentrations measured in the three tests after quenching:

- Compared to unreacted groundwater, the chloride content of filtered reacted water is usually decreased in hotter regions of the packing material and increased in cooler regions. The exception occurred in the Phase III control test where increases in chloride level were evident for both the hotter and cooler regions. Nevertheless, there was still the same general behavior in terms of higher chloride in the cooler regions.

- Compared to unreacted groundwater, the sulfate content of filtered reacted water is always increased. The increase is larger in the cooler regions of the packing material.

- For unfiltered reacted groundwater the concentrations of chloride, sulfate, and especially SiO_2 and total iron, are significantly increased. This shows that the colloidal particles present in the groundwater contain relatively high concentrations of these three constituents.

- In terms of the effect of thermal gradients on the concentration differences across the packing it was found that chloride and sulfate differences were largest for the Phase II test, which had the smallest thermal gradient. These concentration trends were very similar for Phase I and Phase III even though the temperature differentials across the packing were quite different (viz. 37 and 73°C, respectively). It is, therefore, unclear what factors controlled the changes in concentration along the thermal gradient.

Similar increases in chloride concentrations were reported by Wood (RHO-BW-SA-219P, 1983), who studied changes in ionic concentrations with time for closed non-irradiated systems containing Umtanum basalt (free of fines) or Baroid National Western[12] bentonite and GR-3 synthetic groundwater at 300°C

[12]The Baroid bentonite contained 85% montmorillonite, 5% quartz, 5% feldspar, 2% illite, and 1% calcite and gypsum.

and 29.9 MPa for one month. However, in Wood's work, the sulfate concentration was lower in the reacted bentonite/groundwater system and was unchanged in the reacted basalt/groundwater system. This would seem to indicate that for these particular systems basalt and bentonite are sources of chloride and that the bentonite can act as a sink for sulfate. An additional experiment containing bentonite/basalt/groundwater reacted under the same hydrothermal conditions for three months showed that sulfate concentration was slightly increased at 28 days and was significantly decreased at the 56-day sampling. In the same test, chloride concentration increased and reached a maximum between 28 and 56 days.

Also, in Wood's study it was found that the iron concentrations in reacted groundwater were highest in the bentonite/water system (up to 0.14 ppm) and similar for basalt/water and basalt/bentonite/water systems (up to 0.08 ppm). This indicates that bentonite is a prime source of iron in the water. In another study, carried out at a 200°C test temperature, a basalt/water system gave a reacted water containing 35.4 ppm of iron after 718 hours (RHO-BW-ST-21P, 1982). The trend to higher total iron concentrations, as the test temperature is decreased from 300 to 200°C, is evident from Wood's work. In the BNL study, however, much of the iron originated from the carbon steel present in the system and iron was present in colloidal form which was not reported as present in Wood's work.

5.6 SEM-EDX Analysis of Colloidal Material

A part of R sample from each of the tests was passed through a 0.025-μm membrane filter to collect colloidal material for analysis. The latter was removed as a film from the filter when it dried. They were mounted with epoxy on a graphite holder and examined by SEM-EDX (17-kV electrons). It should be noted that comparatively less colloidal material was extracted from the Phase III (non-irradiated) test.

5.6.1 SEM-EDX Analysis of Colloidal Material Removed From Phase I Test Solution

A micrograph of the dried colloidal material film from the Phase I test is given in Figure 9. A rod-shaped phase and a small rectuangular particle are seen to be embedded in the colloidal material. SEM-EDX analyses given in Figures 10 through 12 show that the colloidal material is rich in Si, Fe, Ca and Al with smaller quantities of Mg and K. The rod-shaped phase also contains Si with significant amounts of Mg, Ca, Ba, Zn K and Al present. In the case of the small particle, the dominant element detected is Ca with a minor proportion of Si. The colloidal material substrate in Figure 9 has an elemental composition consistent with that for clay particles, as expected (Table 1). The small calcium-rich phase is possibly calcite which has been found in bentonite by other workers (ANL-83-19, 1983). At the present time, the identification of the rod-shaped phase is unknown. Zinc has been observed in small crystals found in bentonite (ANL-83-19, 1983) but this phase could have also originated from the basalt component of the packing material. More work is needed to characterize the colloidal material obtained from the current studies.

An interesting effect was observed as the colloidal material was bombarded with 17-kV electons in the SEM as shown in Figure 13. Small protuberances developed in the sample film which could have been caused by vaporization of residual moisture.

5.6.2 SEM-EDX Analysis of Colloidal Material Removed From Phase II Test Solution

Micrographs of the dried colloidal material recovered from the Phase II test heater and wall regions are shown in Figures 14 and 15. Both of these samples were analyzed by EDX and were found to be high in Si and Al along with some Fe and Ca. This is similar to the composition determined by EDX for the Phase I test material, except that no K or Mg was detected (see Figure 10).

However, several differences are evident upon comparison of the two micrographs taken at the same magnification. The material from the heater region is much coarser in texture. This may be due to different thicknesses of material deposited on the filter. Additionally, there is a dendritic structure lying on the substrate in the material taken from the wall region (see Figure 15). The structure was analyzed by EDX and found to contain large amounts of Ca and S. See Figure 16 for a micrograph taken at alower magnification (300X) of the material recovered from the heater region in the Phase II test. Analysis by EDX of the nodule present shows a high content of Ca, S and Si along with some Al.

5.6.3 SEM-EDX Analysis of Colloidal Material Recovered from the Phase III Test Solution

Micrographs of the colloidal material recovered from the heater and wall regions of the Phase III control test are shown in Figures 17 and 18. Corresponding EDX analyses for these materials are given in Figures 19 and 20. Both have essentially the same composition: high Si and Al content with moderate Fe and Ca amounts along with some trace elements. No differences in composition were noted for localized variations in substrate texture. Additionally, the presence of oxygen was confirmed in the sample taken from the wall region by use of transmission electron microscopy (TEM)-EDX (see Figure 21). The dried sample taken from the heater region was too thick to permit an analysis by TEM-EDX.

5.6.4 Comparison of SEM-EDX Analyses of Colloidal Materials

A comparison of the information gained by use of SEM-EDX techniques in the three test systems yields the following conclusions:

- The bulk composition of all colloidal materials, from both the wall and heater regions, is essentially the same. There is a high Si and Al content, some Ca and Al, along with trace elements. Oxygen is believed to be present in all samples but was only confirmed by TEM-EDX in the colloidal material taken from the wall region of the Phase III test.

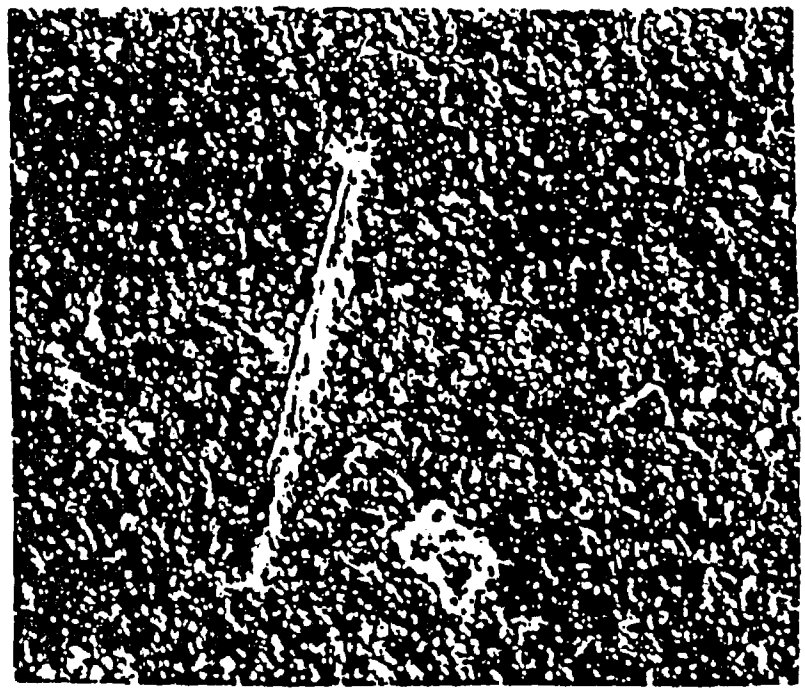

Figure 9. Micrograph of colloidal material recovered from the Phase I test (800X).

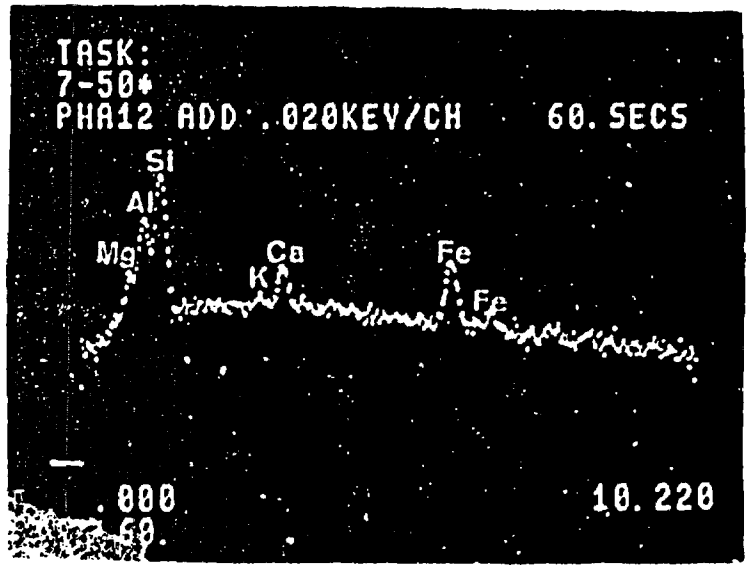

Figure 10. EDX analysis of colloidal material recovered from the Phase I test.

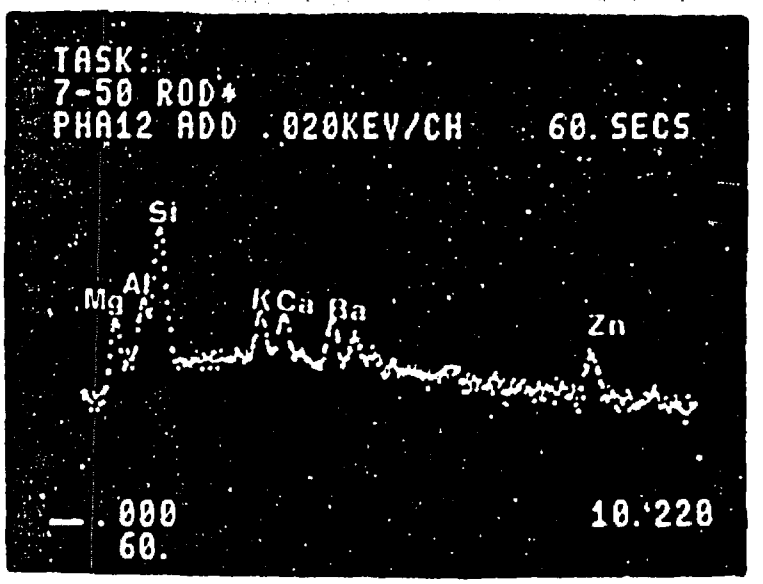

Figure 11. EDX analysis of rod in colloidal material recovered from the Phase I test.

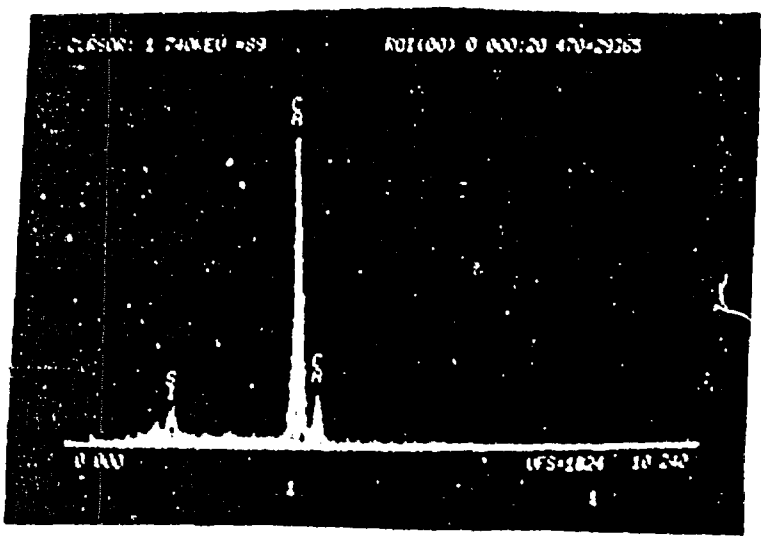

Figure 12. EDX analysis of crystal in colloidal material recovered from the Phase I test.

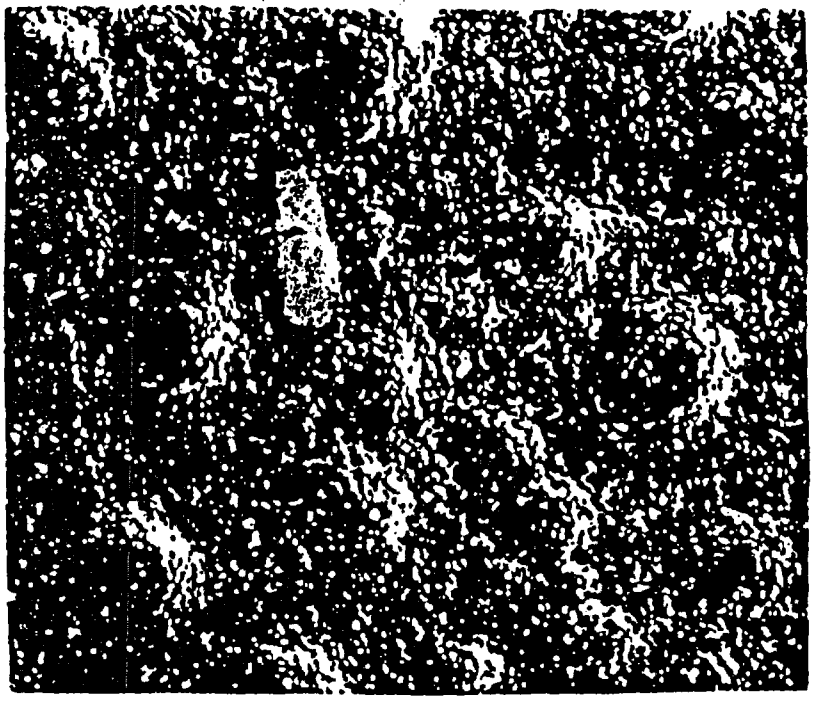

Figure 13. Micrograph of protuberances appearing in colloidal material recovered from the Phase I test after bombardment with 17-kV electrons (1000X).

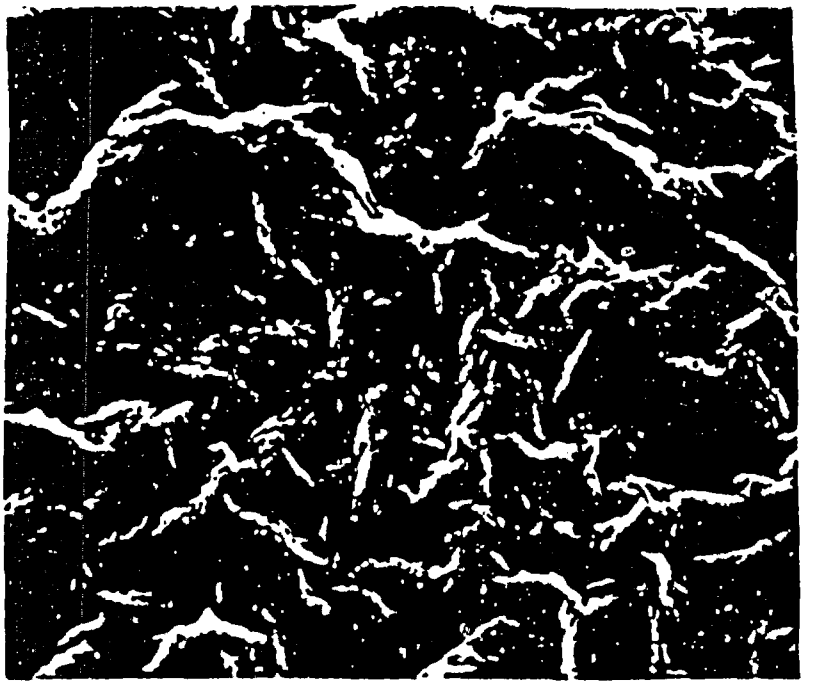

Figure 14. Micrograph of colloidal material recovered from the Phase II test heater region (1000X).

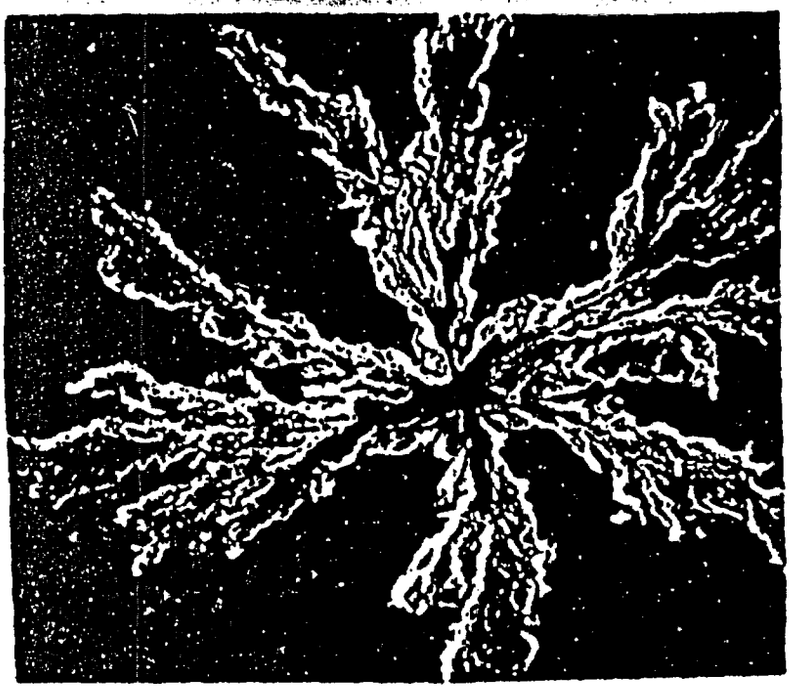

Figure 15. Micrograph of colloidal material recovered from the Phase II test wall region (1000X).

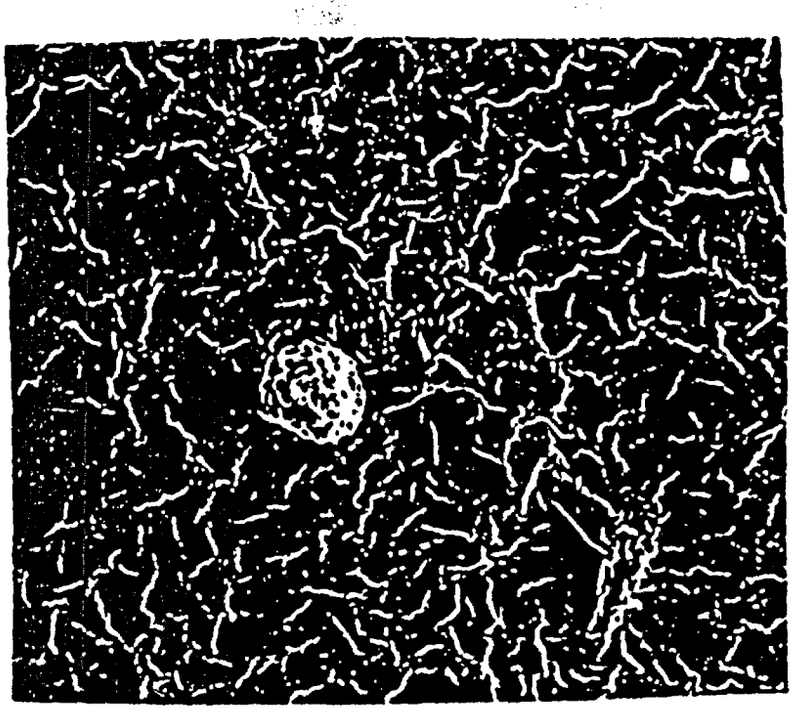

Figure 16. Micrograph of colloidal material recovered from the Phase II test heater region (300X).

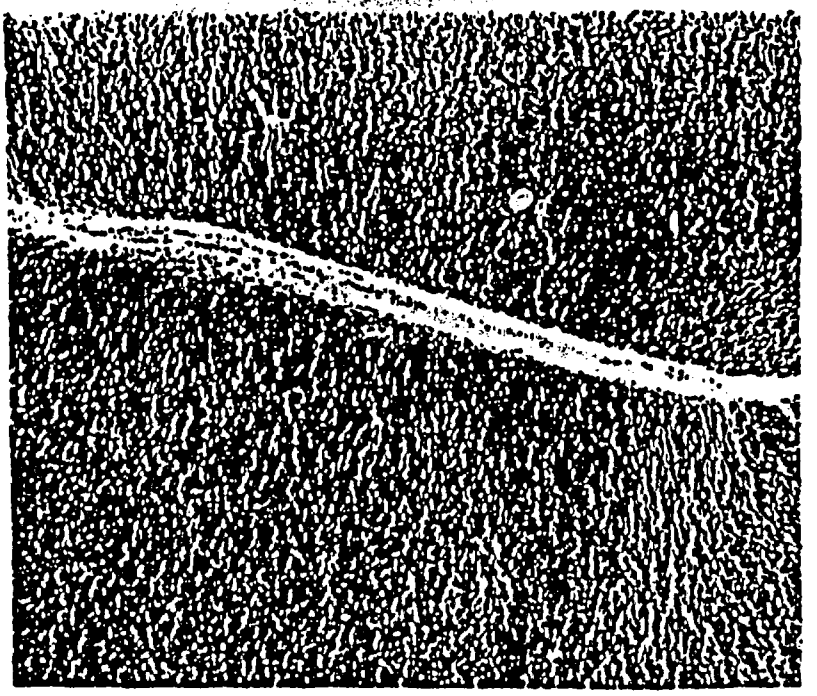

Figure 17. Micrograph of the colloidal material recovered from the Phase III test heater region (100X).

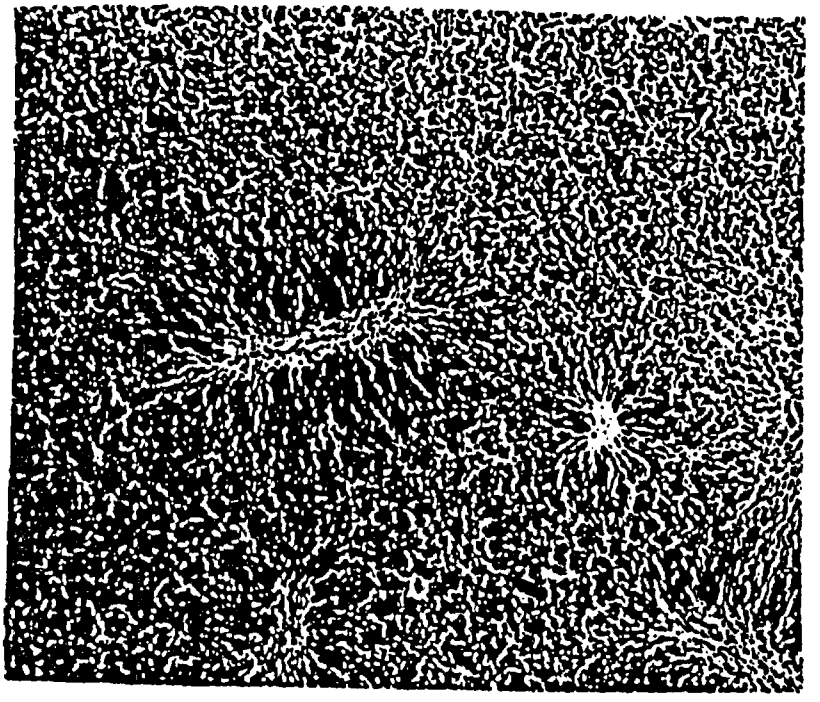

Figure 18. Micrograph of the colloidal material recovered from the Phase III test wall region (100X).

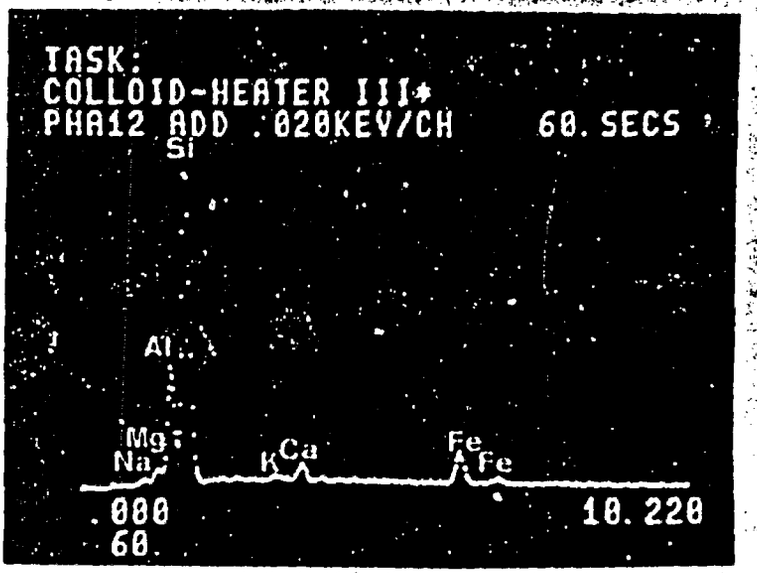

Figure 19. EDX analysis of colloidal material recovered from the Phase III test heater region.

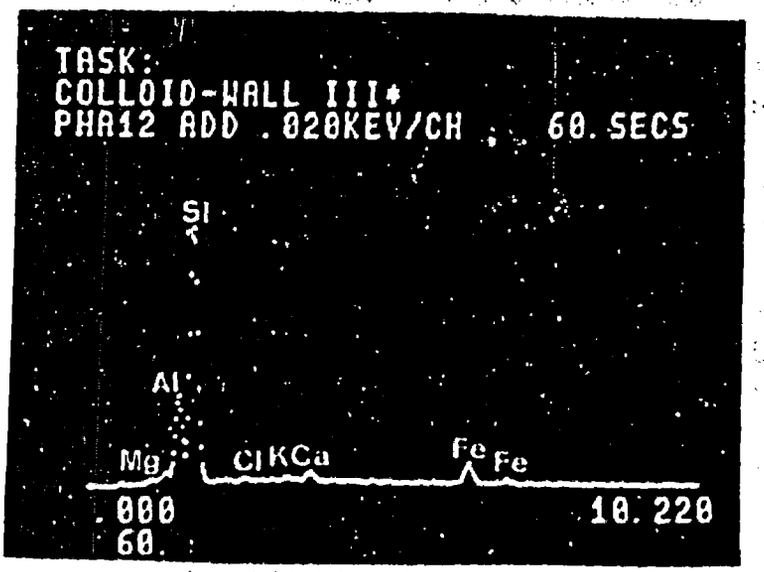

Figure 20. EDX analysis of colloidal material recovered from the Phase III test wall region. The presence of oxygen was confirmed by EDX, see Figure 21.

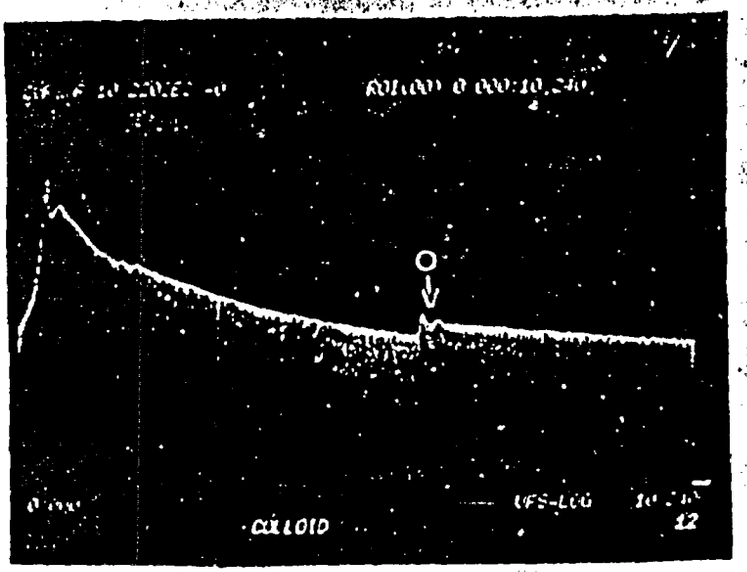

Figure 21. EDX(TEM) analysis of colloidal material recovered from the Phase III test wall region.

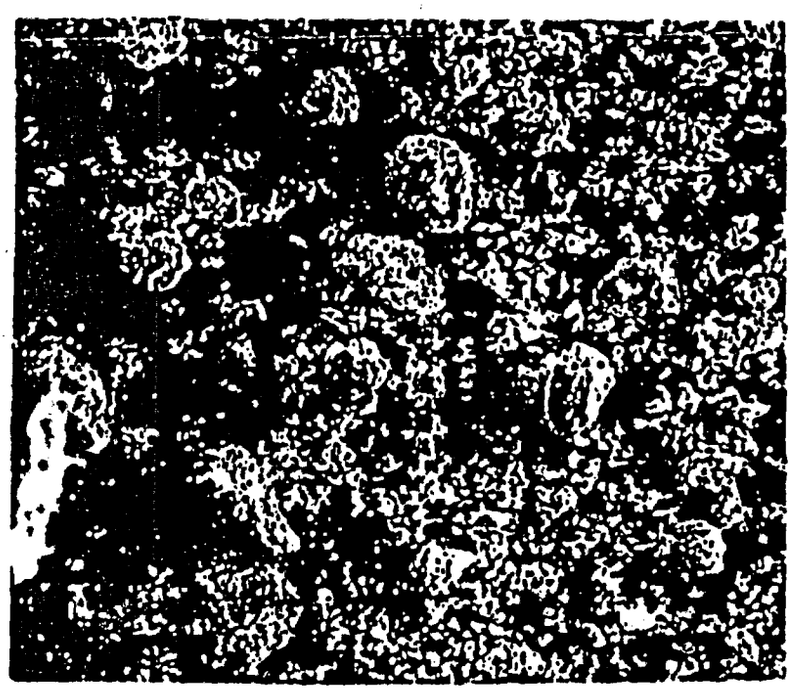

Figure 22. Micrograph of unreacted bentonite clay (100X).

- o A variety of embedded and deposited phases that differ in shape and composition can be seen in the micrographs of the colloidal material recovered from the Phase I and Phase II tests. None of these was seen in the colloidal material recovered from the Phase III test. This indicates that radiation plays some role in the formation of these phases.

5.7 Analysis of Unreacted Bentonite and Reacted Bentonite Portion of Slurry

5.7.1 Analysis of Bentonite

A micrograph of unreacted SWy-1 bentonite is given in Figure 22. The semi-quantitative EDX analysis shows that the following elements were present at two locations in the sample: Si (≈75%), Al (≈15%), Fe (≈6%), 4% (Mg, K, Ca, V, Na, Cu, Zn, Ti).

Reacted bentonite portions of the packing material were centrifuged, and the solid placed on a glass slide and allowed to dry. There were no basalt pellets in any of these specimens. They were examined with an X-ray diffractometer in the range $2\theta = 3\text{-}37°$ using Cu K_α radiation and the resulting patterns are shown in Figures 23, 24, 25. The 2θ values were converted into d-spacings using standard tables (Rose, A. J., 1957). A comparison is given in Table 7. It is clear that differences exist in the d-spacings of the Phase I, Phase II and Phase III test samples. For illustrative purposes, the materials remaining after centrifugation and removal of the supernatant liquid in the Phase I test are shown in Figure 26. This appearance is similar to those for materials from the Phase II and Phase III tests. Samples from near the heater (Tubes A and D in Figure 26) were a combination of orange, white and tan in color. Material samples near the wall (Tubes B and E in Figure 26) was mostly tan and white in color. A tube of unreacted slurry (Tube C in Figure 26) was centrifuged for comparison purposes and was tan in color. See Section 5.8.1 for the results of solids analysis performed in the study by Wood (RHO-BW-SA-219P, 1983).

5.7.2 Analysis of Montmorillonite Portion of Bentonite

The major peaks attributable to the montmorillonite in the control samples appear in the range $2\theta = 7.1$ ($d = 12.4$ Å) to $2\theta = 7.8$ ($d = 11.3$ Å). These single peaks are shown for Phase I, Phase II and Phase III test samples in Figures 27b, 28b and 29b, respectively. These peaks shift in the reacted, glycolated, and heat-treated slurry samples.

5.7.2.1 Montmorillonite XRD Phase I Test

The two reacted samples in the Phase I test gave very similar results but the strongest peak obtained was significantly shifted compared to the equivalent peak for the control, which may indicate that the incorporation of a large cation in the interlayer sites occurred and that the distance between successive layers of the smectite (i.e. basal spacing) increased due to swelling. There is some illite present in the samples before and after reaction, as evidenced by the peak at $\approx 2\theta = 9°$ ($d \approx 9.9$ Å). See the last three columns of Table 8 for a tabulation of these data.

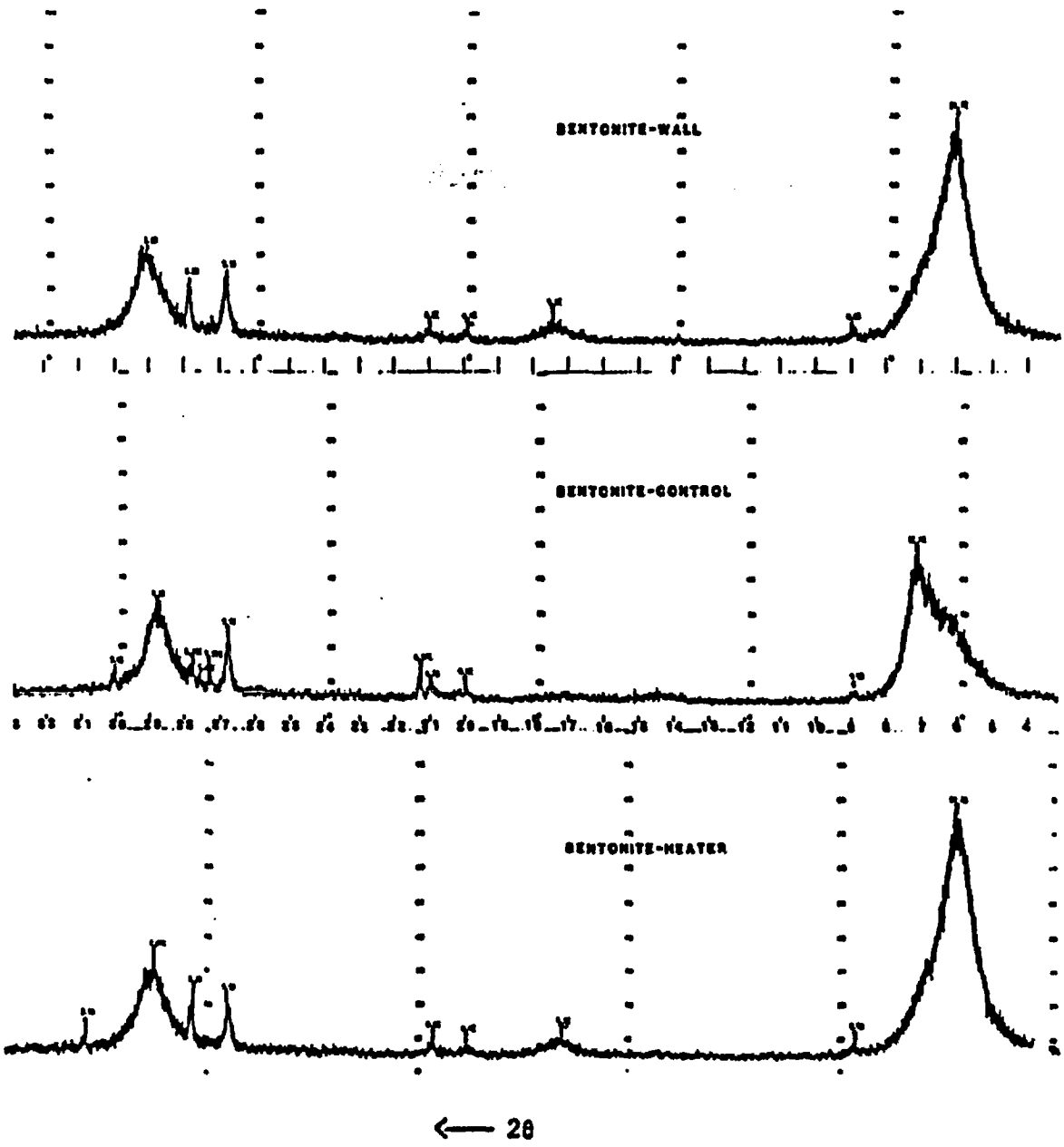

Figure 23. Comparison of X-ray diffraction patterns of reacted and unreacted bentonite present in the Phase I centrifuged packing material slurry samples prepared as oriented clay mounts by evaporation of slurry on glass slides. [Range of scan: 2θ = 3-37° (d = 2.43-29.4 Å).] (Control sample consisted of a slurry of bentonite and basalt with synthetic groundwater.)

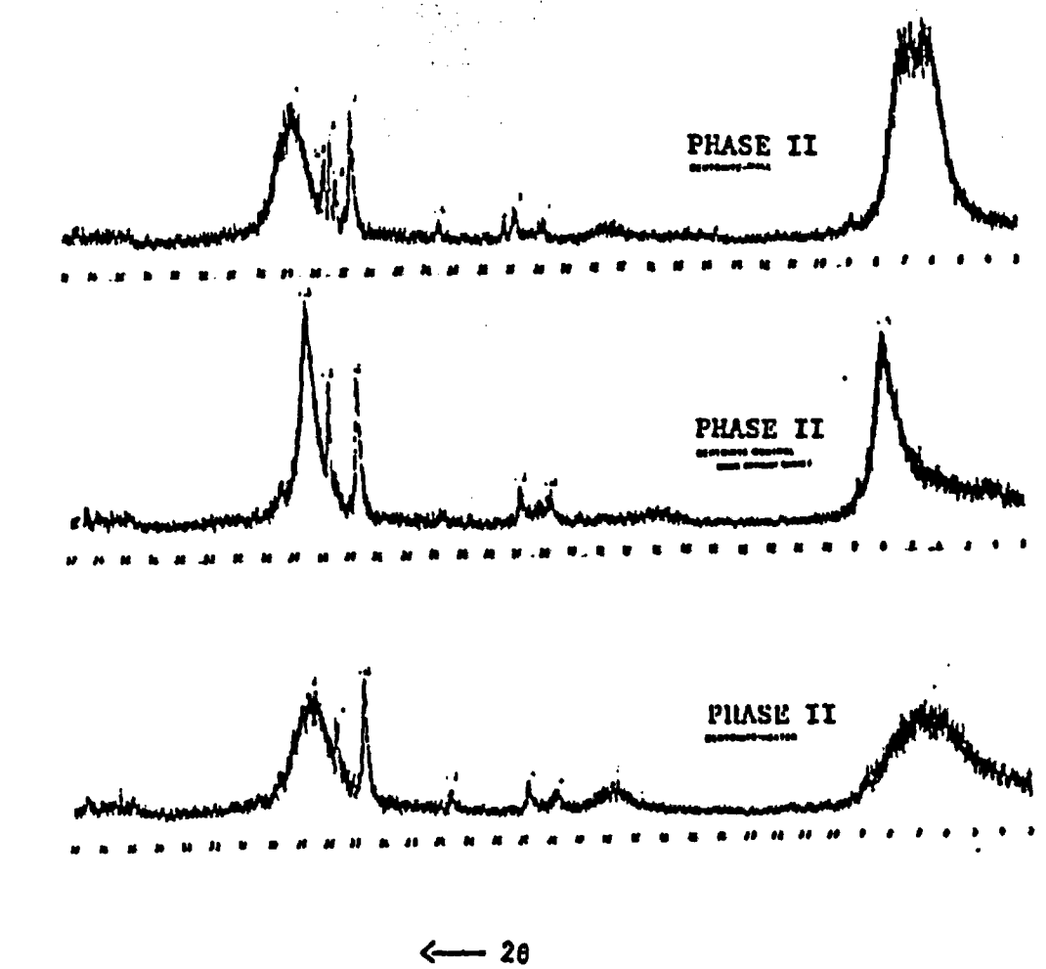

Figure 24. Comparison of X-ray diffraction patterns of reacted and unreacted bentonite present in the Phase II test centrifuged packing material slurry samples prepared as oriented clay mounts by evaporation of slurry on glass slides. [Range of scan: 2θ = 3-37° (d = 2.43-2.94 Å)]. (Control sample consisted of a slurry of bentonite with synthetic groundwater.)

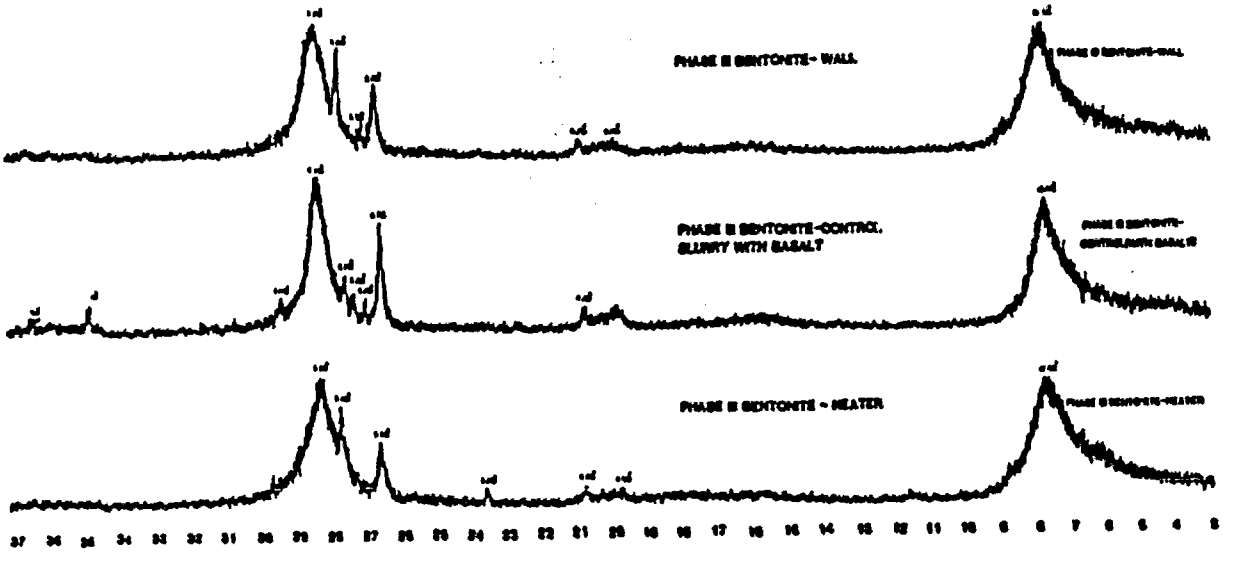

← 2θ

Figure 25. Comparison of X-ray diffraction patterns of reacted and unreacted bentonite present in the Phase III test centrifuged packing material slurry samples prepared as oriented clay mounts by evaporation of slurry on glass slides. [Range of scan: $2\theta = 3\text{-}37^{\circ}$ (d = 2.43-29.4 Å)]. (Control sample consisted of a slurry of bentonite and basalt with synthetic groundwater.)

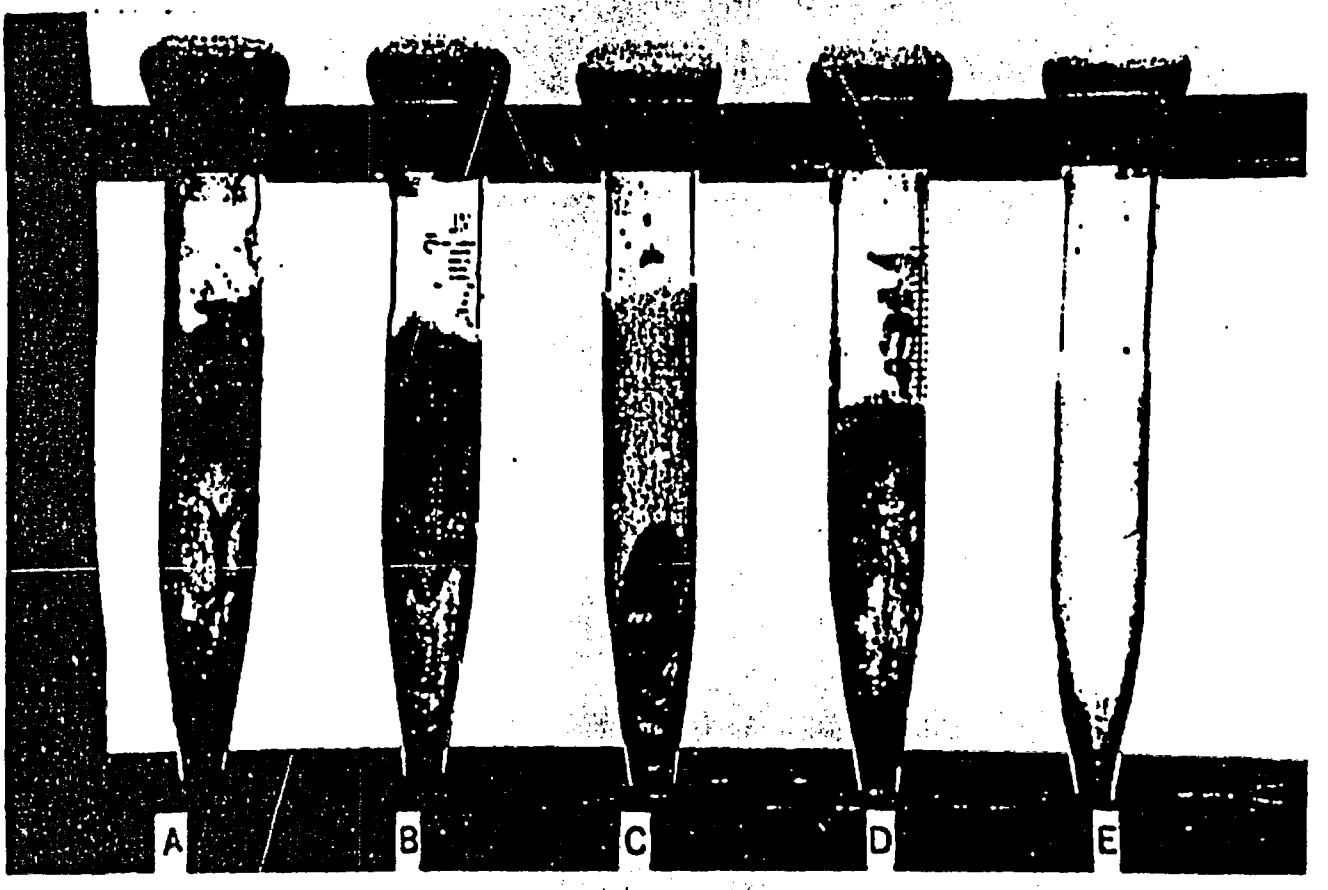

Figure 26. Appearance of Phase I centrifuged packing material slurries before and after reaction. (Tubes are shown full-scale. Black material in bottom of tubes is basalt fines.)
(A) Sampled near heater
(B) Sampled near autoclave wall
(C) Control unreacted
(D) Sampled near heater
(E) Sampled near autoclave wall.

Table 7. Comparison of (00ℓ) d-spacings based on X-ray diffractometer studies of reacted and unreacted bentonite portions of centrifuged packing material slurries prepared as oriented clay mounts by evaporation of centrifuged slurry on glass slides. [Intensities not specified. Range of scan: 2θ = 3-37° (d = 2.43-29.4 Å).]

d (Å) Wall Sample	d (Å) Heater Sample	d (Å) Control Sample[a]
Phase I Test		
14.7	14.7	12.4
----	9.9	9.9
5.1	5.1	----
4.4	4.4	4.4
4.2	4.2	4.2
----	----	4.17
3.3	3.3	3.3
----	----	3.26
----	----	3.23
3.2	3.2	3.22
3.1	3.09	3.1
----	----	3.0
Phase II Test		
13.6	13.4	11.3
6.50	----	----
----	----	5.53
5.09	5.01	----
4.47	4.48	4.49
4.27	4.27	4.25
3.77	3.77	3.77
3.34	3.35	3.34
3.28	----	----
3.25	----	----
3.23	3.22	3.22
3.11	3.13	3.14
Phase III Test		
11.3	11.5	11.5
4.44	4.48	4.49
4.25	4.26	4.28
----	3.77	----
3.34	3.34	3.35
3.30	----	3.29
----	----	3.26
3.22	3.21	3.23
3.15	3.14	3.14
----	----	3.03
----	----	2.58
----	----	2.46

[a]Control samples for each test were prepared separately and contained bentonite/basalt in Phase I and III tests but contained only bentonite/groundwater for the Phase II test.

Table 8. Comparison of (00ℓ) d-spacings based on X-ray diffractometer studies of Phase I test reacted and unreacted montmorillonite, prepared as oriented clay mounts by evaporation of centrifuged packing material slurry on glass slides; treatment by glycolation at 60°C, followed by heating to 300°C for one hour. [Intensities not specified. Range of scan: 2θ = 3-9.5° (d = 9.30-29.4 Å).]

d (Å)								
Heater Wall Samples Glycolated		Control	Heater Wall Samples Glycolated and Heat Treated		Control	Heater Wall Samples Untreated		Control
17.0	16.0	16.6	15.2*	15.2*	15.5*	14.7	14.7	12.4
9.9	9.7	9.9	——	9.9	——	9.9	9.8	9.9

*Peak intensity is drastically reduced when compared to the peak intensities in the diffraction patterns of the untreated and glycolated samples. This decrease in intensity is due to the collapse of the smectite structure.

The slides, coated with centrifuged reacted and unreacted (control) packing material slurries, were subsequently given standard glycolation[13] and heat treatments to study the changes in the (001) reflections of the montmorillonite clay (Carroll, D., 1970). The first treatment consists of glycolation. See the first three columns of Table 8 for tabulation of the data on the glycolated samples and Figures 27d, 27e, and 27f for the diffraction patterns of the glycolated samples. An expandable clay such as montmorillonite will characteristically swell upon glycolation due to the increase in basal spacing between layers because of the incorporation of organic molecules in the interlayer sites and this will be evidenced by a shift in the d-spacing at ≈12-15 Å to ≈16-18 Å. Compare Figures 27a and 27d; Figures 27b and 27e; Figures 27c and 27f. The sample taken from the heater region had the largest d-spacing value, followed by that for the control sample, followed by that for the sample taken from the wall region.

[13]Samples are glycolated by placing the coated slides in a desiccator, which contains ethylene glycol in the well normally filled with desiccant, and by heating in an oven at 60°C for at least an hour.

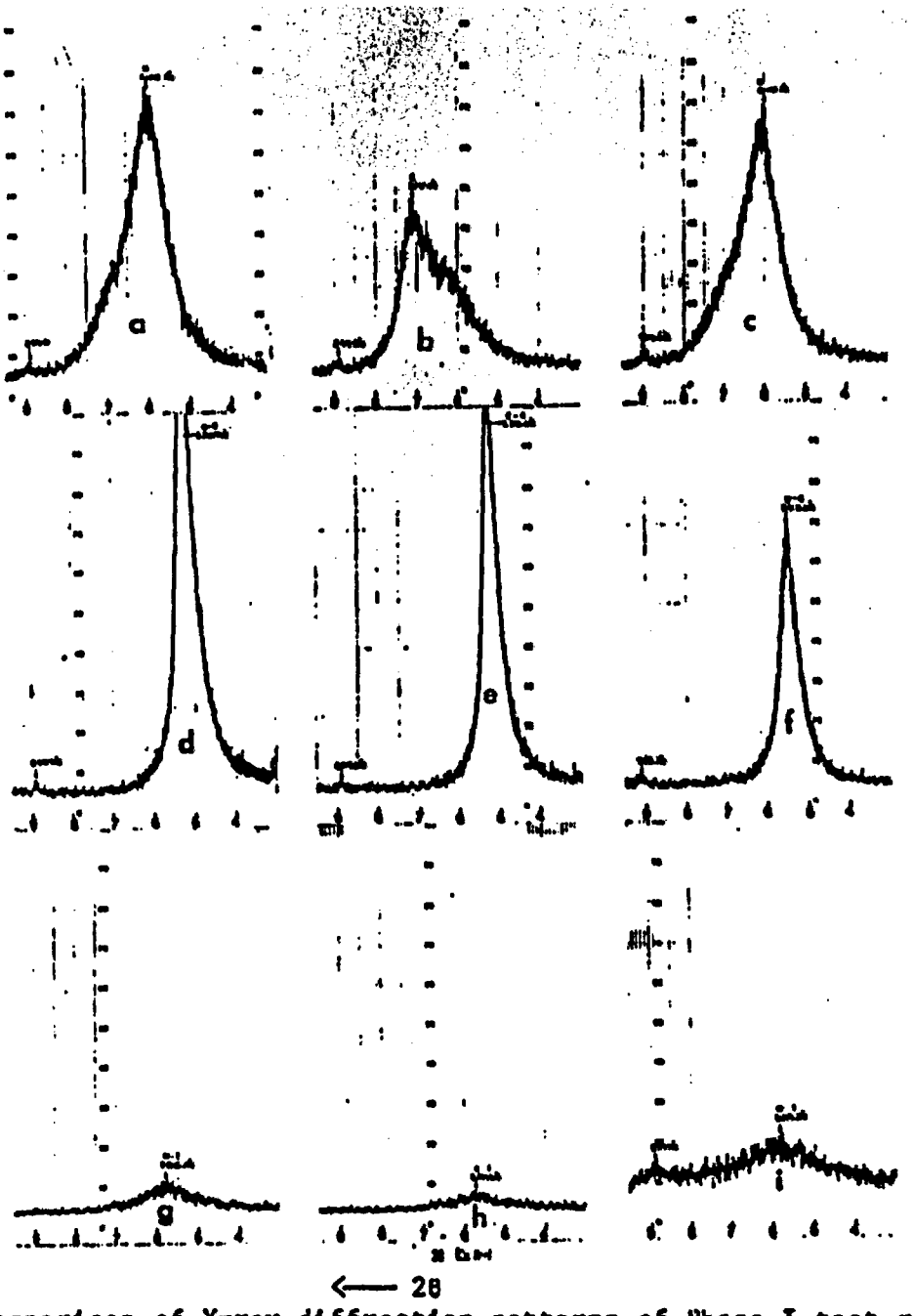

Figure 27. Comparison of X-ray diffraction patterns of Phase I test reacted and unreacted montmorillonite present in the centrifuged packing material slurry samples prepared as oriented clay mounts by evaporation of slurry on glass slides; treatment by glycolation, followed by heating to 300°C for one hour. [Range of scan: 2θ = 3.9-5° (d = 9.30-29.4 Å)].
(a) Untreated slurry sampled from heater region
(b) Untreated slurry (control)
(c) Untreated slurry sampled from wall region
(d) Glycolated (60°C) slurry sampled from heater region
(e) Glycolated (60°C) slurry (control)
(f) Glycolated (60°C) slurry sampled from wall region
(g) Heat-treated (300°C) slurry sampled from heater region
(h) Heat-treated (300°C) slurry (control)
(i) Heat-treated (300°C) slurry sampled from wall region.

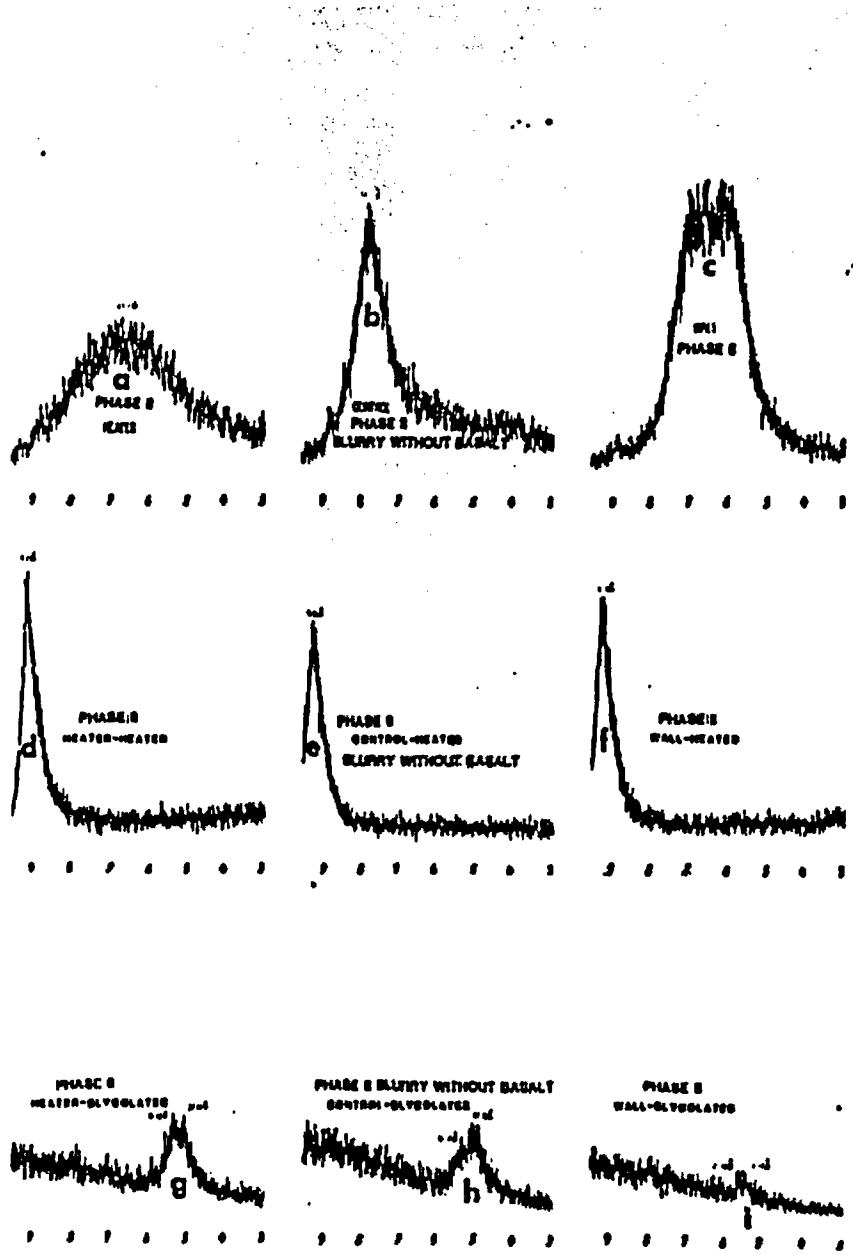

Figure 28. Comparison of X-ray diffraction patterns of Phase II test reacted and unreacted montmorillonite present in the centrifuged packing material slurry samples prepared as oriented clay mounts by evaporation of slurry on glass slides; heat-treated at 300°C for 18 hours, followed by glycolation at 60°C. [Range of scan: 2θ = 3-9.5° (d = 9.30-29.4 Å)].

(a) Untreated slurry sampled from heater region
(b) Untreated slurry (control)
(c) Untreated slurry sampled from wall region
(d) Heat-treated (300°C at 18 h) slurry sampled from heater region
(e) Heat-treated (300°C at 18 h) slurry (control)
(f) Heat-treated (300°C at 18 h) slurry sampled from wall region
(g) Glycolated (60°C) slurry sampled from heater region
(h) Glycolated (60°C) slurry (control)
(i) Glycolated (60°C) slurry sampled from wall region.

The second standard treatment for a smectite consists of heating the glycolated samples to 300°C for at least one hour. The interlayer water is removed by this procedure and, characteristically the original (001) reflection collapses and is replaced by one in the ≈9-10 Å region. This is evident upon comparison of Figures 27a and 27g; Figures 27b and 27h; and Figures 27c and 27i. See Columns four through six of Table 8. Although these heat-treated samples were not rehydrated to see if the (001) reflection due to swelling would reappear, it is obvious that after heating to 300°C, the expandability has been drastically reduced. The reflection at ≈9-10 Å attributable to the formation of a non-expandable clay was not observed. Additional heating at 300°C may be needed to see this effect. With the loss of interlayer water, montmorillonite may be transformed into hydromica (illite) if sufficient potassium is available, or into chlorite, if sufficient magnesium is present. The main effect of pressure and temperature on a hydrous mineral will be dehydration. Reviews of the literature concerning the hydrothermal stability of the packing material can be found in NUREG/CR-2482, Vols. 3 and 5 (1983) and NUREG/CR-3091, Vols. 1 and 2 (1983).

5.7.2.2 Montmorillonite XRD Phase II Test

Similar treatments were given to the Phase II test samples, except that the order of glycolation and heating was reversed. This was done in order to see to what extent swelling would occur after heating. See Figures 28a-28i. The shifts in d-spacings evident in the diffraction patterns after these treatments are summarized in Table 9.

Table 9. Comparison of (00ℓ) d-spacings based on X-ray diffractometer studies of Phase II reacted and unreacted montmorillonite, prepared as oriented clay mounts by evaporation of centrifuged packing material slurry on glass slides; treatment by heating to 300°C for 18 hours, followed by glycolation at 60°C. [Intensities not specified. Range of scan: 2θ = 3-9.5° (d = 9.30-29.4 Å).]

d (Å)								
Heater	Wall Samples Heat-Treated	Control	Heater	Wall Samples Heat-Treated and Glycolated	Control	Heater	Wall Samples Untreated	Control
9.7	9.5	9.60	17.7*	16.0*	17.8*	13.8	13.6	11.3
----	----	----	16.7*	15.6*	16.8*	----	----	----

*Peak intensity is drastically reduced when compared to the peak intensities in the diffraction patterns for the untreated and heated samples.

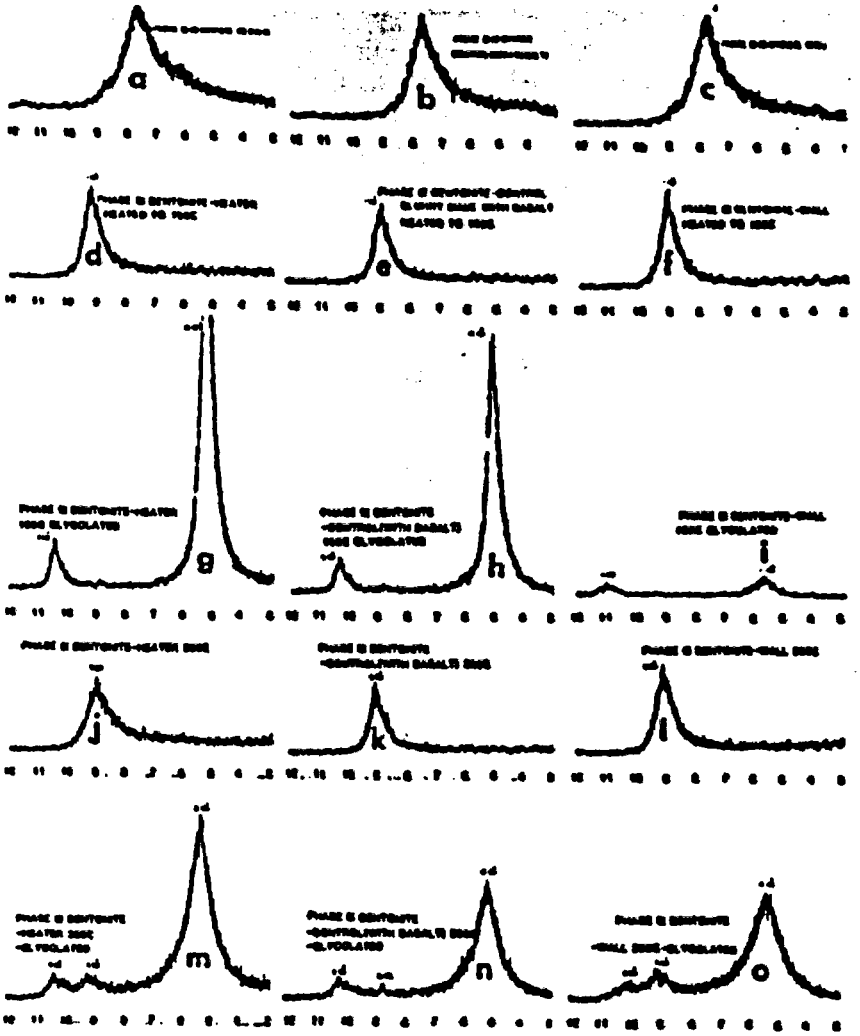

Figure 29. Comparison of X-ray diffraction patterns of Phase III test reacted and unreacted montmorillonite present in the centrifuged packing material slurry samples prepared as oriented clay mounts by evaporation of slurry on glass slides; heat-treated at 150°C, followed by glycolation at 60°C, followed by heat-treatment at 300°C, followed by glycolation at 60°C. [Range of scan: 2θ = 3-9.5° (d = 9.30-29.4 A)].

(a) Untreated slurry sampled from heater region
(b) Untreated slurry (control)
(c) Untreated slurry sampled from wall region
(d) Heat-treated (150°C) slurry sampled from heater region
(e) Heat-treated (150°C) slurry (control)
(f) Heat-treated (150°C) slurry sampled from wall region
(g) Glycolated (60°C) slurry sampled from heater region after heating to 150°C
(h) Glycolated (60°C) slurry (control) after heating to 150°C
(i) Glycolated (60°C) slurry sampled from wall region after heating to 150°C
(j) Heat-treated (300°C) slurry sampled from heater region
(k) Heat-treated (300°C) slurry (control)
(l) Heat-treated (300°C) slurry sampled from wall region
(m) Glycolated (60°C) slurry sampled from heater region after heating to 300°C
(n) Glycolated (60°C) slurry (control) after heating to 300°C
(o) Glycolated (60°C) slurry sampled from wall region after heating to 300°C)

Swelling of the montmorillonite occurred in the Phase II test as evidenced by the shift in d-spacing from 11.3 Å to 13.8 Å (in the sample taken from the heater region) and to 13.6 Å (in the sample taken from the wall region). This is shown in Figures 28a-28c. Upon heating of the samples to 300°C, the d-spacings of the major montmorillonite peak shifted to a range of 9.5-9.7 Å, indicative of dehydration and collapse of the smectite structure. See Figures 28d-28f for the XRD patterns of the heated samples. These samples were subsequently glycolated and some swelling did occur as can be seen in Figures 28g-28i by the shift in the d-spacings to a range of 15.6-17.8 Å. However, the intensity of the peaks is drastically reduced when compared to the intensity of the peaks of the hydrated montmorillonite (Figures 28a-28c). This seems to indicate that dehydration may not be reversible.

5.7.2.3 Montmorillonite XRD Phase III Test

The X-ray diffraction patterns of the samples from the Phase III unirradiated test are shown in Figures 29a-29c. Various treatments were applied and X-ray diffraction studies subsequently made to determine the effects of the treatments on the expandability of the montmorillonite. The d-spacings for each of the patterns are given in Table 10. There was a slight increase in the basal spacing of the untreated reacted samples when compared to the untreated unreacted sample. See Figures 29a-29c. After heating the samples to 150°C for 12 hours, dehydration with the accompanying decrease in basal spacing occurred, as shown in Figures 29d-29f. Up to this point, all XRD patterns for the Phase III test samples were very similar to each other. The samples were subsequently glycolated at 60°C to determine differences in expandability. The XRD patterns of the glycolated Phase III test control sample and the Phase III test sample taken from the heater region shown in Figures 29g and 29h show a large increase in the montmorillonite basal spacing, along with the appearance of a new peak. Intensities of these two peaks are similar and are much greater than the corresponding intensities in the XRD patterns of the untreated samples. The XRD pattern of the glycolated heat treated sample taken from the wall region of the Phase III test system shows less expandability of the montmorillonite and decreased intensities of the montmorillonite major peak and of the newly formed one. These samples were then heated to 300°C for several hours and XRD patterns were obtained. Significant and similar decreases in basal spacings are evident in all three samples, as shown in Figures 29j-29l. Samples were then subjected to glycolation at 60°C. Similar expansion of the basal spacing occurred in all samples, indicating that swelling of the montmorillonite was still occurring and that dehydration was apparently reversible in the case of these samples and their successive treatments.

Table 10. Comparison of (00ℓ) d-spacings based on X-ray diffractometer studies of Phase III reacted and unreacted montmorillonite, prepared as oriented clay mounts by evaporation of centrifuged packing material slurry on glass slides; heat-treatment at 150°C, followed by glycolation at 60°C, followed by heat-treatment at 300°C, followed by glycolation at 60°C. [Intensities not specified. Range of scan: 2θ = 3-9.5° (d = 9.30-29.4 Å).]

	d(Å)		
	Heater	Wall	Control
Untreated	11.5	11.3	11.5
Heat-treated (150°C)	9.6	9.7	9.8
Glycolated (60°C)	17.0	15.8*	17.1
	8.6	8.0	8.6
Heat-treated (300°C)	9.8	9.7	9.7
Glycolated (60°C)	16.5	16.2	17.0
	9.5	9.7	10.1
	8.5	8.7	8.6

*Peak intensity is drastically reduced when compared to the peak intensities in the diffraction pattern of the untreated sample.

5.7.2.4 Comparison of Montmorillonite XRD Studies For All Tests

A comparison of the d-spacings obtained for untreated and treated montmorillonite samples from the three tests yielded the following conclusions:

- The basal spacings in the samples taken from the wall and heater regions of the irradiated systems are increased in comparison to an unreacted control sample. This suggests that irradiation may enhance expandability.

- The shape and intensity of the major montmorillonite peak in the Phase II test samples differs significantly for the heater sample and the wall sample. This is not true for the corresponding samples of the Phase I and Phase II tests.

- Expandability may be affected by heat treatments. After heating the samples from the Phase II tests for 18 hours at 300°C, and subsequent glycolation, it was apparent that the major montmorillonite peak had almost disappeared. This did not occur in the case of the Phase III test samples after heating at 300°C for several hours. But it should also be noted that other peaks appeared in the Phase III test XRD patterns, indicating that other minerals had been produced. This is also supported by the XRD patterns obtained over the entire range. Qualitatively it can be seen by comparison of the overall patterns that differences exist between the reacted and unreacted clays in each test and in the three different test systems.

5.8 Analysis of Reacted Basalt

5.8.1 Comparison of XRD Patterns of Pulverized Basalt

The basalt pellets removed from regions near the heater and near the wall in each of the three phases and an unreacted control sample were pulverized and analyzed by XRD to detect any differences due to reaction. Interpretation of the complex diffraction patterns to identify specific changes in mineralogical composition would require a significant effort and is beyond the scope of this work. Polished thin section basalt samples were also prepared and examined with a polarizing microscope to help detect changes in basalt mineralogy.

The XRD patterns for all basalt samples are reproduced in Figure 30. The data for the observed (hkℓ) reflections are summarized in Table 11. If a comparison of the patterns shown in Figure 30 is made, it is obvious that there are differences among the patterns, showing that changes occur in the mineralogical composition of the basalt upon reaction. For example, there is a d-spacing of 4.67 Å for samples taken from the heater region in the irradiated systems which is not present in the samples taken from the wall or heater regions in the unirradiated system. More detailed and comprehensive studies are needed to characterize the changes that occur and to determine the effects of these changes in composition on the repository environment.

A preliminary solids analysis and solution analysis performed in the Wood hydrothermal bentonite/basalt/groundwater non-irradiated experiment (RHO-BW-SA-219P, 1983) at 300°C and 28.9 MPa suggests that the primary reaction in the basalt-bearing system is the dissolution of basalt glass followed by the precipitation of a pure silica phase (that is, cristobalite and/or quartz) and smectite, illite, and mordenite (zeolite). It was thought that some alteration of the bentonite to illite may have occurred but this was not seen when a bentonite/groundwater system was tested in a similar manner.

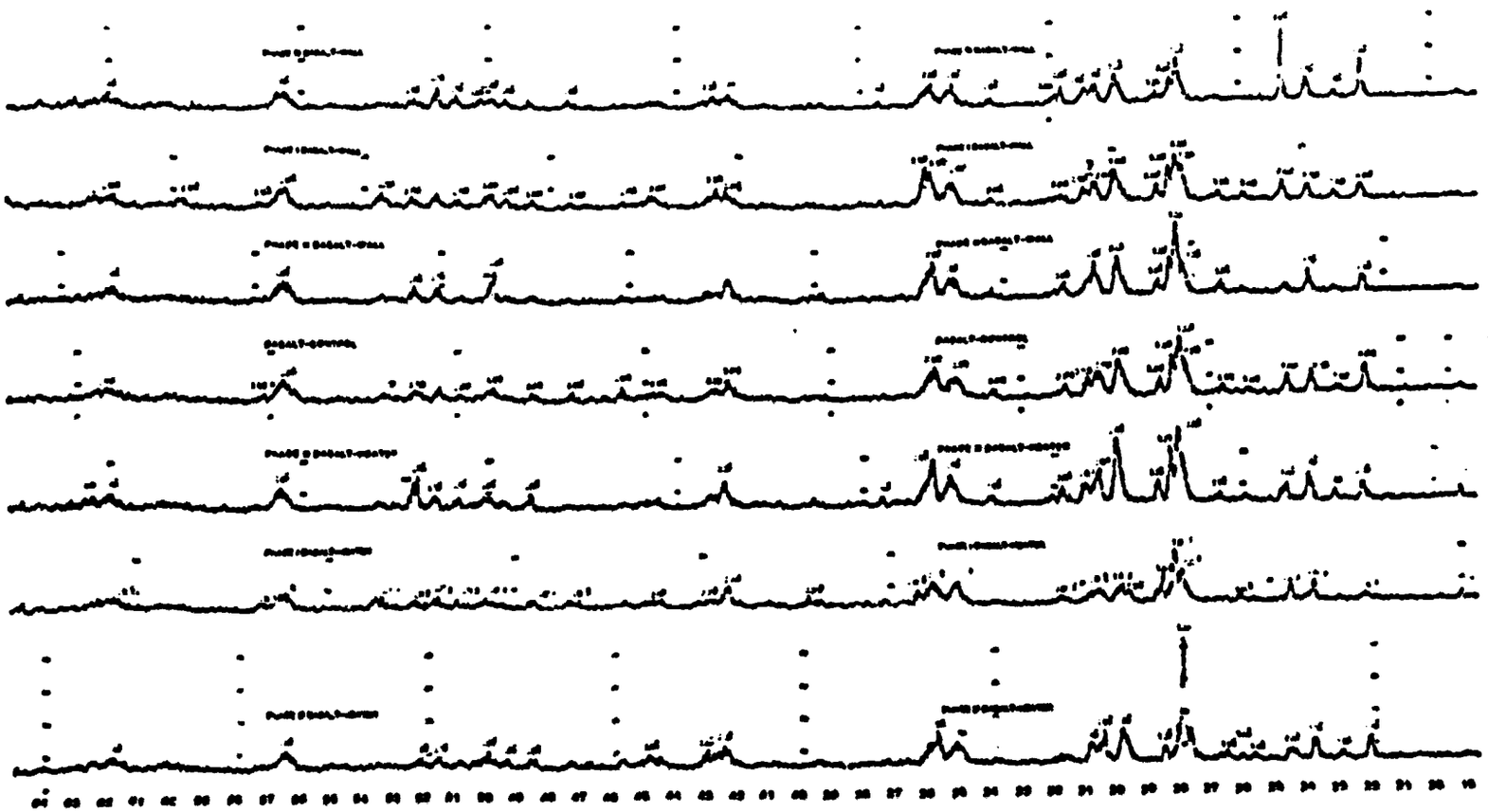

Figure 30. Comparison of X-ray diffraction patterns for reacted and unreacted basalt, prepared as unoriented mounts of pulverized basalt. [Range of scan: 2θ = 3-65° (d = 1.43-29.4 A)].

Table 11. Comparison of (hkℓ) d-spacings based on X-ray diffractometer studies of reacted and unreacted basalt, prepared as unoriented mounts of pulverized basalt. [Intensities not specified. Range of scan: 2θ = 3-65° (d = 1.43-29.4 Å).]

d (Å)						
Wall Sample Phase I Test	Wall Sample Phase II Test	Wall Sample Phase III Test	Heater Sample Phase I Test	Heater Sample Phase II Test	Heater Sample Phase III Test	Control Sample
----	----	----	4.67	4.67	----	----
4.04	4.04	4.04	4.04	4.03	4.04	4.05
3.89	3.88	3.89	----	3.88	3.89	3.90
3.76	3.75	3.75	3.77	3.74	3.74	3.77
3.64	3.64	3.67	3.64	3.64	3.64	3.64
3.47	----	3.47	----	3.46	3.48	3.48
----	3.45	----	3.44	----	3.42	----
3.37	3.37	----	----	3.35	3.37	3.37
3.22	3.23	----	----	----	3.23	3.23
3.20	3.21	3.21	3.21	3.19	3.21	3.21
3.18	3.18	3.18	3.18	3.17	3.18	3.18
3.14	3.14	3.13	3.14	3.13	3.13	3.14
----	----	----	3.02	----	----	----
3.00	3.01	3.01	3.00	2.99	2.99	3.00
2.94	----	2.94	2.94	2.94	2.94	2.95
2.93	2.93	2.93	----	----	----	----
2.90	2.92	2.90	----	2.90	2.90	2.91
2.84	2.84	2.83	2.83	2.83	2.84	2.85
----	2.82	2.82	----	2.80	2.81	----
2.65	2.65	2.66	----	2.65	2.65	2.65
2.56	2.56	2.56	2.57	2.55	2.56	2.57
2.52	2.52	2.52	2.51	2.51	2.52	2.52
2.51	----	2.51	2.48	----	----	----
2.41	----	2.41	----	2.41	----	----
----	----	----	2.27	2.27	----	----
2.14	2.14	2.14	2.14	2.13	2.13	2.14
2.12	2.11	2.12	2.10	2.11	2.11	2.12
2.03	----	2.03	2.02	2.02	2.02	2.03
1.99	1.99	----	----	----	1.99	1.99
----	----	----	----	----	1.95	----
1.92	1.92	1.92	1.92	----	1.93	1.93
1.88	1.87	1.88	1.87	1.88	1.88	1.87
1.85	1.85	1.84	----	1.85	1.85	----
1.83	1.83	1.83	1.83	1.83	1.83	1.83
1.79	1.80	1.79	1.79	1.79	1.79	1.80
1.77	1.77	1.77	1.77	1.77	1.77	1.77
1.75	1.74	1.75	1.75	1.75	1.76	1.75
1.72	1.72	1.72	1.71	1.71	----	1.72
1.63	1.63	1.63	1.62	1.63	1.63	1.63
1.61	1.61	----	1.60	----	----	1.61
1.55	----	----	----	----	----	----
1.50	1.49	1.49	1.50	1.50	1.49	1.50

5.8.2 Comparison of Micrographs of Polished Basalt Thin Sections

Examination of polished basalt thin sections under a polarizing microscope revealed the presence of at least three mineralogical phases: plagioclase, pyroxene, and olivine. These were identified by their respective characteristic shapes and optical properties (Kraus, E. H., 1959; Deer, W. A., 1966). The three phases are shown in Figure 31. Examination of reacted basalt samples taken from the heater region for each test under the polarizing microscope indicates that plagioclase and olivine appear to be relatively unchanged. However, the pyroxene appears to have been altered, as evident from the alteration features observed on pyroxene grains from a Phase I test sample shown in Figure 32. Additionally, there are red-brown areas in the reacted basalt that are not present in the unreacted basalt in samples from the three tests. See Figure 33. There do not seem to be gross differences in the irradiated and non-irradiated basalt thin sections under the polarizing microscope. It was observed that there were very few red-brown areas in the Phase III specimen. In the Phase III specimen, they were mainly yellow-brown in color. Compare Figures 33 and 34. An additional observation is that these areas not present in the unreacted basalt specimen appear to be more numerous in the samples taken from the wall region than in the samples taken from the heater region in all three tests.

Work has been done at BWIP on identifying alteration products resulting from the reaction under hydrothermal conditions at 150°C for 120 days of basalt/bentonite/groundwater (BWIP/NRC Geochemistry Workshop, 1984). It was observed that (1) partial dissolution of basalt mesostasis and clay occurred, (2) smectite structure was preserved, and (3) iron and potassium were substituted in the smectite structure. The reaction product was identified as Fe-smectite. In the present work, XRD analysis of the powdered basalt samples did not reveal any basal spacings $\geq$ 9.6 Å, which is the minimum basal spacing a smectite can display and corresponds to the fully collapsed state (Deer, W. A., 1966)[14].

Much work needs to be conducted to identify the specific mineralogical changes that are occurring in the basalt after reaction. In particular, the effects of the repository conditions on the basaltic glassy phases needs to be determined. Also, correlations need to be made between the changes seen microscopically and the changes seen in the XRD patterns.

5.9 Metallography of Carbon Steel Sleeve and Identification of Surface Products

In the three phases of the test program, individual 1020 carbon steel sleeves were used to simulate the waste container. End caps were welded on to isolate the internal heater. The sleeves (25.4-mm diameter, 155-mm length and

[14]The observable range of d-spacings was 1.43-29.4 Å. Any d-spacings greater than 29.4 Å would not have been seen.

Figure 31. Minerals in unreacted basalt as determined with a polarizing microscope under crossed polars (100X). (Key: Pl = plagioclase, P_y = pyroxene and O = olivine.)

Figure 32. Minerals in Phase I test reacted basalt sampled from the heater region as determined with a polarizing microscope under crossed polars (100X). (Key: Pl = plagioclase, P_y = pyroxene and O = olivine.)

Figure 33. Minerals in Phase I test reacted basalt sampled from the wall region as determined with a polarizing microscope under crossed polars (100X). (Red-brown areas are indicated by R in photo.)

Figure 34. Minerals in the Phase III test reacted basalt sampled from the wall region as determined with a polarizing microscope under crossed polars (100X). (Yellow-brown areas are indicated by y in photo.)

2-mm thick) were removed from the stainless steel autoclave after the packing material slurries had been examined after the 60-day test periods. Figure 35 shows the reacted sleeve after the Phase I test and compares it to one which was not tested. It should be noted that the sleeve for the Phase I test was in the as-received condition whereas the Phase II and Phase III test sleeves were polished through 600-grit silicon carbide paper, in an attempt to remove the decarburized surface layer which was introduced by tube manufacturing processes.

5.9.1 Metallography of Phase I Test Sleeve

Figure 36 shows a metallographic section perpendicular to the axis of the Phase I steel sleeve. The steel consists primarily of white ferritic grains interspersed with dark pearlitic regions. A thin gray oxide layer is observed on the outer surface, which was in contact with the packing material. The oxide is adherent but in certain locations is found to be fractured. Within the two-month testing period at 150°C, no obvious surface pitting or intergranular corrosion was observed. Small indentations which were present originated in the starting material. Immediately above the oxide, a slightly thicker black layer (indicated by arrow) is just discernible between the oxide and plastic compound used to mount the sample for metallographic preparation. Figure 37 is a micrograph taken at a different location and shows a thicker dark layer (between the arrows). This represents an adherent orange-red clay layer which remained after most of the basalt/bentonite mixture contacting it was removed. Samples of this layer were mechanically removed and subjected to X-ray diffraction. It seems from a comparison of Figures 36 and 37 that the metal oxide layer is thinner in regions where the orange-red layer is thick. This indicates that this adherent layer minimized uniform corrosion.

Analysis by SEM-EDX of the sleeve surface product revealed the presence of a material similar in composition to a sample of bentonite that was examined separately. However, there were some compositional differences at various locations on the sleeve, as the semi-quantitative elemental analyses revealed. The elemental analysis of bentonite clay by SEM-EDX shows that Si is the most abundant element (≈75%), with some Al (≈15%) and Fe (≈6%), and minor amounts of other elements (≈4%). At some sites on the sleeve, the surface products that were probed showed more Fe relative to the amount indicated in bentonite. For some sites, the Fe and Si peaks were similar in intensity but in others the Fe peaks were much stronger than those for Si. One surface product sample, shown in Figure 38, is a layered material whose elemental composition was mainly Fe with some Si and a small amount of Mg. There was not sufficient material, however, to pursue more quantitative experiments.

As noted above, the Phase I test sleeve, which was used in the as-received condition, was decarburized to a depth of approximately 50 microns (Figures 36 and 37). Figure 39, showing a section through a non-reacted steel tube, proves that decarburization was a result of standard manufacturing processes rather than from hydrothermal testing.

During the Phase I test, the slurry level inside the autoclave had fallen to a level below the top of the carbon steel sleeve. Above this waterline,

Figure 35. Appearance of carbon steel sleeve prior to reaction (left) and subsequent to Phase I test reaction (right). (Sleeves are shown full-scale.)

Figure 36. Micrograph of outside diameter of carbon steel sleeve subsequent to Phase I test rection showing metal oxide and thin clay deposition layer (marked by arrow) (250X).

Figure 37. Micrograph of outside diameter of carbon steel sleeve subsequent to Phase I test reaction showing metal oxide and thick clay deposition layer between arrows (250X).

Figure 38. SEM-EDX micrograph of iron-rich layered material in Phase I test carbon steel surface product (1000X).

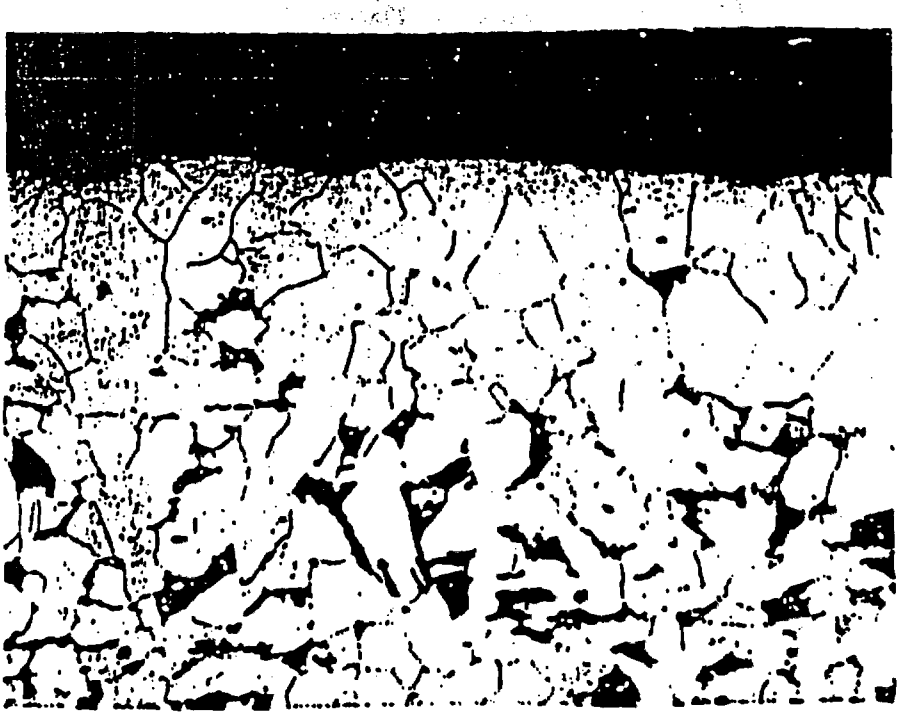

Figure 39. Micrograph of outside diameter of carbon steel sleeve prior to Phase I test reaction (250X). (Note the presence of decarburized surface.)

accelerated corrosion at the welded end cap was evident (Figure 35). The occurrence of more severe corrosion on the steel exposed to vapor has been reported in another study (PNL-4452, 1983). In that work, cast ductile iron was placed in an autoclave with oxic basaltic groundwater and crushed basalt at a temperature of 250°C, a pressure of 5.2 MPa (700 psi) and a gamma dose rate of $\approx 2 \times 10^5$ rad/h for periods up to three months with no bentonite present. Between the one- and three-month test periods, the autoclave operated in the vapor phase for several days, apparently because of a slightly elevated temperature. The present observation of accelerated corrosion in the vapor phase could, therefore, be associated with higher oxygen levels or, possibly, with waterline corrosion.

Figure 40 shows the appearance of weld metal at the top of the Phase I test steel sleeve. A thin broken oxide layer is just visible. Fusion of the metal has removed the decarburized layer and ferrite-rich grain boundary regions are formed. Again, no pitting or intergranular attack was detected.

5.9.2 Metallography of Phase II Test Sleeve

In the Phase II test, prior polishing of the sleeve had removed the decarburized surface layer (Figure 41). A very thin, irregular surface oxide is seen above which is a thin clay layer (between arrows). Several hemispherically-shaped pits are present. These are approximately 12 microns in depth after the 60-day reaction period. If one makes the highly conservative assumption that the pit depth increases linearly with time, then the depth after the minimum 300-year radionuclide containment period would be 2.2 cm. This would be insufficient to penetrate any of the carbon steel containers specified by Westinghouse Electric Corporation for conceptual waste package designs (AESD-TME-3142, 1982). For these, the container wall thicknesses vary between 5.3 and 8.7 cm.

The adherent materials on the Phase II test sleeve were studied with SEM-EDX, electron diffraction, and electron energy loss spectroscopy (EELS) in an attempt to identify the orange-brown portion and magnetic green-yellow portion. Micrographs of these materials are shown in Figures 42 and 43, respectively. The EDX analyses of these samples showed that (1) the orange-brown material contained large amounts of Si, Fe and Al with some Ca, Mg and S in the darker areas, and some Ca, Mg and K in the lighter areas and (2) the green-yellow material contained large amounts of Fe and Si with some Al, Mg and Ca. The samples were shown to be well-defined crystalline materials that contained oxygen by use of EELS. See Figure 44 for the two-point plot of the EELS spectrum of the orange-brown material. A similar one was obtained for the green-yellow specimen. Subsequently Debye-Scherrer patterns were obtained (see Figures 45 and 46). The d-spacings were calculated by measuring the patterns, which had been calibrated against a gold standard and are listed in Table 12. They did not match any of the spacings reported for common iron-silicate materials. It is believed that these specimens contain hydroxyl groups and/or water molecules because they were degraded by an electron beam. The identify of these materials is not presently known.

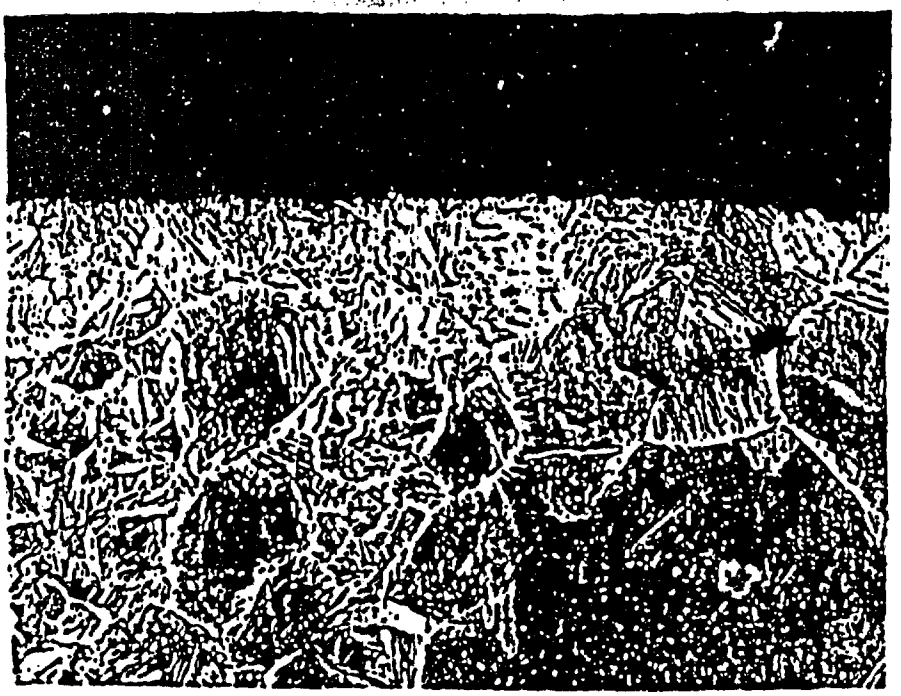

Figure 40. Micrograph of weld metal in carbon steel sleeve subsequent to Phase I test reaction (250X).

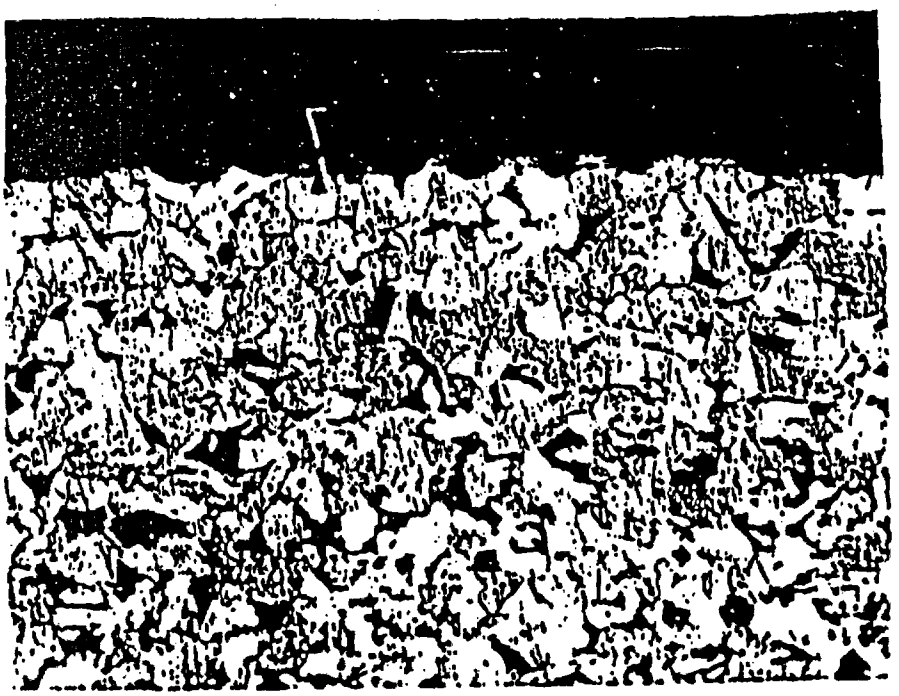

Figure 41. Micrograph of outside diameter of carbon steel sleeve subsequent to Phase II test reaction showing metal oxide and thin clay deposition layer (marked by arrows) (250X).

Figure 42. Micrograph (SEM) of orange-brown sleeve surface product from Phase II test (100X).

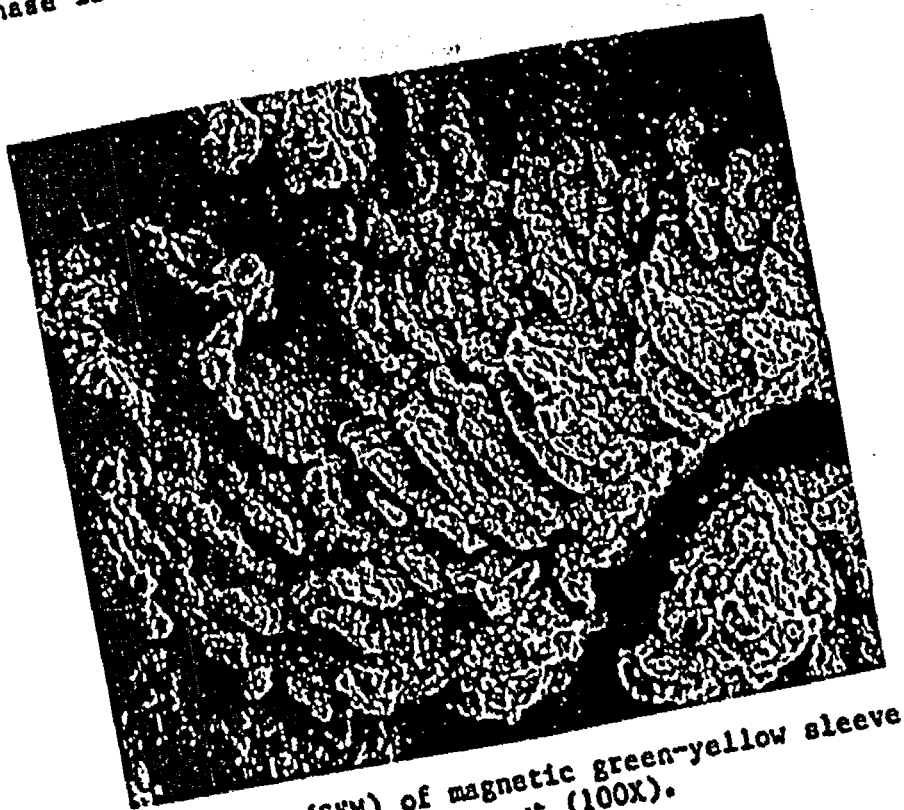

Figure 43. Micrograph (SEM) of magnetic green-yellow sleeve surface product from Phase II test (100X).

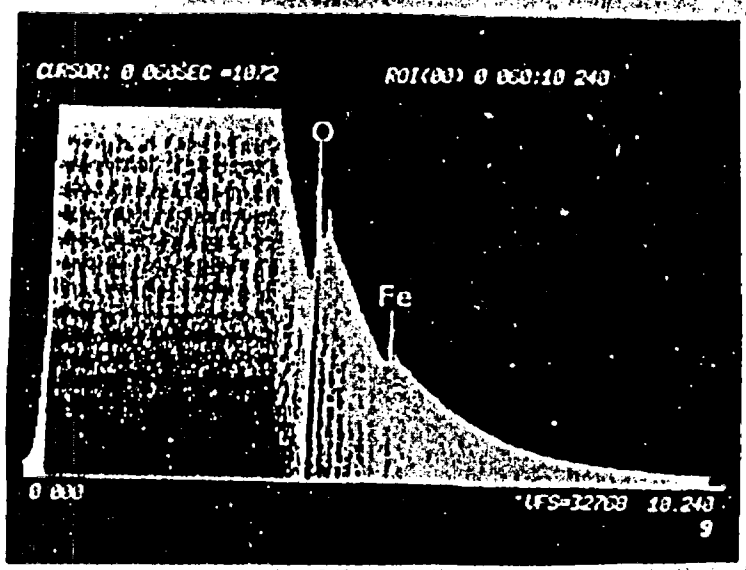

Figure 44. Point plot of EELS spectrum of orange-brown sleeve surface product from the Phase II test showing well-defined crystalline material containing iron and oxygen.

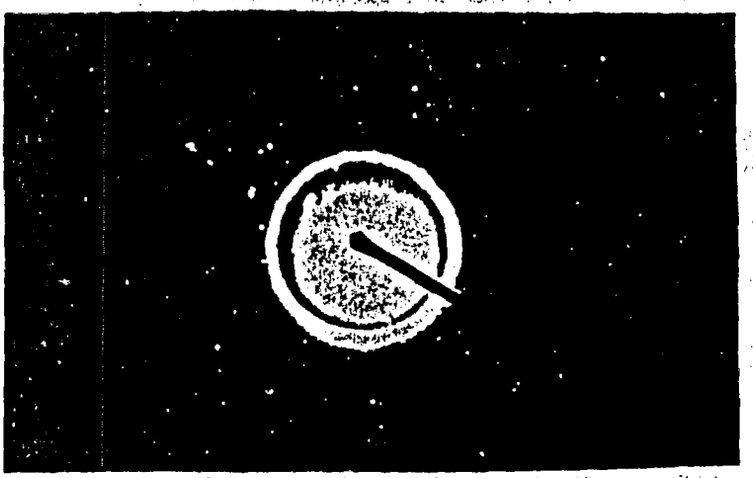

Figure 45. Debye-Scherrer powder pattern for orange-brown sleeve surface product from Phase III test.

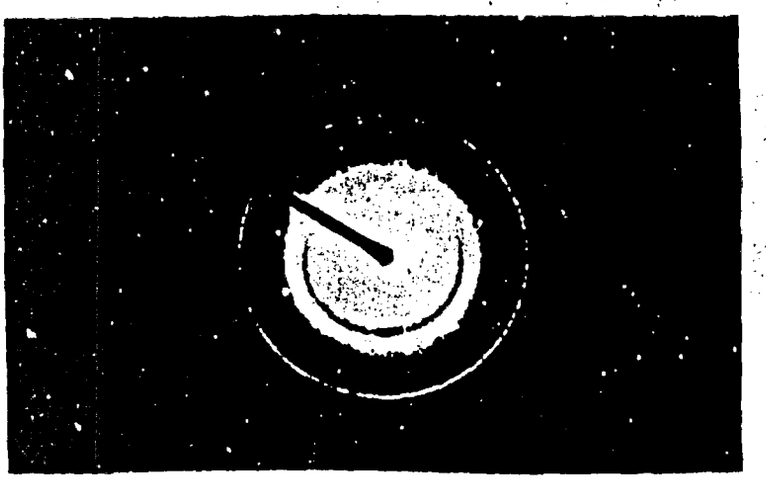

Figure 46. Debye-Scherrer powder pattern for green-yellow sleeve surface product from Phase II test.

Table 12. Calculated d-spacings of Phase II test sleeve surface product based on measured Debye-Scherrer electron diffraction powder patterns.[a]

d (Å) Green Oxide[b]	d (Å) Red (Orange) Oxide[b]
4.69	4.40
2.60	2.49
1.76	1.63
1.55	1.47
1.36	1.26
1.00	

[a]Spacings were calculated based on the measured patterns. A gold standard was used for calibration.
[b]Oxygen was determined to be present by use of EELS (electron energy loss spectroscopy).

5.9.3 Metallography of Phase III Sleeve

In the Phase III control test, carried out in a non-irradiation environment, pitting is also observed (see Figure 47). The pits in this case are more shallow and more closely spaced than those in the Phase II experiment (Figure 41). Based on an assumed linear pit propagation rate, the pit depth after 300 years would be about 1.5 cm. It should be noted that polishing the carbon steel sleeve prior to testing did not completely remove the surface-decarburized layer. Therefore, pit initiation and growth do not seem to be dependent on the presence of carbide phases. Figure 47 also shows a thin oxide layer which was detached from the metal substrate. It is approximately seven microns in thickness, which is similar to the oxide thickness for the Phase I test sleeve shown in Figure 36. If the oxide is assumed to be magnetite (Fe_3O_4), it may be shown that the 7-μ oxide layer was formed from 3.2 μ of steel during the 60-day test period[15]. Again, a highly conservative assumption of a linear rate for uniform corrosion gives a metal loss of 0.6 cm in 300 years. Thus, uniform corrosion will not be a significant failure mode for a carbon steel container in a basalt repository.

The material adhering to the Phase III test carbon steel sleeve was analyzed by SEM-EDX and X-ray diffraction to determine if an identification could be made. One product was green in color. A micrograph and EDX analysis of

[15]The amount of O_2 present in this amount of magnetite is estimated to be ≈140 mg. There is a maximum of 22 mg of O_2 in the plenum and dissolved in the water. The remaining O_2 probably originates from adsorbed oxygen and/or radiolysis of water.

Figure 47. Micrograph of outside diameter of carbon steel sleeve subsequent to Phase III test showing pitting, and a thin detached oxide layer (250X).

this material are shown in Figures 48 and 49. The other product was orange-brown in color and relevant information is given in Figures 50 and 51. Both materials contain large amounts of Si and Fe. The green product also has a high Ca content. Some Mg, Al, and Cl are also present in each. The XRD diffraction pattern (scan range 2θ = 3-68°) of the orange-brown material yielded five sets of d-spacings: 3.03-3.08 Å, 2.51-2.56 Å, 2.10-2.11 Å, 1.91-1.93 Å and 1.88-1.89 Å. This compound or mixture of compounds was not identifiable.

5.9.4 Comparison of Pitting Corrosion For All Tests

The results of the carbon steel corrosion evaluations show that pitting may occur during 60-day tests at 150°C in the presence of basalt/bentonite packing material. Gamma irradiation and surface decarburization of the steel did not have a significant influence on the initiation of pitting. Pits were only found, however, on pre-polished metal surfaces exposed to methane-containing water. It is not clear whether the surface polishing or the methane was responsible for this type of corrosion. Although the pitting rates obtained in this study were found to be too low to penetrate a typical steel container for a basalt repository, it must be realized that the test temperature of 150°C is much lower than the maximum value of about 300°C relevant to actual container conditions.

6. SUMMARY

The objective of this program was to determine the chemical environment that will be present within high level nuclear waste packages emplaced in a basalt repository. For this purpose, low carbon 1020 steel (current BWIP reference container material), synthetic basaltic groundwater and a mixture of bentonite and basalt were exposed in an autoclave to a specific repository condition after sealing (150°C, 1500 psi) in a gamma radiation environment with a dose rate of $(3.8 \pm 0.5) \times 10^4$ rad/h. The experiment consisted of three test phases.

The Phase I test involved a two-month irradiation test in an argon environment. The Phase II test is a similar test in a methane environment in the presence of radiation. These two tests were followed by a Phase III control test which is similar to the Phase II study but which was conducted in the absence of radiation.

A summary of findings is given below:

- Over the two-month test periods, the gas pressure in the autoclave ranged from 9.3-9.7 MPa in the Phase I test, from 11.1-13.2 MPa in the Phase II test and from 9.8-11.7 MPa in the Phase III test. There was a trend to decreasing pressures followed by a trend to pressures approaching or slightly exceeding the initial values.

- In all three tests, hydrogen was produced and oxygen was consumed, as determined by gas analyses and dissolved oxygen measurements. More hydrogen was produced in the Phase II test than in the Phase I and III

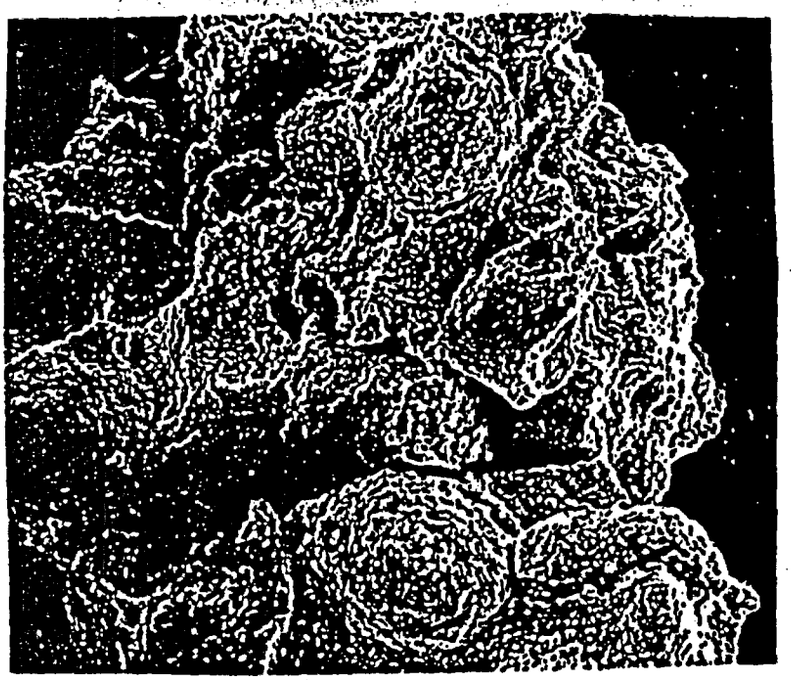

Figure 48. Micrograph of Phase III test green carbon steel surface product (100X).

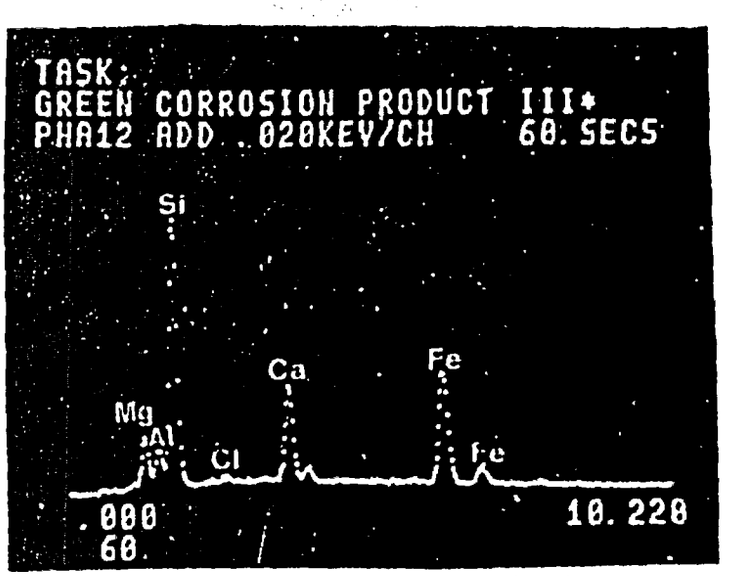

Figure 49. EDX of Phase III test green carbon steel surface product.

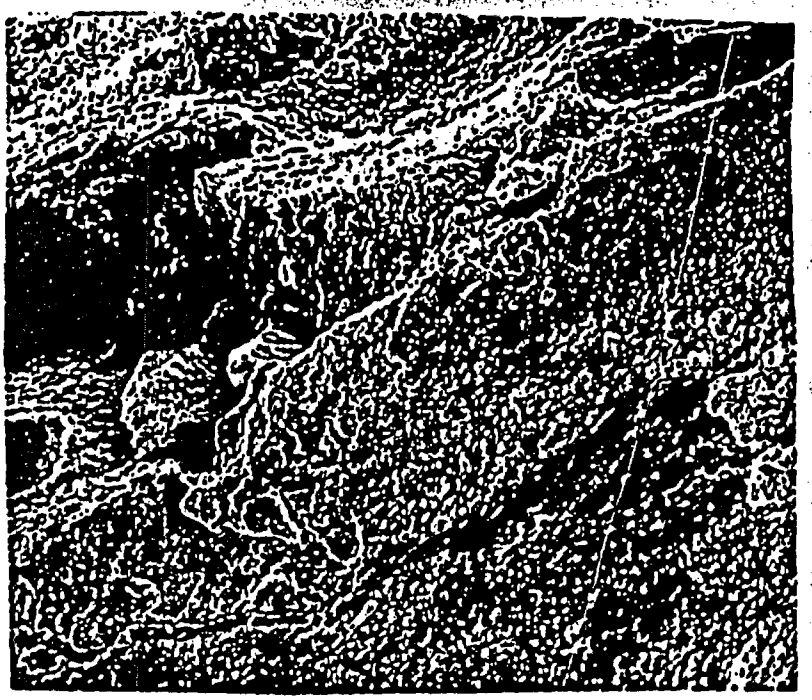

Figure 50. Micrograph of Phase III test orange-brown carbon steel surface product (100X).

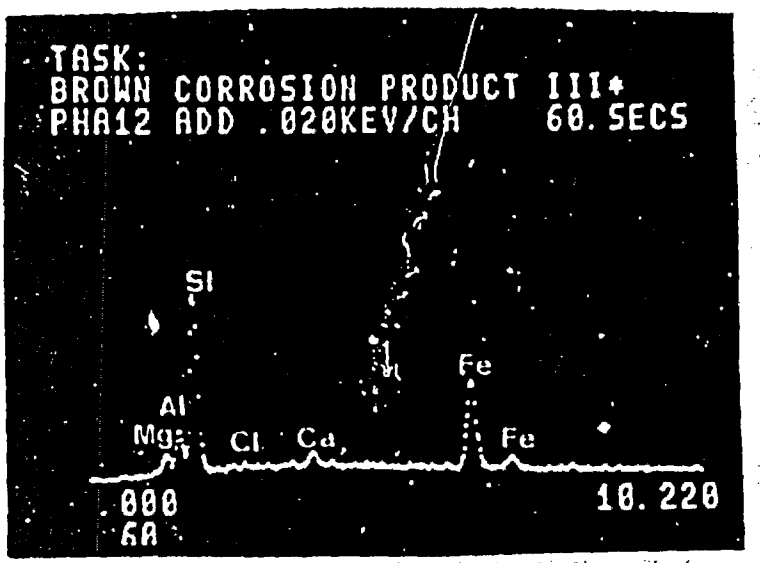

Figure 51. EDX of Phase III test orange-brown carbon steel surface product.

tests due to the radiolysis of methane. Similar amounts of hydrogen were produced in the irradiated Phase I test and in the non-irradiated Phase III test.

- After cooling the autoclave over a period of 25 minutes, the pH of the water in the basalt/bentonite packing material measured at room temperature was nearly neutral. There did not appear to be a significant change in pH across the thermal gradient in the packing material in any of the three tests.

- There did not appear to be a significant change in DO across the thermal gradient of the packing material in any of the three tests.

- The calculated Eh values indicated that an oxidizing environment existed after quenching the contents of the autoclave. Radiolysis of groundwater did not appear to increase the oxidizing potential overall.

- The concentration of Cl^- and SO_4^{2-} measured at room temperature were significantly greater near the cooler end of the thermal gradient in the tests.

- The bulk of the Fe and Si content of the reacted water is present as colloidal material that is filterable. Gamma radiation enhanced colloid formation.

- Hydrothermal conditions cause some change in the bentonite component of the packing material.

- Optical and XRD studies indicate that some changes occur in the mineralogical content of basalt during hydrothermal testing.

- There was no pitting on the carbon steel sleeve or the steel weldment in the Phase I test. There were hemispherically-shaped pits approximately 12 μ in depth after 60 days of irradiation in the Phase II test. In the Phase III test, shallower (approximately 8 μ in depth) and more closely-spaced pits were formed on the carbon steel sleeve. Based on a highly conservative assumption of linear pitting rates the maximum pit depth after 300 years is about 2.2 cm.

- Adherent surface products removed from the carbon steel sleeve in the Phase I test contained mainly montmorillonite clay. SEM-EDX analysis indicated the presence of other materials containing more Fe than that found in the montmorillonite. Surface products removed from the carbon steel sleeve in the Phase II test were analyzed by SEM-EDX and electron diffraction but were not readily identifiable. (An orange-brown product contained large amounts of Si, Fe, and Al, while the green-yellow product was largely composed of Fe and Si.) Identification was also not possible for the Phase III surface products, which were analyzed by SEM-EDX and XRD. Both Phase III surface products contained large amounts of Si and Fe, with the green phase also containing a large amount of Ca.

7. RECOMMENDATIONS FOR FUTURE WORK

The following recommendations are made for additional and confirmatory experiments:

- o A number of identical experiments need to be performed to establish statistical variations.
- o Longer term experiments should be performed to determine changes in gas composition and pressure buildup.
- o The effect of quenching the autoclave on the measured values of pH, DO, Cl^-, SO_4^{2-} and Fe needs to be determined.
- o Changes in the clay and basalt during hydrothermal reaction need to be specified and explained to predict long term performance.
- o Full characterization of the colloidal material in terms of composition and size distribution needs to be performed.
- o Mineralogical changes in the basalt, especially with regard to the glassy phases, need to be fully evaluated. Correlations could be made with predictions generated by use of geochemical codes, such as WATEQ and PHREEQE.
- o Long term corrosion studies are needed to determine the extent of localized corrosion in container steels. Hydrogen uptake by steel, and its effect on embrittlement also needs to be established.
- o Applicability of the current laboratory data to repository environments needs to be established by in situ experiments. These experiments should simulate hydrothermal conditions and may involve pressurizing a test borehole. Similar tests will need to be developed and conducted for waste package performance experiments. Repository field tests, such as those which have been carried out by WIPP (SAND 83-1516C, 1983), may provide a basis for designing tests relevant to a basalt repository.

8. REFERENCES

AESD-TME-3142, "Waste Package Conceptual Designs for a Nuclear Repository in Basalt," C. R. Bolmgren and others, Westinghouse Electric Corporation, 1982.

ANL-83-19, "Fuel Cycle Programs - Quarterly Progress Report, October-December 1982," J. J. Steindler and others, Argonne National Laboratory, 1983.

Arai, H., S. Nagai, K. Matsuda and M. Hatada, "Effect of Irradiation Temperature on the Radiolysis of Methane," Radiat. Phys. Chem. 17, 151-157, 1981.

Bonham, L. C., "Solubility of Methane in Water at Elevated Temperatures and Pressures," American Association of Petroleum Geologists Bulletin 62, 2478-2488, 1978.

Braker, W. and A. L. Mossman, Gas Data Book, Matheson Gas Products, Inc., Secaucus, New Jersey, 1980.

Brunauer, S., P. H. Emmett and E. Teller, "Adsorption of Gases in Multimolecular Layers," J. Amer. Chem. Soc. 60, 309-319, 1938.

BWIP/NRC Geochemistry Workshop, January 9-12, 1984, Richland, Washington.

Carroll, D., Clay Minerals: A Guide to Their X-Ray Identification, Geological Society of America, Boulder, Colorado, 1970.

Dean, J. A., Lange's Handbook of Chemistry, McGraw-Hill, 1979, p. 10-5.

Deer, W. A., R. A. Howie and J. Zussman, An Introduction to the Rock-Forming Minerals, London, Longnam Group Ltd, 1966.

DOE/RL 82-3, Vol. II, "Site Characterization Report for the Basalt Waste Isolation Project," November 1982.

DP-1464, "Radiolytic Gas Production From Concrete Containing Savannah River Plant Waste," N. E. Bibler, Savannah River Laboratory, January 1978.

DP-MS-76-51, "Radiolytic Gas Production During Long-Term Storage of Nuclear Wastes," N. E. Bibler, Savannah River Laboratory, October 1976.

Draganic, I. G. and Z. D. Draganic, The Radiation Chemistry of Water, New York, Academic Press, 1971.

Greenberg, A. E., J. T. Connors and D. Jenkins, Standard Methods for the Examination of Water and Wastewater, American Public Health Association, Washington, D. C., 1981.

Grimshaw, R. W., The Chemistry and Physics of Clays and Other Ceramic Materials, New York, John Wiley and Sons, 1971.

Hall, E. E., "Corrosion of Cast Iron and Low Carbon Steel Nuclear Waste Containers in a Basalt Repository," U. S. Nuclear Regulatory Commission, August 1982.

Himmelblau, D. M., "Solubilities of Inert Gases in Water, 0°C to Near the Critical Point of Water," J. Chem. Eng. Data, Vol. 5, 10-15, 1960.

Kraus, E. H., W. F. Hunt and L. S. Ramsdell, Mineralogy, New York, McGraw-Hill, 1959.

Krumhansl, J. L., "Mineralogic Stability of a Bentonite Backfill in a Bedded Salt Repository Environment," Abstract for 1982 Meeting Geological Society of America.

Lerman, A., Geochemical Processes Water and Sediment Environments, New York, Wiley, 1979, p. 389.

Maurin, J., "Etude de la Radiolyse due Methane en Phase Gazeuse, J. Chim. Phys. 59, 15-26, 1962.

Norfolk, D. J. and T. Swan, "Gamma Radiolysis of Methane Adsorbed on Gamma-Alumina - Part I: Development of Sites Active in Energy Transfer," J. Chem. Soc. Faraday Trans. I 73, 1454-1466, 1977.

Norfolk, D. J., R. F. Skinner and W. J. Williams, "Hydrocarbon Chemistry in Irradiated $CO_2/CO/CH_4/H_2O/H_2$ Mixtures - I," Radiat. Phys. Chem. 21, 307-319, 1983.

NUREG-0960, Vol. 2, "Draft Site Characterization Analysis of the Site Characterization Report for the Basalt Waste Isolation Project," U. S. Nuclear Regulatory Commission, March 1983.

NUREG/CR-2482, Vol. 3, BNL-NUREG-51494, "Review of DOE Waste Package Program: Subtask 1.1 - National Waste Package Program, April 1982-September 1982," P. Soo and others, Brookhaven National Laboratory, March 1983.

NUREG/CR-2482, Vol. 4, BNL-NUREG-51494, "Review of DOE Waste Package Program: Subtask 1.1 - National Waste Package Program, October 1982-March 1983," P. Soo and others, Brookhaven National Laboratory, September 1983.

NUREG/CR-3091, Vol. 1, BNL-NUREG-51630, "Review of Waste Package Verification Tests: Semiannual Report Covering the Period April-September 1982," P. Soo and others, Brookhaven National Laboratory, April 1983.

NUREG/CR-3091, Vol. 2, BNL-NUREG-51630, "Review of Waste Package Verification Tests: Semiannual Report Covering the Period October 1982-March 1983," P. Soo and others, Brookhaven National Laboratory, August 1983.

NUREG/CR-3091, Vol. 3, BNL-NUREG-51630, "Review of Waste Package Verification Tests: Biannual Report," B. Siskind and others, December 1983.

NUREG/CR-3389, "Valence Effects on the Sorption of Nuclides on Rocks and Minerals," R. E. Meyer, W. D. Arnold and F. I. Case, Oak Ridge National Laboratory, February 1984.

PNL-4452, "Nuclear Waste Package Materials Testing Report: Basalt and Tuffaceous Environments," D. J. Bradley and others, Pacific Northwest Laboratory, March 1983.

RHO-BW-SA-219P, "Experimental Investigation of Sodium Bentonite Stability in Hanford Basalt," M. I. Wood, Rockwell Hanford Operations, 1983.

RHO-BW-SA-303P, "Repository and Waste Package Designs for High Level Nuclear Waste Disposal," M. J. Smith and others, Rockwell Hanford, 1983.

RHO-BW-SA-315P, "Gamma Radiolysis Effects on Grande Ronde Basalt Groundwater," W. J. Gray, Pacific Northwest Laboratory, October 1983.

RHO-BW-ST-21P, "Evaluation of Sodium Bentonite and Crushed Basalt as Waste Package Backfill Materials," M. I. Wood, G. D. Aden and D. L. Lane, Rockwell Hanford Operations, October 1982.

RHO-BWI-C-66, "Preliminary Geochemical and Physical Testing of Materials for Plugging Man-Made Accesses to a Repository in Basalt," C. L. Taylor and others, Rockwell Hanford, April 1980.

RHO-BWI-C-105, "The Geochemical Behavior of Supercalcine Waste Form: Its Stability in a Basalt Environment," J. R. Halloway and others, Rockwell Hanford Operations, June 1981.

RHO-RE-SR-5, "Reference Material Chemistry - Synthetic Groundwater Formation," T. E. Jones, Rockwell Hanford Operations, April 1982.

Rose, A. J., Tables permettant le depouillement des diagrammes de rayons X et Abaques de reglage des monochromateurs a lame caurbe, Paris, Centre National de la Recherche Scientifique, 1957.

SAND 83-1516C, "The Waste Package Materials Field Test in S. E. New Mexico Salt," M. A. Molecke and T. M. Torres, Sandia National Laboratories, November 1983.

SD-BWI-TP-022, "Barrier Materials Test Plan," Rockwell Hanford Operations, March 1984.

Seyfried, W. E., Jr. and J. L. Bischoff, "Low Temperature Basalt Alteration by Seawater: An Experimental Study at 70°C and 150°C," Geochimica et Cosmochimica Acta 43, 1937-1947, 1979.

Stevens, G. C., R. M. Clarke and E. J. Hart, "Radiolysis of Aqueous Methane Solutions," J. Phys. Chem. 76, 3863-3867, 1972.

Stoessell, R. K. and P. A. Byrne, "Methane Solubilities in Clay Slurries," Clays and Clay Minerals 30, 67-72, 1982.

Van Olphen, H., An Introduction to Clay Colloid Chemistry, New York, Wiley, 1977.

Van Olphen, H. and J. J. Fripiat, Data Handbook for Clay Materials and Other Non-Metallic Minerals, Oxford, England, Pergamon Press, 1979, p. 19.